ISSN 2355-3286

ULTIMA Computing

Jurnal Sistem Komputer

Engineering | Vol. 14 | No. 1 | Page 1 - 47 | June 2022 | ISSN 2355-3286

UMN

UNIVERSITAS
MULTIMEDIA
NUSANTARA

ISSN 2355-3286

EDITORIAL BOARD

EDITORIAL ADDRESS

Universitas Multimedia Nusantara (UMN)
Jl. Scientia Boulevard
Gading Serpong
Tangerang, Banten - 15811
Indonesia
Phone. (021) 5422 0808
Fax. (021) 5422 0800
Email : ultimacomputing@umn.ac.id

Ultima Computing : Jurnal Sistem Komputer is a Journal of Computer Engineering Study Program, Universitas Multimedia Nusantara which presents scientific research articles in the field of Computer Engineering and Electrical Engineering as well as current theoretical and practical issues, including Edge Computing, Internet-of-Things, Embedded Systems, Robotics, Control System, Network and Communication, System Integration, as well as other topics in the field of Computer Engineering and Electrical Engineering. The Ultima Computing : Jurnal Sistem Komputer is published regularly twice a year (June and December) and is jointly managed by the Computer Engineering and Electrical Engineering Study Program at Universitas Multimedia Nusantara.

Call for Papers

International Journal of New Media Technology (IJNMT) is a scholarly open access, peer-reviewed, and interdisciplinary journal focusing on theories, methods and implementations of new media technology. Topics include, but not limited to digital technology for creative industry, infrastructure technology, computing communication and networking, signal and image processing, intelligent system, control and embedded system, mobile and web based system, and robotics. IJNMT is published twice a year by Faculty of Engineering and Informatics of Universitas Multimedia Nusantara in cooperation with UMN Press.

Ultimatics : Jurnal Teknik Informatika is the Journal of the Informatics Study Program at Universitas Multimedia Nusantara which presents scientific research articles in the fields of Analysis and Design of Algorithm, Software Engineering, System and Network security, as well as the latest theoretical and practical issues, including Ubiquitous and Mobile Computing, Artificial Intelligence and Machine Learning, Algorithm Theory, World Wide Web, Cryptography, as well as other topics in the field of Informatics.

Ultima Computing : Jurnal Sistem Komputer is a Journal of Computer Engineering Study Program, Universitas Multimedia Nusantara which presents scientific research articles in the field of Computer Engineering and Electrical Engineering as well as current theoretical and practical issues, including Edge Computing, Internet-of-Things, Embedded Systems, Robotics, Control System, Network and Communication, System Integration, as well as other topics in the field of Computer Engineering and Electrical Engineering.

Ultima InfoSys : Jurnal Ilmu Sistem Informasi is a Journal of Information Systems Study Program at Universitas Multimedia Nusantara which presents scientific research articles in the field of Information Systems, as well as the latest theoretical and practical issues, including database systems, management information systems, system analysis and development, system project management information, programming, mobile information system, and other topics related to Information Systems.

ISSN 2355-3286

FOREWORD

ULTIMA Greetings!

Ultima Computing : Jurnal Sistem Komputer is a Journal of Computer Engineering and Electrical Engineering at Multimedia Nusantara University which presents scientific research articles in the field of Computer Systems as well as the latest theoretical and practical issues, including Edge Computing, Internet-of-Things, Embedded Systems, Robotics, Control Systems, Network and Communication, System Integration, and other topics in the field of Computer Engineering and Electrical Engineering.

In this June 2022 edition, ULTIMA Computing enters the 1st Edition of Volume 14. In this edition there are six scientific papers from researchers, academics and practitioners in the fields of Computer Engineering and Electrical Engineering. Some of the topics raised in this journal are: Comparison of FIR Window Filter Variation Results on Pink Noise Audio, Indoor Positioning System Infrastructure Based on Triangulation Method through Visible Light Communication, Specification Design and Performances Using Computational Fluid Dynamics for Mini-Remotely Operated Underwater Vehicle, The Development of an IoT-based Indoor Air Monitoring System Towards Smart Energy Efficient Classroom, Sensor Design for Building Environment Monitoring System based on Blynk and Preliminary Study on Indonesian Word Recognition for Elder Companion Robot.

On this occasion we would also like to invite the participation of our dear readers, researchers, academics, and practitioners, in the field of Engineering and Informatics, to submit quality scientific papers to: International Journal of New Media Technology (IJNMT), Ultimatics : Jurnal Teknik Informatics, Ultima Infosys: Journal of Information Systems and Ultima Computing: Journal of Computer Systems. Information regarding writing guidelines and templates, as well as other related information can be obtained through the email address ultimacomputing@umn.ac.id and the web page of our Journal here.

Finally, we would like to thank all contributors to this June 2022 Edition of Ultima Computing. We hope that scientific articles from research in this journal can be useful and contribute to the development of research and science in Indonesia.

June 2022,

M.B.Nugraha, S.T., M.T.
Editor-in-Chief

ISSN 2355-3286

TABLE OF CONTENT

ISSN 2355-3286

Comparison of FIR Window Filter Variation Results on Pink Noise Audio

John Christopher[1], Nabila Husna Shabrina[2], Cindy Cornelia[3], Yoel Zakhary[4]
[1,3,4] Department of Physics Engineering, Universitas Multimedia Nusantara, Tangerang, Indonesia
[2] Department of Computer Engineering, Universitas Multimedia Nusantara, Tangerang, Indonesia
[1] john.christopher@student.umn.ac.id, [2] nabila.husna@umn.ac.id, [3] cindy.cornelia@student.umn.ac.id, [4] yoel.zakhary@student.umn.ac.id

Accepted on 14 June 2021
Approved on 29 March 2022

***Abstract*— IIR and FIR filters are the most used digital signal filters. The application of each filter type depends on the needs of the user. IIR filters are generally used for applications with limited memory. In comparison, FIR filters are usually used for applications where the linear phase is essential. In this study, the implementation of FIR filters on pink noise audio samples was observed. Various FIR window method filters such as rectangular, hamming, hanning, and Blackman will be compared. Each type of filter will have a different filter order due to computing the frequency cut-off point for each filter. The comparisons were made by observing the gain response, the time domain signal, the frequency response, and the phase response. The results indicated that the Hanning window method is a better filter because it produces low delay and good attenuation. Things to be considered in designing FIR filters are fluctuations in frequency response and phase shift. Alterations on cut-off points on the filters and delay usage can be deployed for some improvement.**

***Index Terms*— digital filter, FIR, gain response, phase response, time domain.**

I. INTRODUCTION

A. Background

Digital filters use mathematical algorithms to remove interference with digital data in the signal. The commonly used filters are IIR and FIR filters, whereas IIR filters are generally used for applications where the linear phase is not crucial, and memory is limited. These filters are commonly used in audio signal management, biomedical sensor signal processing, and high-speed telecommunications applications. Whereas FIR filters are generally used for applications where the linear phase is important and there is sufficient memory available. This filter is commonly used in audio signal enhancement and biomedical applications [1]. Filters can also be used to create audio equalizers applicable to many situations.

Many methods to design FIR filters such as frequency sampling, window method, and optimal design method. In this paper, the window method is chosen as the method used to design the filter. The Window Method is an easy, effective, and most commonly used method in designing FIR filters [2]. In addition, the window method also has good scalability and ease of calculating window coefficients [3]. However, the FIR filter has some problems when using the Fourier transform. Oscillations in the passband and stopband could appear. This is due to sudden signal truncation when converted using the Fourier transform and the convergence of the Fourier transform, which is quite long, especially near the discontinuity point. This problem can be solved by selecting the correct type of window method on the signal [4].

The method window itself is divided into several types based on the equation used, such as Rectangular Window, Hamming Window, Hanning Window, and Blackman Window [5].

B. Objectives and research methods

Through the discussion carried out in the background, it can be concluded that each variation of the FIR filter could filter out audio data interference or its own noise. This directly affects the results of the audio data equalizer due to the different filtering capabilities. To determine the ability of each variation of the FIR filter, the authors make an equalizer system design that includes 6 filter bands for all audio signals. The results of the equalizer for each variation of the FIR filter will be compared by the author.

The type of research used is experimental on pink noise audio as audio data to be filtered. Using the pink noise audio, a comparison of each type of FIR filter will be the objective of this research. The window methods will be compared such as Rectangular Window, Hamming Window, Hanning Window, and Blackman Window. To simplify the analysis, the x-axis time-domain graph is from 0 to 0.1 seconds and the y-axis is limited from -1 to +1. For the frequency-domain, the x-axis is limited from 0 to 7000 Hz and the y-axis is limited from 0 to 3000 samples. For the phase-domain, the x-axis is limited from 0 to 7000 Hz and the y-axis is limited from -1000 to 1000 samples.

II. LITERATURE REVIEW

A. Audio Signal Processing

In a world with increasingly sophisticated technological developments, communication systems are also developing and increasingly pampering their users. The development of communication systems forced the production of the best and optimal audio quality possible. To produce audio quality that spoils the ears of its users, we need a system that processes the audio signal. Audio signals can appear in the form of analogue signals or digital signals, and both have a range from 20 Hz to 20000 Hz according to the limits of human hearing ability.

With audio signal processing technology, an audio signal can be manipulated to produce a better output. Some examples of audio signal processing techniques include analogue-to-digital conversion (ADC), echo cancellation, filtering, equaliser, and noise removal [6].

B. Audio Equalizer

One of the audio signal processing techniques is equalisation, also known as the equalizer. Basically, an equalizer is a set of filters, either employing software or hardware filters used to adjust the amplitude level of a specific frequency range. At first, the equalizer was created to adjust the sound characteristics in places that have less than ideal sound results. Over time, the equalizer has evolved its use to a wider range of needs. The equalizer works in a frequency range, also known as bands. At its simplest, a two-band equalizer adjusts the treble and bass. The more bands available, the narrower the adjustable frequency range will be, so that it can provide more flexible control [7].

C. Frequency Response

Frequency response is a measure of the output of any system to an input signal of the varying frequency with a constant amplitude, as can be seen in Fig.1. This is usually characterized by the magnitude of the system response which is measured in decibel and degree [8]. In addition, the frequency response is often thought of as a filter that can increase or decrease the input signal to change the sound. The frequency response can be said to be ideal when the resulting response does not match the bass or treble volume of the audio used [9].

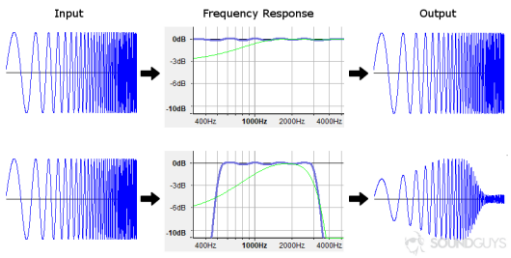

Figure 1. Frequency Response

D. Phase Response

The phase of the frequency response is the phase response. This response shows the delay of the filter at each frequency point [10]. Ideally, the filter is expected to have a linear phase response so that the audio signal being passed is not distorted and degraded. Linear phase filter (linear response filter) has a physical meaning that every frequency that passes through the filter will have the same delay so that the phase response will increase as the frequency increases [11]. The example of phase response can be seen at Fig.2.

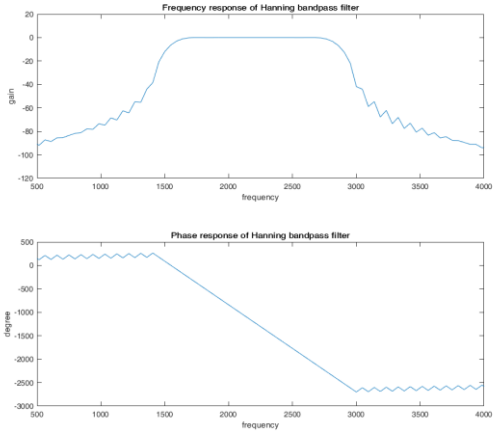

Figure 2. Phase Response

E. Finite Impulse Response (FIR)

Finite Impulse Response is a filter that has an impulse response with a limited period. The FIR filter design method is based on the ideal filter approach, where this filter will approach perfect characteristics because the filter order will increase so filter making, and its implementation will be more complicated [12]. FIR filters are usually implemented using delays, multipliers, and enhancers to produce the desired output. Fig. 3 Shows a basic diagram of an FIR filter of length N. The value of *hk* in the figure is the coefficient used for multiplication, so the output at time n is the sum of all pending samples multiplied by the appropriate coefficient.

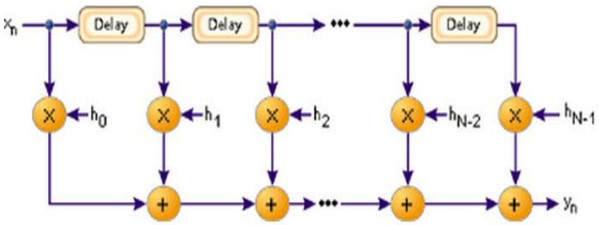

Figure 3. FIR Filter Structure [13]

The process of selecting filter lengths and coefficients is called filter design. The purpose of the filter design is to adjust the existing parameters so that the desired results are produced through this filter [13].

F. Window Method for Designing FIR Filter

The Window Method is an effective, fast, and easy-to-use filter design method. However, in general, this method is less than optimal [14]. Windowing causes smearing so that the cut-off frequency cannot be determined accurately to get the desired stop band frequency range and fit frequency band. For this reason, the window method is more suitable for the needs of design prototypes [15]. To find the equivalent representation of the time domain, the window method can be calculated using the inverse Fourier transform. The following is the equation in the window method [16]:

$$h_d[n] = \frac{1}{2\pi} \int_{-\pi}^{+\pi} H_d(w) e^{jwn} dw \quad (1)$$

G. Hamming Method for Designing FIR Filter

Hamming Method is an FIR filter method that has an amplitude formed by the cosine function, this filter is limited to degrees N. When the value of n is in the range

$$-\frac{N-1}{2} \leq n \leq \frac{N-1}{2} \quad \text{(N odd)}$$

$$-\frac{N}{2} \leq n \leq \frac{N}{2} \quad \text{(N even)}$$

Then the value of w(n) is as follows:

$$w(n) = 0.54 + 0.46 \cos\left(\frac{2\pi}{N}\right) \quad (2)$$

H. Hanning Method for Desinging FIR Filter

Hanning Method is an FIR filter method which has an amplitude that is also formed by the cosine function, and is limited to degrees N. Different from the hamming method, hanning touches the 0 point at both ends of the signal [17].

$$w(n) = 0.5\left(1 - \cos\left(2\pi \frac{n}{N+1}\right)\right) R_N(n) \quad (3)$$

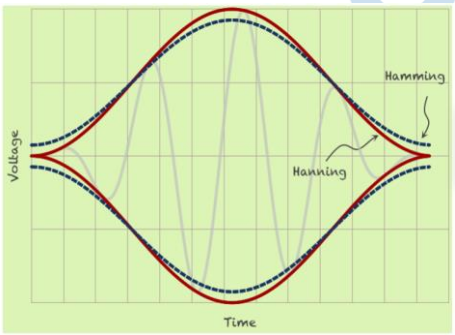

Figure 4. Comparison of Hamming and Hanning Powers [17].

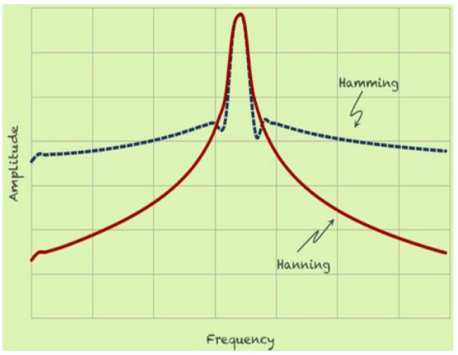

Figure 5. Comparison of Hamming and Hanning Amplitudes [17].

The comparison between Hamming and Hanning windows in terms of powers and bandwidth can be seen in Fig.4 and 5.

I. Blackman Method for Designing FIR Filter

The Blackman method is used to reduce the variance. When compared with other methods, the Blackman method has a better improvement in damping the stopband. The Blackman method has good characteristics for filtering an audio [18]. The equation of the function of this method is as follows:

$$w(n) = \left(0{,}42 - 0{,}5 \cos\left(\frac{2\pi n}{N-1}\right) + 0{,}08 \cos\left(\frac{4\pi n}{N-1}\right)\right) R_N(n) \quad (4)$$

J. Rectangular Method for Designing FIR Filter

The Rectangular method is a method that has a constant function between the interval range and the value of zero. The equation of the function of this method is as follows. When the range n is at 0<n<N-1, then the value of w(n) is as follows:

$$w(n) = R_N(n) \quad (5)$$

and worth

$$w(n) = 0 \quad (6)$$

if it is out of range.

K. Comb Filtering

Comb filtering occurs when a signal and a signal equal to the delay are combined into a single signal. Comb Filtering creates peaks and troughs in the frequency response and results in a thin, odd sounding sound. [19]. To reduce it, it is necessary to use delay compensation on the FIR filter between the two signals to be combined [20]. Comb filtering can be seen at Fig. 6.

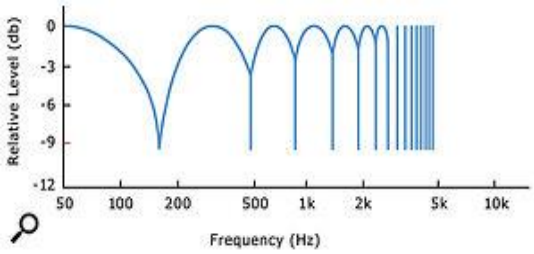

Figure 6. K.1 Comb Filtering [21]

III. METHODOLOGY

The equalizer system design features six bandpass filters covering the entire audio frequency range. The sampling frequency used is 48000 Hz as the standard for digital audio [22]. The filter specifications are shown in the Table 1. [23].

TABLE 1. FIR FILTER SPECIFICATIONS

Filter No	Filter Type	Low Stop Freq	Low Pass Freq	High Pass Freq	High Stop Freq
1	Low-pass	1100 Hz	700 Hz	-	-
2	Band-pass	400 Hz	700 Hz	1700 Hz	2000 Hz
3	Band-pass	1400 Hz	1700 Hz	2700 Hz	3000 Hz
4	Band-pass	2300 Hz	2700 Hz	3900 Hz	4300 Hz
5	Band-pass	3500 Hz	3900 Hz	5300 Hz	5700 Hz
6	High-pass	-	-	5300 Hz	00 Hz

Based on reference [1], it is stated that the audio signal has more energy at low frequencies than high frequencies so that the filter specifications are limited to 5300 Hz. The equalizer design in this paper is divided into six parts; low pass filter, four band pass filter, and high pass filter. The high pass filter serves to filter frequencies above 5300 Hz. Like the equalizer function in general, by changing the amplitude/magnitude of each filter, the character of the sound output can be adjusted as needed.

C. Cut Off Frequency FIR filter

The Fourier Transform design with the window function is called the window method. The window method is used to design the FIR filter used in this equalizer system. By using the equation fc = (fap +fas)/2 , we get the cut off frequency point for each of the six filters as given in Table 2.

TABLE 2. AUDIO EQUALIZER FILTER SYSTEM

Filter No	Filter Type	Cut Off Low	Cut Off High	Normalized Freq Low	Normalized Freq High
1	Low-Pass	900 Hz		0,0375	
2	Band-Pass	550 Hz	1850 Hz	0,0229	0,0771
3	Band-Pass	1550 Hz	2850 Hz	0,0646	0,1188
4	Band-Pass	2500 Hz	4100 Hz	0,1042	0,1708
5	Band-Pass	3700 Hz	5500 Hz	0,1542	0,2292
6	High-Pass		5000 Hz		0,2083

D. Filter Order

Based on the frequency limits of cut off low, cut off high, normalized low, and normalized high, the filter order value is obtained to get the same transition width on the six filters for each of the three types of filters. Filter order is obtained by the equation f =|fas-fap| /fs and N=3.1/delta F(Hanning), N=3.3/delta F (Hamming), and N=5.5/delta F(Blackman).. The result can be seen in Fig. 3. Based on the study in [23], the order of the filter is determined by the equation that has been shown previously. The filter order is determined to get the same transition width for all four filter types. That way, the gain response diagram filter is easier to compare.

TABLE 3. FILTER ORDER

Filter No	Filter Type	Rectangular	Hanning	Hamming	Blackman
1	Low-pass	108	372	396	660
2	Band-pass	144	496	528	880
3	Band-pass	144	496	528	880
4	Band-pass	108	372	396	660
5	Band-pass	108	372	396	660
6	High-pass	72	248	264	440

IV. RESULT AND ANALYSIS

After performing the simulation using MATLAB, the graphs of each method were obtained. Fig. 7-8. shows a graph of a pink noise audio sample in the time-domain, frequency domain, and phase domain before being filtered along with a graph of each method used.

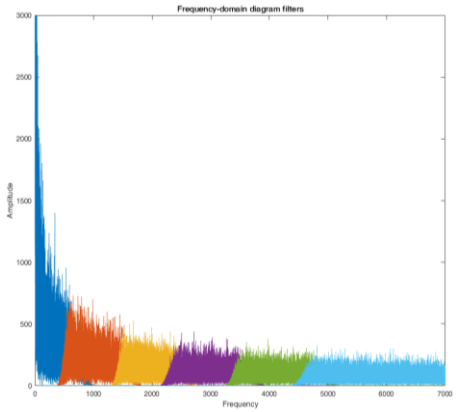

Figure 7. Frequency Division Graph 6 band filter

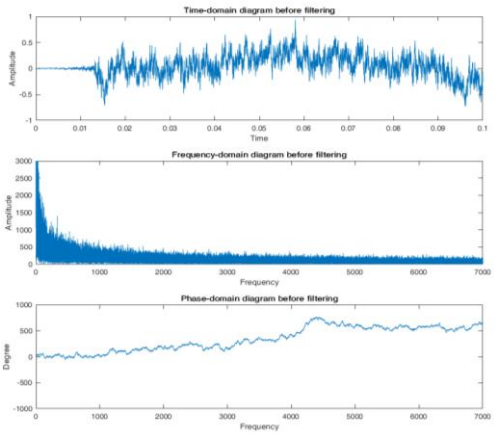

Figure 8. Pink Noise Graph in Time Domain, Frequency Domain and Phase Domain before filtering

A. *Gain Response Diagram*

The gain response for rectangular, hanning, hamming and Blackman windows are given in Fig. 9-12. In the gain response filter diagram, it can be seen that the hanning window has the best attenuation compared to the other two types of filters. The attenuation of the rectangular window filter starts in the range of -30 dB. The attenuation of the hanning window filter starts from the range of -60 dB. The attenuation of the hamming window filter starts from the range of -70 dB. The attenuation of the Blackman window filter starts from the range of -80 dB. Although the hamming window has a lower attenuation than the hanning window, the hanning window has a more drastic attenuation slope. That is, the further away from the cut off point, the hanning window attenuation is greater than the hamming window. If it is correlated between filter order and gain response on the four filters, it can be said that the higher the order, the more the frequency is attenuated at points outside the cut off.

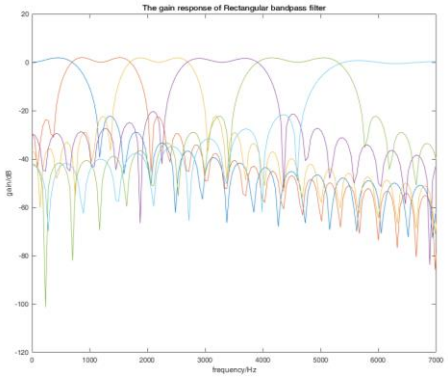

Figure 9. Rectangular Window Gain Response Graph

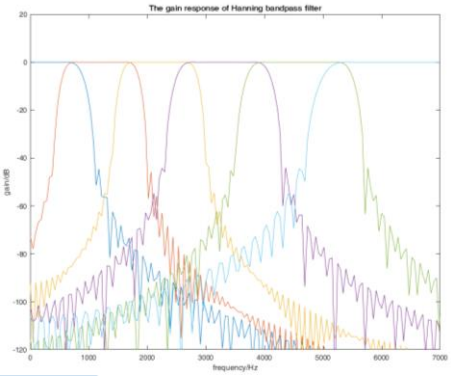

Figure 10. Gain Response Hanning Window Chart

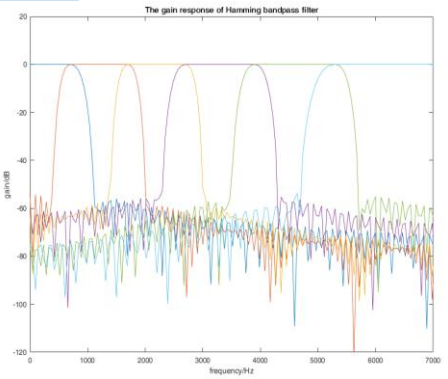

Figure 11. Hamming Window Gain Response Chart

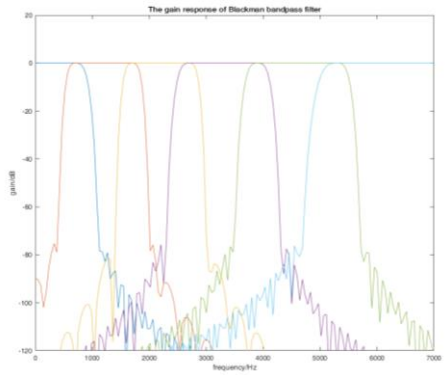

Figure 12. Blackman Window Gain Response Chart

B. *Time-Domain Diagram*

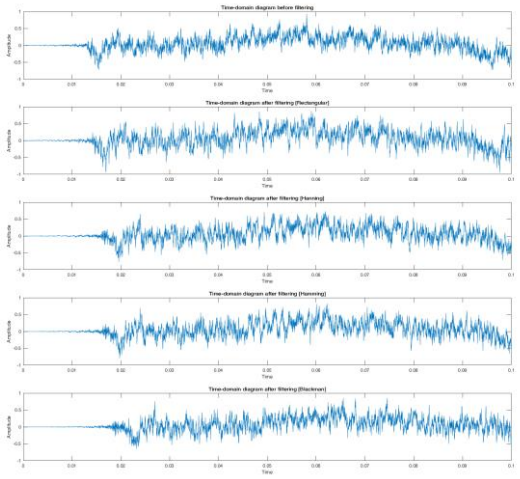

Figure 13. Time-Domain Graphics

On the time-domain graph, as shown in Fig. 13, can be seen that the audio starts sounding at about 10 ms (0.01 sec). Then, after filtering, the results shown by the time-domain graph on the four types of FIR filters indicate a shift in the audio, also known as delay. This delay occurs due to filtering at low frequencies carried out by each type of filter. In the graph given, it can be seen that the rectangular window has the lowest delay. In addition, in Table 3 Filter Order in the low pass section, it can be seen that the rectangular window has a lower filter order than the hanning window, hamming window, and Blackman window method. This indicates that if the required filter order calculation is larger, then the delay that occurs will increase.

C. *Frequency Domain*

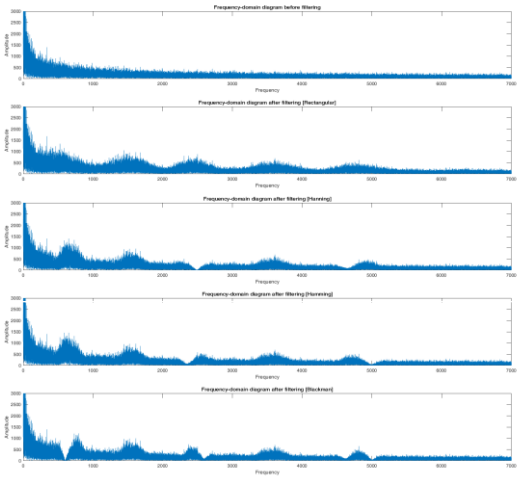

Figure 14. Frequency domain signal for Rectangular, Hanning, Hamming, and Blackman Windows.

On the frequency-domain graph given in Fig. 14, the four types of filters create fluctuations when compared to the frequency of the audio response before using the filter. This change can be caused by combining the outputs of each band filter at the cut off point. This fluctuation in output pooling occurs due to overlapping filter cut-offs. The first low-pass filter has a cut-off at 900 Hz, while the second band-pass filter has a cut-off from 550 Hz to 1850 Hz. It can be seen that the audio from 550 Hz to 900 Hz comes from two filters so that there is an increase in amplitude in that frequency range. This overlap also occurs in subsequent filters. On the other hand, for the frequency area with an amplitude close to zero (lost). This is due to the comb filtering phenomenon. This phenomenon is a phenomenon of frequency overlapping in two filters with different time-delays. When there is overlap at the same frequency value, fluctuations and faults will occur in the audio energy.

D. *Phase Domain*

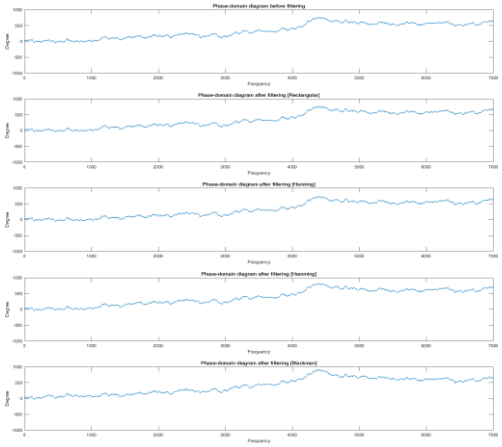

Figure 15. Phase Domain signal for Rectangular, Hanning, Hamming, and Blackman Windows.

For phase domain graph, given in Fig.15, there is a slight phase shift in the four types of filters used. The phase shift is also caused by the different time-delays for each filter.

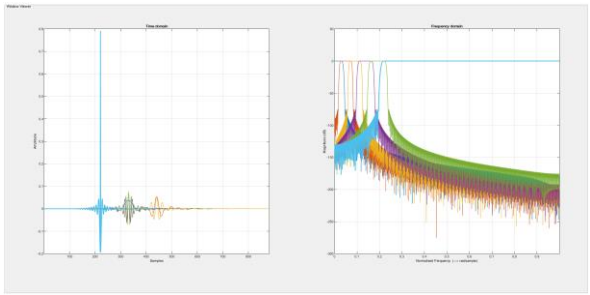

Figure 16. Blackman calculated filter order

V. CONCLUSION

From the simulation results that have been carried out, it can be concluded that the hanning window method is the best method because it produces low delay and good attenuation. To compensate the fluctuations in frequency response and phase shift, some improvements can be made. First, the cut-off

points on the six filters could be altered so that there is no overlapping frequency range between two or more filters. Furthermore, both time-delays can be compensated by adding a delay for each filter.

REFERENCES

[1] Admin, "Difference between IIR and FIR filters: A practical design guide," *ASN Home*. https://www.advsolned.com/difference-between-iir-and-fir-filters-a-practical-design-guide/. (Accessed: 26-Aug-2021).

[2] G. K. Agordzo and H. Adjei, "A design of a low-pass FIR filter using Hamming window functions in Matlab," *Computer Engineering and Intelligent Systems*, Vol. 11, No. 2, 2020. pp. 24

[3] K. Priya & L. Singh, "Analysis of FIR Filter Design Techniques," *International Journal of Computer Science and Technology*, Vol. 4, Issue 1, 2013. pp 92

[4] P. Podder, T. Z. Khan, M. H. Khan, & M. M. Rahman, "Comparative Performance Analysis of Hamming, Hanning and Blackman Window," *International Journal of Computer Applications*, vol. 96, no. 18, 2014. pp 1-7

[5] H. Rakshit & M.A. Ullah, "A Comparative Study on Window Functions for Designing Efficient FIR Filter," Proceeding of *2014 9th International Forum on Strategic Technology (IFOST)*, 2014.

[6] "Audio signal PROCESSING- Understanding digital & analog audio signal processing," PathPartnerTech. https://www.pathpartnertech.com/audio-signal-processing-understanding-digital-analog-audio-signal-processing/. (Accessed: 26-Aug-2021).

[7] Y. Trivedi, "What is an equalizer, and How does it work?,"Howtogeek.com. .https://www.howtogeek.com/59467/htg-explains-what-is-an equalizer-and-how-does-it-work/. (Accessed 26-Aug-2021)

[8] FADG,"Term: Frequency response (audio)," Frequency response (audio) - Glossary - Federal Agencies Digitization Guidelines Initiative.http://www.digitizationguidelines.gov/term.php?term=frequencyresponseaudio. (Accessed: 26-Aug-2021)

[9] R. Triggs, "What is frequency response and how does it affect my music?," SoundGuys. https://www.soundguys.com/frequency-response-explained-16507/. (Accessed: 26-Aug-2021).

[10] Admin, "Phase response," CCRMA. https://ccrma.stanford.edu/~jos/filters/Phase_Response_I.html. (Accessed: 26-Aug-2021).

[11] "Phase response," Phase Response - an overview | Science Direct Topics. https://www.sciencedirect.com/topics/computer-science/phase-response. (Accessed: 26-Aug-2021).

[12] E. *, "What is FIR FILTER? - FIR filters for digital signal processing," ElProCus, https://www.elprocus.com/fir-filter-for-digital-signal-processing. (Accessed: 26-Aug-2021).

[13] M. Barr, "Introduction to finite impulse Response filters for DSP," Barr Group Software Experts, https://barrgroup.com/embedded-systems/how-to/digital-filters-fir-iir. (Accessed: 26-Aug-2021).

[14] Stanford Edu, "Window method for fir filter design", Stanford.edu.https://ccrma.stanford.edu/~jos/sasp/Window_Method_FIR_Filter.html. (Accessed: 26-Aug-2021).

[15] A. Roychowdhury, "FIR Filter Design Techniques," M.Tech. credit seminar report,Electronic Systems Group, EE Dept, IIT Bombay, Nov. 2002.

[16] S. Arar, "FIR filter design BY Windowing: Concepts and the rectangular window - technical articles," All About Circuits. https://www.allaboutcircuits.com/technical-articles/finite-impulse-response-filter-design-by-windowing-part-i-concepts-and-rect/. (Accessed: 26-Aug-2021).

[17] By: "Window functions in spectrum analyzers," Tektronix. https://www.tek.com/blog/window-functions-spectrum-analyzers#:~:text=The%20difference%20between%20them%20is,still%20have%20a%20slight%20discontinuity (Accessed: 26-Aug-2021).

[18] D.-J. Jwo, I.-H. Wu, and Y. Chang, "Windowing design and performance assessment for mitigation of spectrum leakage," E3S Web of Conferences, vol. 94, p. 03001, 2019.

[19] A. Clifford & J. Reiss, "Reducing comb filtering on different musical instruments using time delay estimation," Journal of the Art of Record Production, Issue 5, 2011.

[20]MATLAB, "designfilt," mathworks.com. https://www.mathworks.com/help/signal/ug/compensate-for-the-delay-introduced-by-an-fir-filter.html. (Accessed: 26-Aug-2021).

[21] P. White, "Q. what exactly is comb filtering" soundonsound.com. https://www.soundonsound.com/sound-advice/q-what-exactly-comb-filtering. (Accessed: 26-Aug-2021).

[22] S. Park, G. Hillman, and R. Robles, "A novel structure for real-time digital sample-rate converters with finite precision error analysis," *Proceeding of 1991 International Conference on Acoustics, Speech, and Signal Processing*, 1991.

[23] T. Tajdari, "FIR and IIR Filters for Sound Equalization Systems", *MJTD*, vol. 9, no. 2, pp. 53-57, Jun. 2020.

ISSN 2355-3286

Indoor Positioning System Infrastructure Based on Triangulation Method through Visible Light Communication

Apnan Juanda[1], Willy Anugrah Cahyadi[2], Angga Rusdinar[3], Denny Darlis[4]
[1,2,3] Electrical Engineering, School of Electrical Engineering, Telkom University, Bandung, Indonesia
[4] Telecommunication Technology, School of Applied Science, Telkom University, Bandung, Indonesia
[1] apnanjuanda@student.telkomuniversity.ac.id, [2] waczze@telkomuniversity.ac.id,
[3] anggarusdinar@telkomuniversity.co.id,[4] dennydarlis@telkomuniversity.ac.id

Accepted on 11 September 2021
Approved on 14 December 2021

***Abstract*— Autonomous mobile robots are widely used in industry to help human's work, but the concept has a weakness, that is robot still does not know its position in a room so it can not detect whether the robot has been at destination point. The technology commonly used to determine the position of objects is the Global Positioning System (GPS). However, GPS does not detect objects that are indoors. Previous research used Wi-Fi as a reference for designing an indoor positioning system, but the system could not determine the position in detail because Wi-Fi could only detect object zones. Based on these problems, this research will propose the infrastructure prototype design of an indoor positioning system based on Visible Light Communication (VLC). The main focus of this research is designing a VLC transmitter and receiver system, estimating the distance between the receiver and transmitter based on the received signal strength, and estimating the receiver's position using the triangulation method based on a minimum of 3 distance estimates. The estimating distance system get average accuracy is 76.47%. The estimated accuracy of the x-coordinate position has the best accuracy is 77.05% and the y-coordinate estimate has the best accuracy is 86.54%.**

***Index Terms*— Indoor Positioning System; LED Driver; Log Normal Shadowing; Received Signal Strength (RSS); Triangulation; Visible Light Communication (VLC)**

I. INTRODUCTION

Remotely Operated Underwater Vehicle (ROV) is a submersible robotic systems, used to examine various underwater characteristics and controlled by operators from shore[1].With complex, dangerous and limited areas urgently explored, there is an urgent need for an underwater machine that can replace humans to complete underwater detection. ROV were developed to perform resource exploration tasks in the ocean[2]. The applications of ROV are widely diverse, such as the oil and gas industry, discovery, aquaculture, marine biology, and military purpose [3][4][5][6].

Numerous of ROV designs are assembled around or inside cubic structured frame along with a buoyant on top body. The robotic vehicle utilized umbilical data cable as electrical cable and controlled by operator positioned on surface vessel.

The heavier tools are settled down on lowest possible position to keep the point of center buoyancy is higher than center of gravity, thus adequate stability is obtained. Sufficient stability of ROV meant ROV has capability to withstand against in disturbance for instance moment of rolling and pitch in longitudinal and lateral axis. Steady hydraulic rods suited of lifting and carrying particular equipment for specific purpose and placed in the fore along with cameras and lights.

Underwater ROVs are generally divided categories based on size, weight, capacity, or performance. Two common design of ROV which widely use are: the ROV Micro-Class with weigh not higher than 3 kg, are used especially in narrow area where a diver might not be capable to enter. And the ROV Mini-Class that weigh about 15 kg are also used as a diver alternative, Inspection-Class are typically rugged ROVs for commercial or industrial use, data acquisition and observation ROVs, Light weight duty category has generally no more than 50 hp on propulsion, While Heavy duty type has less than 220 hp with the ability to capability lift at least two handlers and work at depths up to 3500 m, and Trenching & Burial work class is the largest with more than 200 hp propulsion, with the ability to take a cable, put down sleds and working at depths until 6000 m in several cases[7][8][9][10]. The ROV design and construction is a robust solution to encounter the various require of an ROV to be used in wide implementations, it is compact, handy to use and inexpensive, and allow for confined space exploration. The main form of the body is designed to encounter the particular utilization needs. Commonly, almost ROV attached by torpedo form and an hydrodynamic main body was used at high-speeds[11]. Another type is the torpedo-less form, worked mainly in remote control

vehicles (ROVs) that are often worked for shorter period of time purpose or the assessment of other large subsea areas like huge ice floe or water-dams[12]. Toward to emphasize the performance in water resistance, Computational Fluid Dynamics (CFD), drives valuable part in Unmanned vehicle design. Nowadays, CFD approach has been widely applied in underwater vehicle design, as it can simulate the fluid flow field around the bodies and to find out with comprehend the physics of fluid flow phenomenon. CFD captured the flow field such as vortex in very small to major scales which is hard to obtain through field experiments.

CFD methods enable to predict and diagnostic technique for identifying the cause of particular problem in physic phenomena. The latest CFD approaches provide wealth data generated emphasize to visualize the implication of the result requires considerable skill. Due to this CFD become as an integral part of the design process.

From the economic cost, numerical simulation can deliver result within sufficiently short time span in the design process, thus optimization design can be detailed in addition to addressing this issue during the design process. Numeric simulation is considered low cost analysis hence became early stage to understanding along side with experimental test which can be over cost and intensive time.

In this project, the CFD analysis assists in investigate and demonstrate variable model for the hull body form based on initial prototype [13]. In this research, a design of Mini-ROV is developed especially the principal of body device in each element and electric parts is embedded. Furthermore, the hydrodynamic parameter and analysis was provided based on CFD simulation.

II. METHODS

The experimental method was used in this study, where a series of experiments were directly conducted by theoretical studies. The overall block diagram of the system built is shown in Fig. 1.

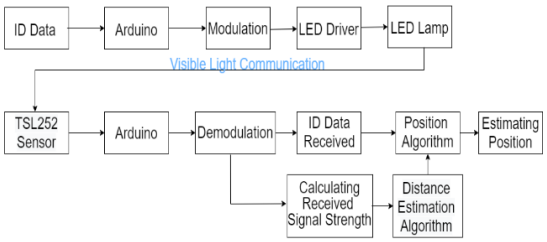

Fig. 1. Block Diagram System

The explanation in Fig. 1 is as follows: first Data ID will be initialized on Arduino, next it converted into ASCII data and will generate binary code that will be sent with serial communication UART (Universal Asynchronous Receiver-Transmitter). The modulation process is carried out, namely the process of converting the information into the carrier signal in the form of LED light. LED Driver is used as a switching circuit that converts the UART signal into LED's light, on the receiver side, the TSL252 sensor works to receive the light intensity and then performs a demodulation process so that the ID data is retrieved, next estimating distance process is based on the received signal strength and estimating position based on the triangulation method.

The prototype that will be made consists of 4 lamps with a height is 80 cm from the floor, between lamps given a distance is 40 cm and the height of the photodetector sensor to the lamp is 65 cm. Based on the existing block diagram, the first step is to initialize the ID data which is the letters of the alphabet a, b, c, d. This ID will be identity and coordinate(x, y) information of each lamp [11]. Next, Arduino Uno which as a microcontroller transmitter will convert data ID into UART serial format and forward it to LED Driver MOSFET IRF520 module. Data will be sent via visible light communication using modulation on-off keying [12].

The receiver device will use the TSL252 sensor to receive the light intensity and convert it into electrical pulses [13]. It is a combination of photodiode and transimpendance amplifier. Photodiode and transimpendance amplifier function to convert light intensity into voltage. The receiver circuit cable configuration is done by connecting the sensor ground pin to the Arduino ground pin, the VCC sensor pin to the 5V Arduino pin, the sensor OUT pin is connected to the Arduino RX pin. The system uses a grid separate and 4 TSL252 sensors to avoid incoming data collisions and cause data bits to be interference and can not be converted to ID data. Identify the incoming signal from which lamp based on the ID data received by the receiver system. Calculating the power of each received signal use log normal shadowing equation to estimate the distance receiver to transmitter. In this research, the process of measuring the distance between the transmitter and the receiver is based on the Received Signal Strength (RSS) method.

Several methods are conceptually capable to solve the problems. Examples of the most common methods are Time Different of Arrival (TDOA) and RSS. Based on TDOA the distance calculates by utilizing the required time to send data from transmitter to receiver so the time will be comparable with the traveled distance. Whereas the RSS used the current signal at the receiver where if the distance between transmitter and receiver is short that received signal will get more power. Because the speed of lights is very high, applying the TDOA method to design a prototype is difficult to calculate how much time it takes for transmitter to send data to receiver at each test point. Therefore an easier method to apply in this research is the RSS method which used the signal strength and

partition between sensors so each sensor only receives one signal from a spesific transmitter and avoids interference of signals from other transmitters.

Based on the RSS method when the received power is greater, the distance between transmitter and receiver is getting closer, and vice versa [14]. The log normal shadowing model is used to calculate the estimated distance by knowing in advance the power value at the reference point, the power at the test point and the pathloss exponent value. The power at the reference point is the power when the receiver is directly under a lamp or transmitter. The pathloss exponent value is a coefficient that indicates a reduction in transmit power when the transmitter sends data until the data is successfully received at the receiver. Next step, estimating receiver position using distance estimation data and triangulation method [15].

The triangulation method can be used to determine the position of an object only by referring to the distance of three existing points. The way to do this is to draw a straight line that connects two points whose distance can be measured directly. The distance between the two points is carefully measured. Then the angle formed by a line connecting one point to the object to be determined is the distance from the line connecting the two points is measured. Then the angle between the line connecting the second point with the object with the line connecting the two points is also measured. Based on the information of two angle values and the distance of three points, the object distance can be calculated.

The design of system will be divided into 3 parts, namely: transmitter device, receiver device, and then design of estimated distance and position. This is an illustration of the overall positioning system that will be created.

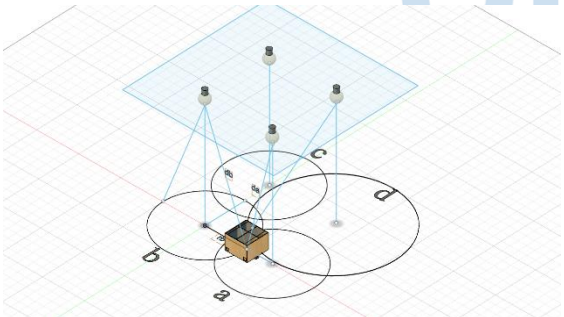

Fig. 2. Illustration Overall System Design

Explanation of Fig. 2 is prototype will be designed to use 4 LED lights as part of the transmitter device that will send ID data, then the illustration of the brown box is the object whose position will be estimated, in which a receiver sensor will be installed to receive data and based on the data and the intensity of the light it will be estimated the distance and position of the object to the transmitter, then the circle in the picture shows the range of data reception

A. Transmitter Device

The transmitter hardware design consists of a 20 Watt 12 VDC LED lamp, LED Driver IRF520, 12 VDC power supply, and an Arduino Uno microcontroller.

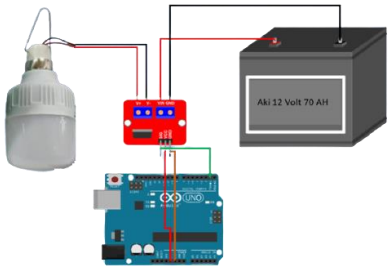

Fig. 3. Wiring Diagram of Transmitter

Next, the software design of the transmitter is shown in flowchart Fig. 3. It explains the sequence of commands when Arduino sends ID data via UART serial communication format and then proceeds to MOSFET IRF520 module to modulate the intensity of LED light.

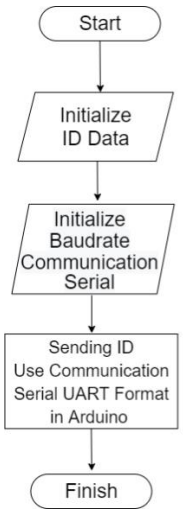

Fig. 4. Flowchart of Transmitter

The explanation in Fig. 4 is a process of sending data by the transmitter. First, the data will be initialized on the Arduino then the baudrate communication will be set for UART format serial communication. The data in the form of an alphabet will be converted into an ASCII code in the form of a binary code, then the process is continued to the LED driver for data adjust the blinking of the lamp to match the transmitted binary data.

B. Receiver Device

The receiver hardware design consists of 4 sets of TSL252 sensors and Arduino Nano, Arduino Mega, and LCD Display 16x2.

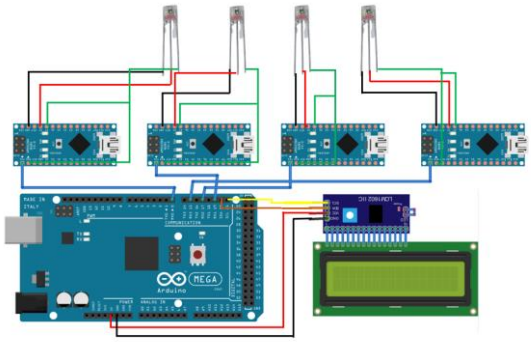

Fig. 5. Wiring Diagram of Receiver

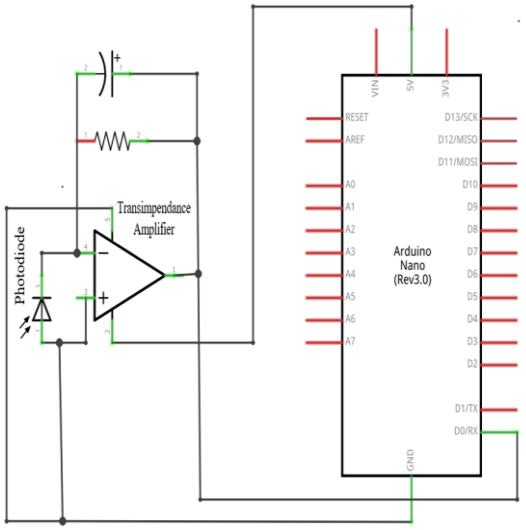

Fig. 6. Schematic of TSL252 Sensor

The TSL252 sensor consists of a photodiode and a transimpendance amplifier function to convert intensity light into voltage or electrical pulses in UART serial format to be translated into ID data. Next, Arduino will calculate the Received Strength for each signal.

The software design of receiver is shown in flowchart Fig. 6. Because the received signal must know 2 types of data, the first stage of the receiver flow diagram is initializing analog pins to read voltage data and the baudrate initialization used must be the same as the transmitter baudrate.

Furthermore, if there is already a data ID in the serial buffer, if there is, then proceed to the data reading process, otherwise the system will wait for the data to be available again. After the ID data is obtained, the process of converting the ADC value to the voltage value is continued. The last process on the VLC Receiver device is the packaging of ID and voltage data which will later be used as input data in the distance estimation process.

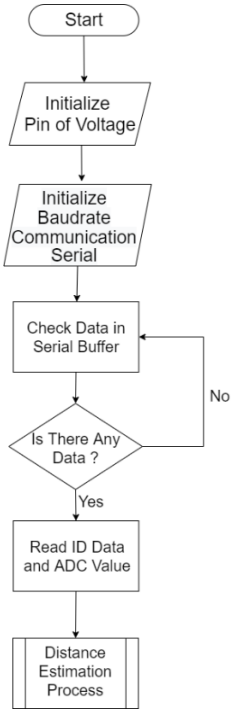

Fig. 7. Flowchart of Receiver

Explanation of Fig. 7 is a process that occurs in the receiver. first, initialize the output pin TSL252 sensor then initialize the baudrate used and must be the same as the baudrate on the transmitter, and then proceed with asynchronous serial communication, if there is data in the serial buffer then, the system detect ID data and ADC value then proceed to the process of estimating the distance from the receiver to the transmitter based on the data ID data and received signal strength.

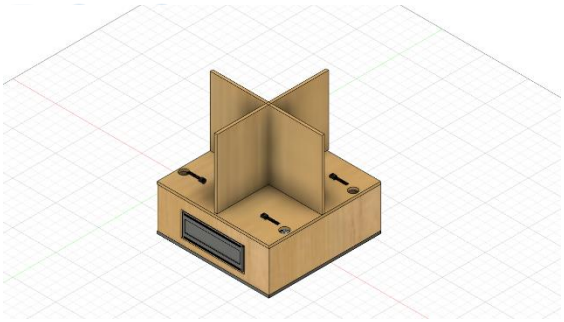

Fig. 8. Mounting and Separation Sensor Design

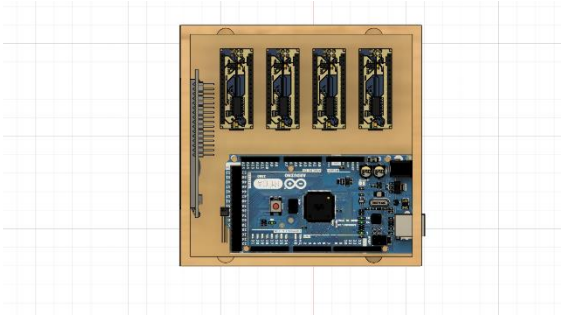

Fig. 9. Components Laying Design

The explanation for Fig. 8 and 9 are the illustration of the object to be estimated position where the TSL252 sensor has been placed to read the data, Arduino to process the data, and a 16x2 LCD to display the estimated position of the object coordinate. The Separator is used so that each sensor only focuses on receiving 1 ID data and avoids the influence of other ID data signals.

C. Design of Estimated Distance and Position Algorithm

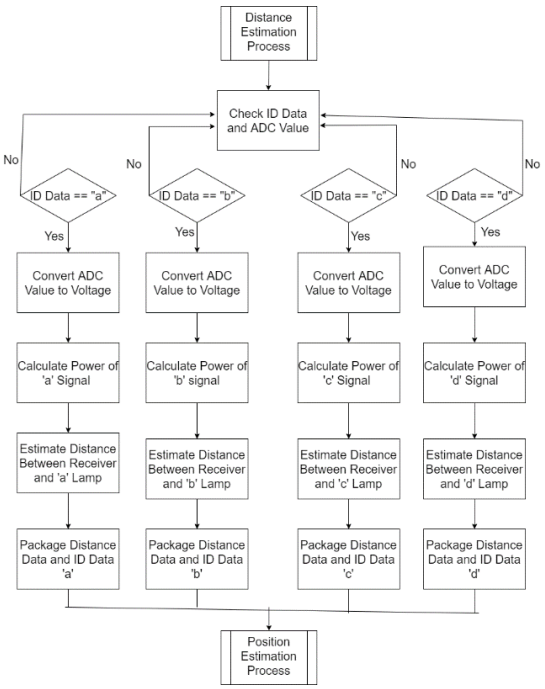

Fig. 10. Flowchart of Estimated Distance

When the ID data is received by the receiver, the system will simultaneously read the signal voltage and calculate the power. Furthermore, the receiving power of each signal will be calculated then the system will use the log normal shadowing equation to estimate the direct distance (d) of the receiver to the lamp that becomes transmitter.

$$Prx = P_0 - 10.n.\log(\frac{d}{d_0}) \quad (1)$$

After that, by using the Pythagoras theorem, the radius distance will be obtained.

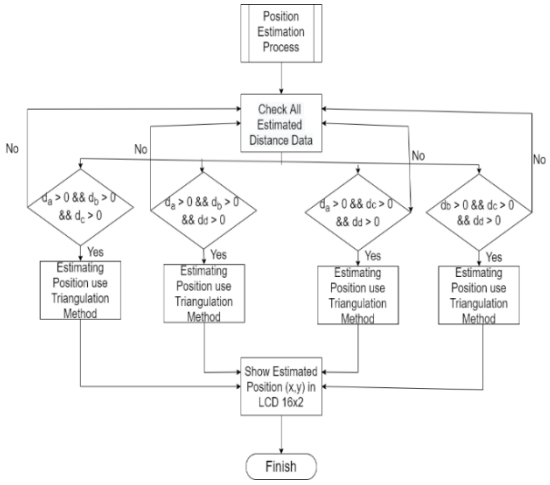

Fig. 11. Flowchart of Estimated Position

The first step in the positioning system flow chart is to check all data on the estimated distance from the receiver to the transmitter. Then check the data based on 4 conditions that have been determined. If one of the conditions is true then the position estimation can be done using the triangulation method.

This is an equation to find the coordinate of an object's position based on estimated distance data and the triangulation method. This equation requires a distance estimate of at least 3 data

$$\begin{bmatrix} x \\ y \end{bmatrix} = \begin{bmatrix} 2(x_2 - x_1) & 2(y_2 - y_1) \\ 2(x_3 - x_1) & 2(y_3 - y_1) \end{bmatrix}^{-1} \begin{bmatrix} r_1^2 - r_2^2 - (x_1^2 + y_1^2) - (x_2^2 + y_2^2) \\ r_1^2 - r_3^2 - (x_1^2 + y_1^2) - (x_3^2 + y_3^2) \end{bmatrix} \quad (2)$$

This is the prototype of the designed system:

Fig. 12. Prototype

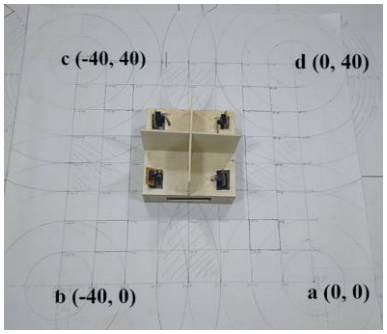

Fig. 13. Reference Coordinates

III. Result and Discussion

The testing in this research is divided into 3 parts: testing of send and receive data through Visible Light Communication (VLC), estimating the distance between receiver and transmitter based on Received Signal Strength (RSS), and estimating the position of object based on triangulation method.

A. Analysis of Sending Data

The analysis is done by observing the transmit signal that appears on the oscilloscope screen, started with connecting the oscilloscope signal cable to the Arduino TX pin as a transmitter and the oscilloscope ground cable to the Arduino ground pin.

a) Signal of ID "a"

The transmit signal is converted into binary data so that ID "a" becomes 0110001, then the oscilloscope will read the signal in the Least Significant Bit (LSB), which is reading data start from the binary data row which has the smallest value, the signal displayed is 0100001101. The number 0 at the beginning start bit and the last 1 indicates the stop bit

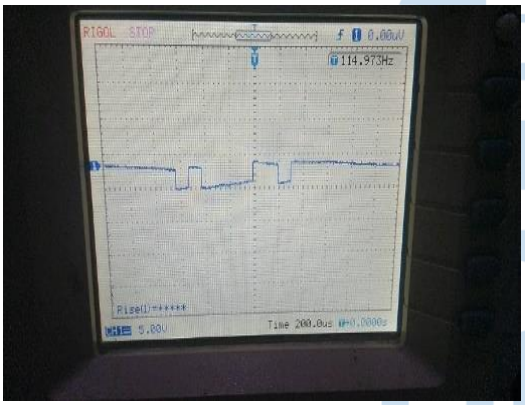

Fig. 14. Signal Form of ID a

b) Signal of ID "b"

The transmit signal is converted to binary data becomes 01100010, on the oscilloscope the signal that appears is 0010001101.

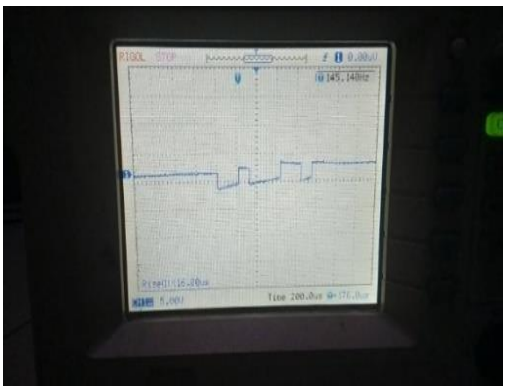

Fig. 15. Signal Form of ID b

c) Signal of ID "c"

The transmit signal is converted to binary data becomes 01100011, on the oscilloscope the signal that appears is 0110001101.

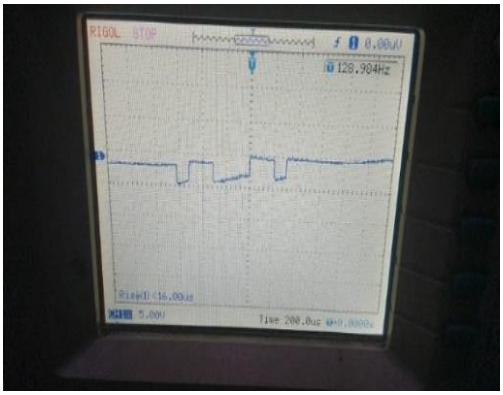

Fig. 16. Signal Form of ID c

d) Signal of ID "d"

The transmit signal is converted to binary data becomes 01100100, on the oscilloscope the signal that appears is 0001001101.

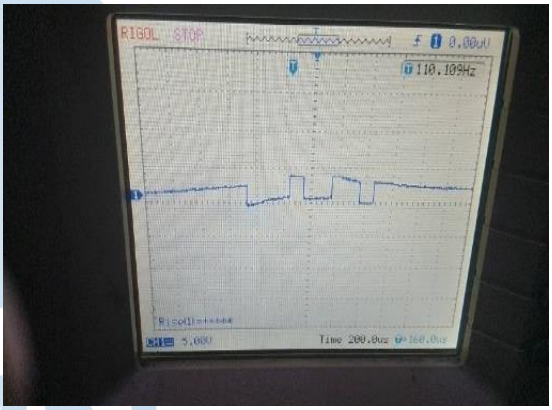

Fig. 17. Signal Form of ID d

B. Analysis of Light Intensity to Radius Distance

This analysis is to determine the value of the light intensity transmitter lamp when the TSL252 sensor can receive ID data at the farthest radius distance from the transmitter. The measurement process uses lux meter HS1010.

TABLE I. Light Intensity to Radius Distance

ID of Lamp	Distance Radius (cm)	Ligth Intensity (Lux)
a	0	362
	5	336
	10	326
	15	366
	20	329
	25	164
b	0	362
	5	347
	10	326
	15	290
	20	214
	25	132
c	0	387

	5	348
	10	340
	15	330
	20	282
	25	219
d	0	371
	5	318
	10	311
	15	290
	20	242
	25	172

Based on Table 1, the signal can be received with a maximum radius distance is 25 cm and the required light intensity in the range of 150 - 370 lux.

C. Analysis of Received Signal

This Analysis is carried out at several points representing positions in center and extreme positions. Center Positions were tested at (-10, 15); (-30, 15); (-30, 25); (-10, 25) while extreme positions were tested at (-10, 30) and (-10, 10). Extreme positions are coordinate position x, y which tend to be very close to one lamp or transmitter but far enough from the other lamp. The purpose of this test is to find out what ID data is received by the receiver device and then it was processed as input to estimate the distance between receiver and transmitter.

TABLE II. RECEIVED SIGNAL AT COORDINATE POSITION TEST

Coordinate Position	Received ID	Signal Strength (mW)	Description
(-10, 15)	a	2.897	Center Position
	d	2.78	
	b	2.781	
(-30,15)	b	2.775	Center Position
	c	2.861	
	a	2.777	
(-30, 25)	c	2.89	Center Position
	b	2.76	
	d	2.72	
(-10, 25)	d	2.98	Center Position
	a	2.8	
	c	2.82	
(-10, 30)	a	2.76	Extreme Position
	c	2.57	
	d	3.08	
(-10,10)	a	2.91	Extreme Position
	d	2.97	
	b	2.85	

Distance Estimation System is done by first calculating the pathloss exponent value of each lamp based on the received signal strength and the log normal shadowing equation. The suitability of the pathloss exponential value is tested by comparing the estimated radius distance based on the system with the real radius distance.

D. Analysis of Estimated Distance between Receiver and Transmitter

a) Calculating Pathloss Exponent Value

Distance Estimation System is carried out by calculating the pathloss exponent value of each lamp based on the received signal strength and the log normal shadowing equation. The suitability of the pathloss exponential value is tested by comparing the estimated radius distance based on the system with the real radius distance.

TABLE III. PATHLOSS EXPONENT VALUE

ID	Radius Distance (cm)	Prx (mW)	d (cm)	n	Average n
a	0	3.066	65	0	3.188
	5	2.9805	65.192	6.674	
	10	2.841	65.765	4.430	
	15	2.797	66.708	2.388	
	20	2.5845	68.007	2.451	
b	0	3.1665	65	0	3.607
	5	3.0535	65.192	8.820	
	10	2.9135	65.765	4.981	
	15	2.8825	66.708	2.521	
	20	2.8295	68.007	1.716	
c	0	3.049	65	0	3.322
	5	2.9245	65.192	9.718	
	10	2.8885	65.765	3.160	
	15	2.786	66.708	2.334	
	20	2.7745	68.007	1.397	
d	0	3.094	65	0	3.276
	5	2.983	65.192	8.664	
	10	2.882	65.765	4.173	
	15	2.8455	66.708	2.206	
	20	2.8315	68.007	1.336	

The pathloss exponential value contained in table III is based on calculations using the log normal shadowing equation.

$$Prx = P_0 - 10.n.\log(\frac{d}{d_0}) \qquad (3)$$

It requires some parameters, namely:

P_0 : Received Signal Strength at reference point when the radius distance is 0 cm (receiver is right below the lamp as transmitter).

P_{rx} : Received Signal Strength at position test.

n : pathloss exponential value.

d : direct distance between receiver, and transmitter.

d_0 : direct distance between receiver and transmitter when radius distance is 0 cm.

After being measured and calculated the results obtained are as follows:

$d_{0a} = d_{0b} = d_{0c} = d_{0d} = 65$ cm, $P_{0a} = 3.066$ mW, $P_{0b} = 3.1665$ mW, $P_{0c} = 3.049$ mW, $P_{0d} = 3.094$ mW. For the value of d and the value of n as represented in Table III. The following graph shows the radius distance will decrease signal strength

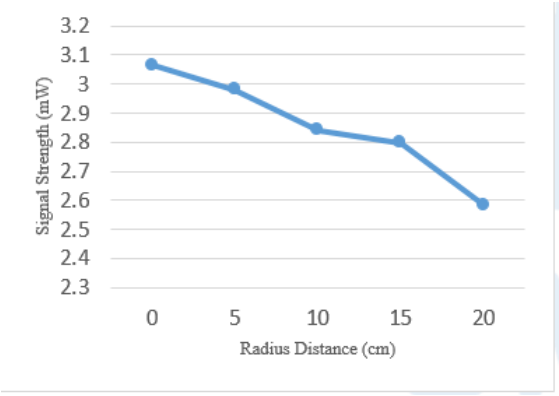

Fig. 18. Radius Distance to "a" Signal Strength Graph

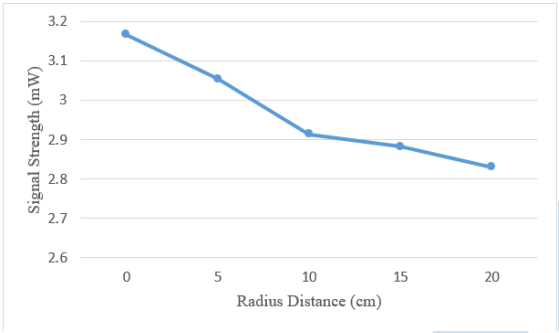

Fig. 19. Radius Distance to "b" Signal Strength Graph

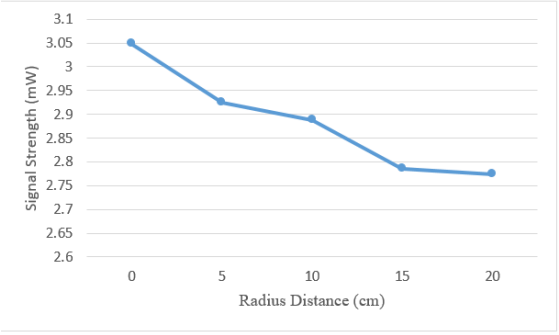

Fig. 20. Radius Distance to "c" Signal Strength Graph

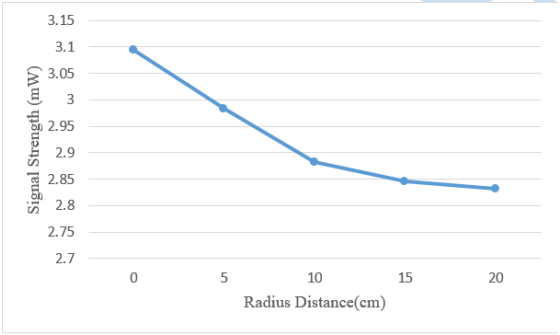

Fig. 21. Radius Distance to "d" Signal Strength Graph

b) Analysis of Estimated Distance Radius with Pathloss Exponent Value

Testing the pathloss exponent value is done by estimating the direct distance (d) using the log normal shadowing equation and then comparing it with the real direct distance (d). Furthermore, the distance d is used to calculate the value of radius distance (r), next it was compared with the actual radius distance r.

TABLE IV. ESTIMATED DIRECT DISTANCE

ID	Prx (mW)	d estimated (cm)	d real (cm)
a	3.066	65	65
	2.981	65.403	65.192
	2.841	66.065	65.765
	2.797	66.275	66.708
	2.585	67.3	68.007
b	3.167	65	65
	3.054	65.471	65.192
	2.914	66.058	65.765
	2.883	66.189	66.708
	2.83	66.413	68.007
c	3.049	65	65
	2.925	65.563	65.192
	2.889	65.727	65.765
	2.786	66.196	66.708
	2.775	66.249	68.007
d	3.094	65	65
	2.983	65.509	65.192
	2.882	65.976	65.765
	2.846	66.145	66.708
	2.832	66.21	68.007

TABLE V. ESTIMATED & ACCURACY RADIUS DISTANCE

r estimated (cm)	r real (cm)	Error (%)	Accuracy (%)	Average Accuracy (%)
0	0	0	100	76.47
7.246	5	44.91	55.088	
11.81	10	18.14	81.865	
12.94	15	13.75	86.252	
17.44	20	12.78	87.219	
0	0	0	100	
7.835	5	56.7	43.299	
11.78	10	17.76	82.237	
12.49	15	16.74	83.262	
13.63	20	31.86	68.141	
0	0	0	100	
8.576	5	71.53	28.473	
9.75	10	2.501	97.499	
12.53	15	16.5	83.502	
12.8	20	35.99	64.007	
0	0	0	100	
8.151	5	63.02	36.975	
11.31	10	13.05	86.948	
12.26	15	18.3	81.704	
12.6	20	36.99	63.011	

The explanation of Table V is showed radius distance data based on estimates and real conditions, after calculated the average accuracy reaches 76.47%

E. Analysis of Estimated Position Based on Triangulation Method

This test uses several coordinate positions that represent positions in center and extreme position such as at the ends of the lamp

a) Center Position area

TABLE VI. ESTIMATED IN CENTER POSITION AREA

Coordinate Test	Received ID	Prx (mW)	d estimated(cm)

(-10, 15)	a	2.897	65.798
	d	2.78	67.306
	b	2.781	66.619
(-30,15)	b	2.775	66.645
	c	2.861	65.853
	a	2.777	66.371
(-30, 25)	c	2.89	65.72
	b	2.76	66.709
	d	2.72	67.59
(-10, 25)	d	2.98	66.366
	a	2.8	66.261
	c	2.82	66.04

The explanation Table VI is showed the test results when the object is positioned in the center of area, then ID and received signal strength are noted on the receiver side next using equation 1 in the method section to obtain the value of d which is the distance between the transmitter and the receiver.

TABLE VII. COORDINATE ESTIMATED IN CENTER POSITION AREA

r estimated (cm)	Coordinate x	Coordinate y
10.218	-18.641	17.49145
17.467		
14.599		
14.715	-19.5446	21.31197
10.562		
13.42		
9.7037	-23.1161	21.63587
15.001		
18.532		
13.398	-20.5402	19.82483
12.864		
11.674		

The explanation of Table VII showed estimated radius distance data from each transmitter to the receiver. Then it is used to find the estimated coordinate position based on equation 2 on method section

b) Extreme Position area

TABLE VIII. d ESTIMATED IN EXTREME POSITION AREA

Coordinate Test	Received ID	Prx (mW)	d Estimated (cm)
(-10, 30)	a	2.76	66.452
	c	2.57	67.194
	d	3.08	65.902
(-10,10)	a	2.91	65.736
	d	2.97	66.413
	b	2.85	66.326

The explanation Table VIII is showed the test results when the object is positioned in an extreme area, then ID and received signal strength are noted on the receiver side next using equation 1 in the method section to obtain the value of d which is the distance between the transmitter and the receiver.

TABLE IX. COORDINATE ESTIMATED IN EXTREME POSITION AREA

r Estimated (cm)	Coordinate x	Coordinate y
13.817	-17.8491	20.91135
17.032		
10.863		
9.8121	-19.026	18.88234
13.627		
13.198		

The explanation of Table IX showed estimated radius distance data from each transmitter to the receiver. Then it is used to find the estimated coordinate position based on equation 2 in the method section.

c) Estimated Coordinate x Position Accuracy

Based on data in table VII and IX, it can be calculated the accuracy of coordinate x is shown in table X.

TABLE X. ACCURACY COORDINATE X

Coordinate Test	Estimated Coordinate x	Accuracy x (%)	Average Accuracy x (%)
(-10, 15)	-18.641	13.59	30.27
(-30,15)	-19.5446	65.14867	
(-30, 25)	-23.1161	77.05367	
(-10, 25)	-20.5402	-5.402	
(-10, 30)	-17.8491	21.509	

(-10,10)	-19.026	9.74	

d) Estimated Coordinate y Position Accuracy

TABLE XI. ACCURACY COORDINATE Y

Coordinate Test	Estimated Coordinate y	Accuracy y (%)	Average Accuracy y (%)
(-10, 15)	17.491446	83.39036	64.67
(-30,15)	21.311972	57.92019	
(-30, 25)	21.635873	86.54349	
(-10, 25)	19.824829	79.29932	
(-10, 30)	20.911346	69.70449	
(-10,10)	18.882339	11.17661	

The explanation of Table X and XI is showed a comparison of coordinate data (x, y) based on estimates and real conditions, next the percentage of accuracy is calculated.

Coordinate Test 1 (-10, 15)
Estimated Coordinate 1 (-18.641, 17.491)

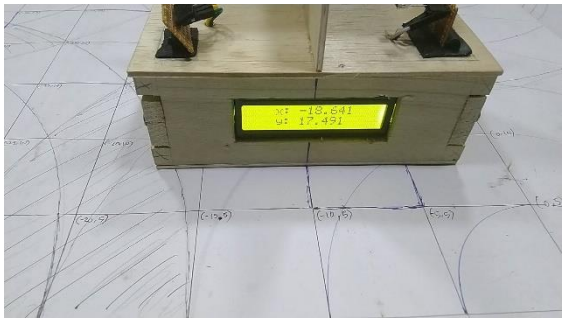

Fig. 22. Coordinate 1

Coordinate Test 2 (-30, 15)
Estimated Coordinate 2 (-19.545, 21.312)

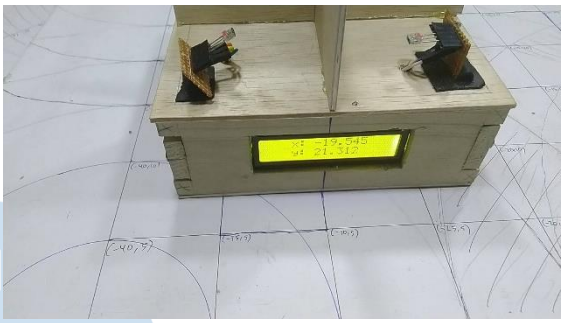

Fig. 23. Coordinate 2

Coordinate Test 3 (-30, 25)
Estimated Coordinate 3 (-23.116, 21.636)

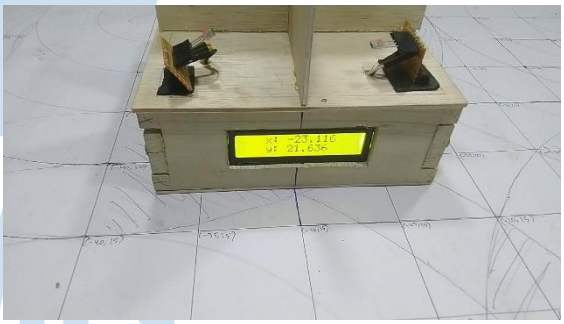

Fig. 24. Coordinate 3

Coordinate Test 4 (-10, 25)
Estimated Coordinate 4 (-20.540, 19.825)

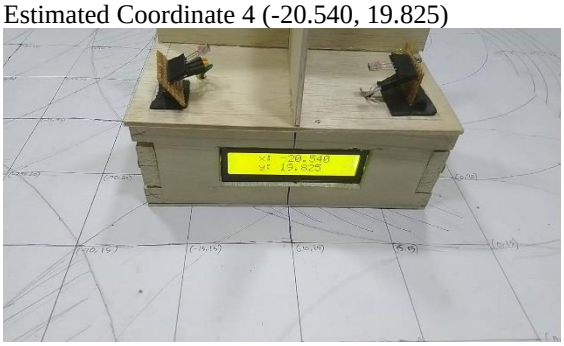

Fig. 25. Coordinate 4

Coordinate Test 5 (-10, 30)
Estimated Coordinate 5 (-17.849, 20.911)

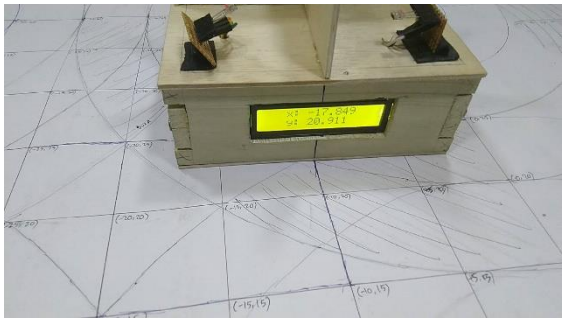

Fig. 26. Coordinate 5

Coordinate Test 6 (-10, 10)
Estimated Coordinate 6 (-19.026, 18.882)

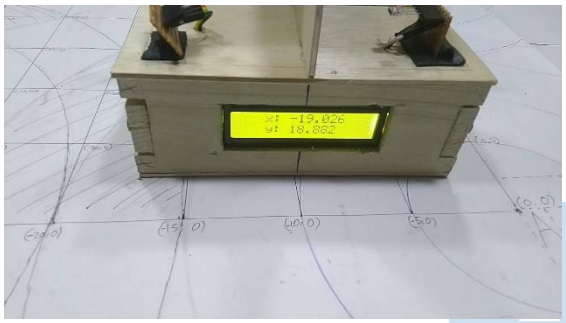

Fig. 27. Coordinate 6

F. *Analysis of Environment Condition*

In this research, the lamp used is limited to 20 watts, because based on testing the transmitter device with specifications of the lamp is good enough to send ID data signal but if the lights used are brighter or dimmer the next research it can be added to the design of the Automatic Gain Controlled (AGC) circuit which is a circuit able regulating the gain in a system and controlling it automatically. This prototype is expected to be able to detect the robot when it reaches the destination point but indeed with all limitations. The focus of this work is only on making the infrastructure of the system which includes sensors, microcontrollers, entering formulas into the programming code and the sequence of processes carried out from receiving data by sensors. To be processed using equations if in a real condition prototype must add some additional parts such as filter circuit and optical lens in the receiver device.

IV. CONCLUSIONS

A. *Research's Results*

The Transceiver device of Visible Light Communication (VLC) succeeded in sending and receiving data in the form of alphabets letters which consists of "a" until "d" with a maximum radius distance is 25 cm and a maximum angle for data transmission is 21.056º.

The design process of positioning estimation system can be solved through several stages are as follows: first step, the receiver of VLC can receive data from the three closest transmitters when tested in the center area and the extreme area. Second step, the distance estimation system between receiver and transmitter can be done with an average accuracy is 76.47%. Furthermore, based on ID and distance estimation data, a positioning estimation system can be carried out and the system get the best accuracy of x-coordinate estimation is 77.05% and the best accuracy of y-coordinate estimation is 86.54%.

Then if it is calculated, the average accuracy of x-coordinate is 30.27% and y-coordinate is 64.67%. The average accuracy is not so good because the data received at a certain test point does not obtain data with maximum accuracy because there are still deficiencies in the positioning of the sensor.

B. *Future Work*

1) Designing device interfaces can display estimated position data.
2) Two-way communication can be implemented by combining with infrared (IR) communication.
3) Design of filter circuits and optical lenses on the receiver so that noise can be minimized and the signal becomes more focused to receive

REFERENCES

[1] I. P. D. Wibawa, A. Rafif, A. Rusdinar, "Design of Tracking System Based on Sensor Fusion (Encoder and Accelerometer) for AGV Position Monitoring,", e-Proceeding of Engineering, vol. 6, no. 2, pp. 1–8, 2019, ISSN : 2355-9365

[2] M. A. Khairul, I. P. Pangaribuan, R. Nugraha, "Food Delivery System Using Augmented Guided Vehicle (AGV) Line Follower Completed Barcode", e-Proceeding of Engineering, vol. 7, no. 2, pp. 3091–3105, 2020, ISSN : 2355-9365

[3] W. Jatmiko1, M. S. Alvissalim2, A. Febrian3, and dan D. R.Y.S4, "Autonomous Robot Localization Method Using The Adoption of Heuristic Searching and Pruning Algorithm for Map Development in Search-And-Safe Case", Jurnal Ilmu Komputer dan Informasi, vol. 2, pp. 114–123, ISSN 1979 – 0732

[4] F. T. Ashegaf, B. A. D. Naipospos, B. B. Bimantoro, "Electric Wheelchair with User Health Monitoring System, Location and Accident Detection Based on IoT", ejournal3.undip.ac.id, vol. 8, no. 2. pp. 119–127, 2019, e-ISSN:2685-0206

[5] H. Liu, and J. L. Houshang Darabi, Pat Banerjee, "Survey of Wireless Indoor Positioning Techniques and Systems", IEEE TRANSACTIONS ON SYSTEMS, MAN, AND CYBERNETICS, vol. 37, no. 6, 2007.

[6] D. P. Yudha, B. I. Hasbi, and R. H. Sukarna, "Indoor Positioning System Based on Fingerprinting Received Signal Strength (RSS) WIFI With K-Nearest Neighbor (K-NN) Algorithm", ILKOM Jurnal Ilmiah, vol. 10, no. 3, pp. 274–283, 2018, e-ISSN 2548-7779 p-ISSN 2087-1716

[7] S. Afifah, R. A. Priramadhi, D. Darlis, "Transceiver On Lighting for Warehouse Navigation System Based On Visible Light Communication", Annual Applied Science and Engineering Conference, 2018

[8] A. P. Ardi, I. S. Aulia, R. A. Priramadhi, and D. Darlis, "VLC-Based Car-to-Car Communication," Jurnal Elektronika dan Telekomunikasi, vol. 20, no. 1, pp. 16-22, Aug. 2020. doi: 10.14203/jet.v20.16-22

[9] C. Xuefen, D. Jing, L. Shuangxing, S. Wenxiao, W. Chunyue, W. Lang, "The Research of Indoor Positioning Based on Visible Light Communication", China Communications, vol. 12, no. 8, pp. 85–92, 2015

[10] M. M. Rahmwati, N. M. Adriansyah, B. Pamukti, "Impact of The Number of Light Emitting Diode (LED) Towards The Accuracy in Indoor Positioning System Based on Visible Light Communication (VLC)", e-Proceeding of Engineering, vol. 7, no. 2, pp. 3758–3765, 2020, ISSN : 2355-9365

[11] R. Irawan, Ilhamsyah, Y. Brianorman, "Application of Short Message Encrytion and Decription Using Android-Based Knapsack Algorithm", Jurnal Coding Sistem Komputer Untan, vol. 3, no. 3, pp. 57–66, 2015, ISSN 2338-493X

[12] Z. Ghassemlooy, S. Arnon, M. Uysal, Z. Xu, and J. Cheng, "Emerging optical wireless communications- advances and challenges," IEEE journal on selected areas in communications, vol. 33, no. 9, pp. 1738– 1749, 2015.

[13] T. Instrument, "LMx58-N Low-Power, Dual-Operational Amplifiers," Texas Instrument, 2014.

[14] S. M. Sheikh, H. M. Asif, K. Raahemifar, and F. Al-Turjman, "Time Difference of Arrival Based Indoor Positioning System Using Visible Light Communication," IEEE Access, vol. 9, pp. 52113–52124, 2021.

[15] W. Dharmawan and A. Kurnianto, "Increasing Accuracy of RSSI Distance Estimation with Normal Log Normal Using Kalman Filter Method on Bluetooth Low Energy", Seminar Nasional Sains dan Teknologi 2016 Fakultas Teknik Universitas Muhammadiyah Jakarta, no. 22, pp. 1–5, 2016, e-ISSN : 2460 – 8416 p- ISSN : 2407 – 1846

ISSN 2355-3286

Specification Design and Performances Using Computational Fluid Dynamics for Mini-Remotely Operated Underwater Vehicle

Muhammad Sawal Baital[1], Fakhruddin Mangkusasmito[2], Mitha Asyita Rahmawaty[2]
[1,2,3] Vocational School, University of Diponegoro, Semarang, Indonesia
[1]sawalbaital@lecturer.undip.ac.id, [2]fakhm17@gmail.com, [3]mithaasyitar@lecturer.undip.ac.id

Accepted on 26 April 2022
Approved on 16 June 2022

***Abstract*— Remotely Operated Underwater Vehicle (ROV) is a submersible robotic system, used to examine various underwater characteristics and controlled by operators from shore. The applications of ROV are widely diverse, especially for exploration and marine industry. This research is to investigate pressure and drag on underwater vehicles using the CFD approach. A low-cost mini ROV with a 300 mm length was used for the research and to determine the hardware and material type required for prototype production by observing pressure and drag from the CFD simulation result. Simulation is solved using CFD software with RANSE method and Shear Stress Transport based k- ω was used as turbulence setting. The result indicated that to pull the mini ROV from the surface to a depth of 50 m requires a thrust of 3,9 kg and the mini ROV receiving the pressure of 7,7 bar.**

***Index Terms*— CFD; Drag; Pressure; ROV**

I. INTRODUCTION

Remotely Operated Underwater Vehicle (ROV) is a submersible robotic systems, used to examine various underwater characteristics and controlled by operators from shore[1].With complex, dangerous and limited areas urgently explored, there is an urgent need for an underwater machine that can replace humans to complete underwater detection. ROV were developed to perform resource exploration tasks in the ocean[2]. The applications of ROV are widely diverse, such as the oil and gas industry, discovery, aquaculture, marine biology, and military purpose [3][4][5][6].

Numerous of ROV designs are assembled around or inside cubic structured frame along with a buoyant on top body. The robotic vehicle utilized umbilical data cable as electrical cable and controlled by operator positioned on surface vessel.

The heavier tools are settled down on lowest possible position to keep the point of center buoyancy is higher than center of gravity, thus adequate stability is obtained. Sufficient stability of ROV meant ROV has capability to withstand against in disturbance for instance moment of rolling and pitch in longitudinal and lateral axis. Steady hydraulic rods suited of lifting and carrying particular equipment for specific purpose and placed in the fore along with cameras and lights.

Underwater ROVs are generally divided categories based on size, weight, capacity, or performance. Two common design of ROV which widely use are: the ROV Micro-Class with weigh not higher than 3 kg, are used especially in narrow area where a diver might not be capable to enter. And the ROV Mini-Class that weigh about 15 kg are also used as a diver alternative, Inspection-Class are typically rugged ROVs for commercial or industrial use, data acquisition and observation ROVs, Light weight duty category has generally no more than 50 hp on propulsion, While Heavy duty type has less than 220 hp with the ability to capability lift at least two handlers and work at depths up to 3500 m, and Trenching & Burial work class is the largest with more than 200 hp propulsion, with the ability to take a cable, put down sleds and working at depths until 6000 m in several cases[7][8][9][10]. The ROV design and construction is a robust solution to encounter the various require of an ROV to be used in wide implementations, it is compact, handy to use and inexpensive, and allow for confined space exploration. The main form of the body is designed to encounter the particular utilization needs. Commonly, almost ROV attached by torpedo form and an hydrodynamic main body was used at high-speeds[11]. Another type is the torpedo-less form, worked mainly in remote control vehicles (ROVs) that are often worked for shorter period of time purpose or the assessment of other large subsea areas like huge ice floe or water-dams[12]. Toward to emphasize the performance in water resistance, Computational Fluid Dynamics (CFD), drives valuable part in Unmanned vehicle design. Nowadays, CFD approach has been widely applied in underwater vehicle design, as it can simulate the fluid flow field around the bodies and to find out with comprehend the physics of fluid flow phenomenon. CFD captured the flow field such as vortex in very small to major scales which is hard to obtain through field experiments.

CFD methods enable to predict and diagnostic technique for identifying the cause of particular problem in physic phenomena. The latest CFD approaches provide wealth data generated emphasize to

visualize the implication of the result requires considerable skill. Due to this CFD become as an integral part of the design process.

From the economic cost, numerical simulation can deliver result within sufficiently short time span in the design process, thus optimization design can be detailed in addition to addressing this issue during the design process. Numeric simulation is considered low cost analysis hence became early stage to understanding along side with experimental test which can be over cost and intensive time.

In this project, the CFD analysis assists in investigate and demonstrate variable model for the hull body form based on initial prototype [13]. In this research, a design of Mini-ROV is developed especially the principal of body device in each element and electric parts is embedded. Furthermore, the hydrodynamic parameter and analysis was provided based on CFD simulation.

II. METHOD

A. Numerical Modelling

Hydrodynamics reference input was set for the mini-ROV. Therefore simulation of the flow around model is accomplished. The moment coefficient of symmetry flow in both xy plane and xz plane tend to be zero. Physical properties of this simulation conducted at $Re = 8.5 \times 10^5$, $\rho = 1025$ kg/m^3, $\nu = 1 \times 10^{-6}$m^2/s and $U = 1$ m/s or $Fr = 0.6$.

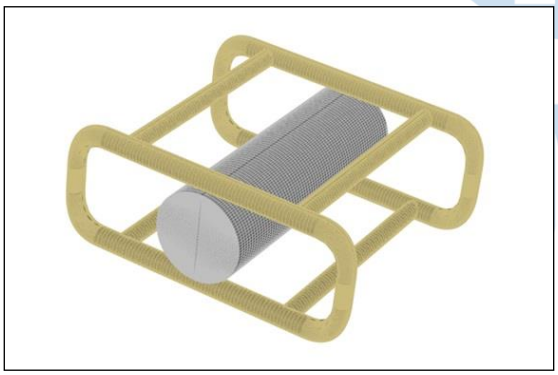

Fig. 1. ROV 3D Model

CFD simulation is used to analyze the total force and pressure difference between horizontal dive, vertical dive, and diagonal dive. The CFD simulation were run on 1:1 scale, 3-Dimension ROV model as shown in Figure 1 and main dimensions of mini-ROV model shown in Table 1.

TABLE I. MAIN DIMENSION

Main Dimension of ROV		
Parts	***Unit***	***Value***
Length over all	cm	30
Breadth over all	cm	34
Height over all	cm	14
Main Hull Diameter	cm	10
Support Frame Diameter	cm	2.25
Displacement	kg	3.1

B. Governing Equation RANS

CFD simulation using Reynolds averaged Navier Stokes (RANS) equations implemented in this project, attained by governed general laws for mass, momentum and energy. This method the flow considered as incompressible. The equation of RANS for incompressible flow shown in the following:

$$\frac{\partial \overline{u_i}}{\partial x_i} = 0$$

$$\frac{\partial \overline{u_i}}{\partial t} + \frac{\partial}{\partial x_j}\left(\overline{u_i u_j} + \overline{u_i' u_j'}\right) = -\frac{1}{\rho}\frac{\overline{\partial p}}{\partial x_i} + \frac{\partial \overline{\tau_{ij}}}{\partial xj} \qquad (1)$$

The derivation of RANS equation from instantaneous of Navier-Stokes equation is the Reynolds decompositions, which refers to separation flow (like velocity u) into mean (time averaged) and fluctuating components (like u') equal to zero.

The subscripts i and j defined the $i^{'}$ and $j^{'}$ components of the cartesian coordinate respectively, $\bar{u}$ and $\bar{p}$ defined the time averaged velocity and pressure respectively, t is the time and ρ is the density of the fluid then $\overline{\tau_{ij}}$ is represent the mean viscous stress tensor.

For the turbulent model adopted k-ω based Shear Stress Transport (SST). Standard k-ω turbulence model is basically combination of k-ω model [14].

The two equation model along with conservation law solved two-transport partial differential equations which acquired turbulence energy diffusion and convection energy. The variables of transport was turbulent kinetic energy (k) indicated turbulent energy and the other was specific turbulent dissipation rate (ω) also known as turbulence scale.

Later k-ω modified with Shear Stress Transport (SST) in order to avoid the k−ω problem of being sensitive to the inlet free-stream turbulence properties [15]. The modified model has capability carried out the transport of the shear stress and satisfied adverse pressure gradient boundary layers and separating flows.

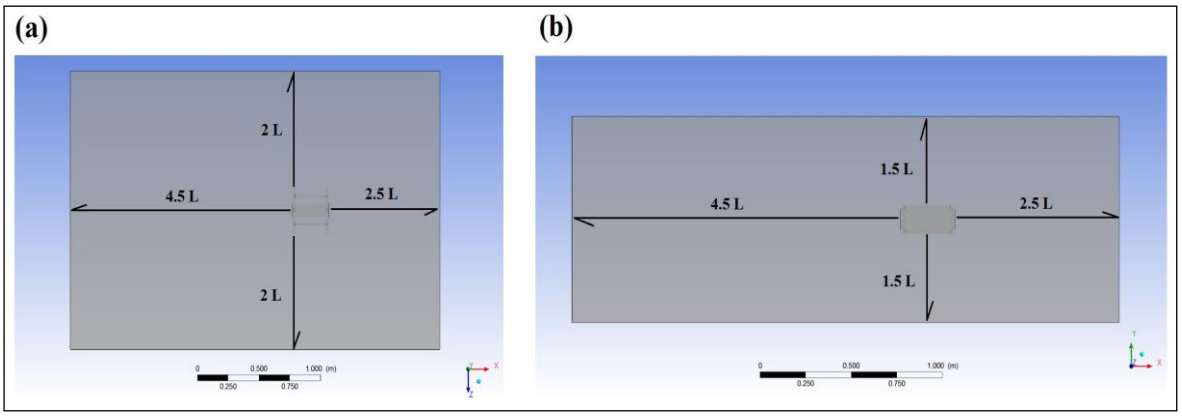

Fig. 2. Computational Domain (a) on XZ plane; (b) on XY plane

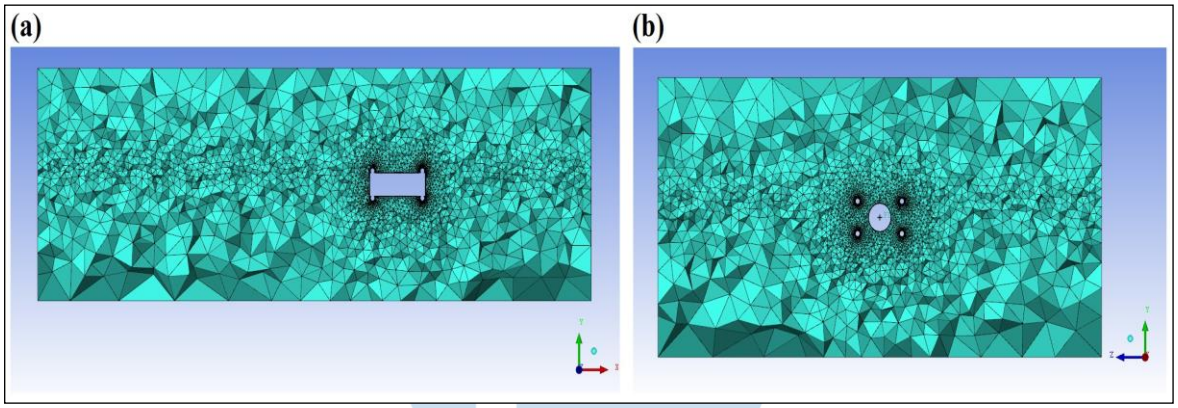

Fig. 3. Unregulated tetrahedral mesh (a) on XY plane; (b) on YZ plane

C. Computational Domain

When conducting CFD numerical simulation, computational domain has significant impact for defining circumstance around the body which engaged with physical condition in fluid dynamics constraint. The space in boundary condition should broad enough to avoid non realistic physic phenomena which lead disrupted the result. The domain spaces where the simulation of numerical solution will be calculated, adequate space let fluid flow surround geometry model did not interfere with boundary domain themselves. The boundary need be discrete in numerous mesh element with structured or unstructured mesh form thus simulation will solved with fluid dynamics equation. The domain came with several shape, in this simulation hexahedron domain was applied. The computational domain for simulation of the ROV model which expressed 2.5L forward the fore of main hull, 4.5L backward the aft of main hull, 2L aside of main hull, 1.5L above upward of the support frame, and 1.5L downward under of the support frame as shown in Figure 2.

D. Boundary and Initial Condition

When attempted CFD analysis, the input of set constraint to the boundary value must be defined and connect the simulation model with its surroundings. Inlet is defined as flow velocity or known as *velocity inlet*. The turbulent length and turbulent intensity were given for fully developed flow. Outlet identified as *pressure outlet* where the gauge pressure is none or equal to zero. The flow was considered a fully develops, there is no switch turn out in the flow direction and the outlet is designed long distant from the geometrical model disturbances. Wall defined as cube around model. The no-slip condition was determined at whole surface of hexahedron, hence the velocity on surface is zero and there is no stream flow passes through the surface of cube. The final boundary is defined as symmetry was placed at the bottom, top and both sides of the computational domain. The conditions at symmetric boundary are no flow across boundary. The normal velocity and normal gradient of all variable are zero it acted as a mirror that reflects all the flow distribution to the other side. Again any variables have same value and gradients at the same distance from the boundary.

TABLE II. NUMERICAL PROPERTIES

Mesh Properties	
Parameter	***Domain Setting***
Mesh type	Unregulated tetrahedral mesh
Number of Element	Approximately 1 million

Mesh Properties	
Parameter	***Domain Setting***
Domain Physics	Continuous fluid (water), SST turbulence model, non buoyant model, reference pressure 1 atm
Boundary Physics	
Parameter	***Domain Setting***
Inlet	Frictional intensity 0.05, Fluid flow speed Fr 0.3
Outlet	Static pressure 0 Pa
ROV model	No slip condition
Solver Setting	
Parameter	***Domain Setting***
Turbulance option	First order
Time scale	Physical time scale function 2 sec
Convergence parameter	RMS with residual target 0.00001
Processing parameter	
Parameter	***Domain Setting***
Run type	Parallel (2 partitions on 4 cores with 16 GB ram)

E. Meshing

CFD is a way of analyzing fluid flows numerically on a computer by a set of algebraic equations. The algebraic equations are obtained by discrete the partial differential equations (PDEs), which may be conservation of mass, momentum, energy etc. The solution is attained at discrete points and hence the computational domains need to be discrete into discrete areas or volume which is the mesh. For this reason, the mesh resolution is of great importance.

The mesh is discrete domain in which the flow problem is to be solved. The flow properties are calculated in every mesh and the density of the cells for instance the mesh resolution is of great importance. Basically, the grid could be either structured or unstructured. In an unstructured mesh such as unregulated tetrahedral, the cells are arranged in an apparently random fashion in contrast to a structured mesh. Mesh generator was carried out to generated mesh for RANS solution.

Unregulated tetrahedral mesh first was generated using Mesh Modeler around the mini-ROV model as shown in Figure 3. Smaller element size of unregulated tetrahedral was used for the ROV model and for the region around the ROV model with refinement is designate to capture the fluid flow properties and to achieve a finer result. The mesh outside the model, defined as fluid then larger mesh built gradually to reduced time computational aspect.

The mesh number is affected the solution, therefore a convergence process was used in order to achieve mesh independent solutions. If mesh independent is obtained, further refinement of the element does not affect the solution.

F. Numerical Solver Setup

The fluid flow analysis is expressed using CFD based RANS method. Turbulence setting using Shear Stress Transport based k-ω with turbulence option first order is used to calculate the simulation. Steady state was used for simulation with total elements about 1 million to satisfy mesh independent criteria. This simulation was converged with Residual RMS level $1x10^{-5}$ was used to investigate. The residual is fundamental measures of an iterative solution convergence, as it directly quantifies the error in the solution of the system of equations. The properties of numerical simulation for fluid flow analysis of ROV model as shown in Table 2.

III. Result and Discussion

A. Mesh Indepedence

The research was performed using the ROV model with horizontal dive simulation to obtain grid independence solution. Mesh independence used for validating simulation result. The sum of element analyze was used to determine the effect of element number on the calculated total force. To build the mesh, the sum of mesh from domain was sequentially reformed, whilst keeping grow rate parameters and the total element ROV models the same. The results of ROV model at different sum of element for Fr 0.6 from simulations are shown in Table 3. In this case, 6 difference meshes was used to validate mesh independence.

TABLE III. Force Result at Different Total Number of Element

Mesh Independent			
Mesh Number	***Number of Element***	***Total Force***	***Simulation Running Time***
1	cm	30	30 min.
2	cm	34	50 min.
3	cm	14	90 min.
4	cm	10	100 min.
5	cm	2.25	120 min.
6	kg	3.1	200 min.

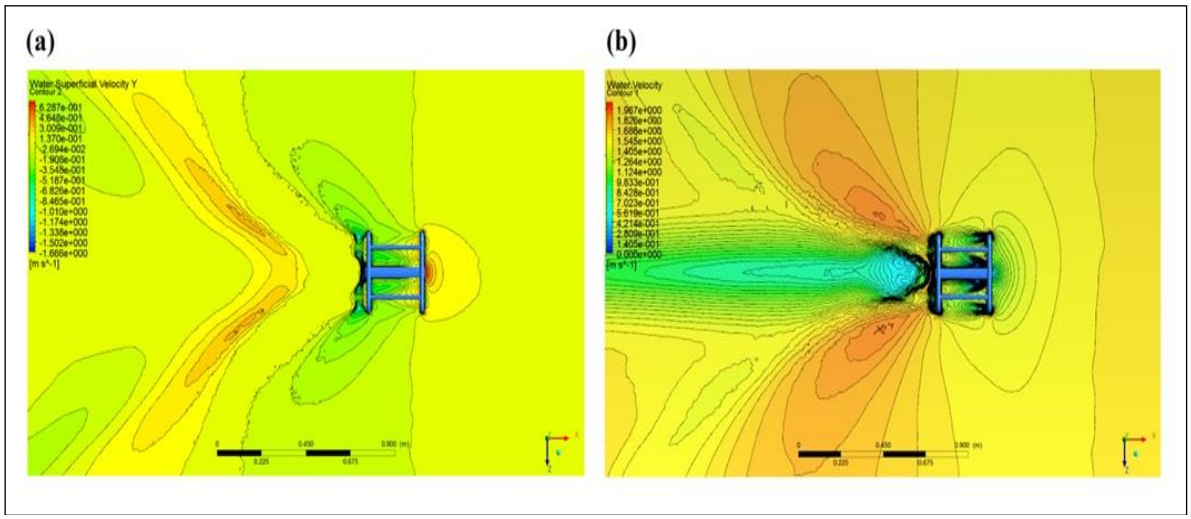

Fig. 4. Flow analysis (a) water superficial velocity contour; (b) velocity contour

The solution converged successfully, with variation of total force as shown in Table 3. In addition, the difference in the total force between Mesh 5 and Mesh 6 are not greater than 2 % [15]. Therefore, the sum of elements on Mesh 5 was chosen and used in all cases of the simulation.

B. The Result of CFD Simulation

Numerical analysis of the ROV model was performed. Computational data was acquired using RANSE code and Turbulence model was selected. The model was run at three particular moves for instance horizontal, diagonal and vertical dive. All cases were run at Fr 0.6 which equals to 2 knots. The model tested in fully submerged simulation which equal 0 to 10 m of depth. The CFD simulation generated physic contour visualization around body mini-ROV model. The movement created phenomena that plot flow pattern in various contour lines. It has color bands that discrete colored regions while the display of a variable on a locator (such as a boundary) shows a finer range of color detail gradually. The contour of water superficial velocity and water velocity are presented in Figure 4(a) and 4(b). The simulation result apparently with diffusion flow of the ROV model respectively. It is mean that the mesh and physical setting was suitable.

Contour of water superficial velocity displayed fluid flow from near to far field that surrounded body mini-ROV model. The contour line appeared caused by fluid mass flow rate through the model. The colors gradation shows difference velocity when fluid flow across the body. The stream assumed the only flow mass rate through passed the model and whereby estimated rapidly the fluid flowing through the medium. In figure 4(a) water superficial velocity has various speed ranges. Superficial velocity performed volumetric flow rate per sectional area. Both in portside and starboard mini-ROV model has interchangeable flow pattern which has similar velocity and considered low. On contrary in front of body has high velocity at middle spot region. It caused by stagnation point on fore body mini-ROV. On rear body has larger flow pattern with few variant fluid flow velocity.

Figure 4(b) illustrate water velocity contour, this velocity contour displayed actual fluid flow velocity. It meant the velocity of fluid flow travelled significant distance per time. Even though has same unit with superficial velocity (m/s), water velocity has detailed in small region. The figure shown on rear body mini-ROV has significant contour, fluid velocity fell dropped compared to other areas. Rear body has transom formed, where body has not streamlined which lead the fluid particle did not fully transmitted far away behind body hence suddenly suffered small turbulence[16].

In CFD simulation, the value of total drag and total pressure caused by ROV movement was obtained directly, the result shown in table 4, 5 and 6. It shows the value at each step Froude number, with unit Newton in total drag and Pascal in total pressure respectively. This value became major lead reference in determining motor thrust. Since the mini-ROV mostly operated in horizontal dive, hence the value at service speed (Fr 0.6) was discussed. Total drag and total pressure 11.863 N and 94.704 Pa. It is meant that motor installed at ROV must be has a thrust of 4 kg, to run ROV at operational speed.

TABLE IV. TOTAL DRAG AND PRESSURE OF ROV MODEL (HORIZONTAL DIVE)

Total Drag Horizontal Dive						
Fr	***Speed in Knot***	***Total drag***		***Total pressure***		
0.30	1.00	2.963 N	0.302 kgf	23.345 Pa	6.663 kg/m2	0.667 kg
0.45	1.50	6.891 N	0.702 kgf	63.364 Pa	10.744 kg/m2	1.809 kg

Total Drag Horizontal Dive						
Fr	***Speed in Knot***	***Total drag***		***Total pressure***		
0.52	1.75	9.971 N	1.016 kgf	81.125 Pa	12.556 kg/m2	2.316 kg
0.60	2.00	11.863 N	1.209 kgf	94.704 Pa	13.940 kg/m2	2.704 kg
0.75	2.50	13.252 N	1.351 kgf	153.424 Pa	19.927 kg/m2	4.381 kg
0.82	2.75	14.034 N	1.431 kgf	168.258 Pa	21.440 kg/m2	4.804 kg

TABLE V. TOTAL DRAG AND PRESSURE OF ROV MODEL (DIAGONAL DIVE)

Total Drag Diagonal Dive						
Fr	***Speed in Knot***	***Total drag***		***Total pressure***		
0.30	1.00	5.024 N	0.512 kgf	40.856 Pa	8.449 kg/m2	1.166 kg
0.45	1.50	10.036 N	1.023 kgf	79.765 Pa	12.416 kg/m2	2.277 kg
0.52	1.75	14.014 N	1.429 kgf	106.585 Pa	15.151 kg/m2	3.043 kg
0.60	2.00	17.536 N	1.788 kgf	124.748 Pa	17.003 kg/m2	3.562 kg
0.75	2.50	20.022 N	2.041 kgf	168.224 Pa	21.437 kg/m2	4.803 kg
0.82	2.75	22.032 N	2.246 kgf	185.752 Pa	23.224 kg/m2	5.304 kg

TABLE VI. TOTAL DRAG AND PRESSURE OF ROV MODEL (VERTICAL DIVE)

Total Drag Vertical Dive						
Fr	***Speed in Knot***	***Total drag***		***Total pressure***		
0.30	1.00	5.962 N	0.608 kgf	14.945 Pa	5.807 kg/m2	0.427 kg
0.45	1.50	11.264 N	1.148 kgf	40.065 Pa	8.368 kg/m2	1.144 kg
0.52	1.75	15.037 N	1.533 kgf	56.675 Pa	10.062 kg/m2	1.618 kg
0.60	2.00	18.785 N	1.915 kgf	71.377 Pa	11.561 kg/m2	2.038 kg
0.75	2.50	21.412 N	2.183 kgf	106.554 Pa	15.148 kg/m2	3.042 kg
0.82	2.75	22.658 N	2.310 kgf	117.145 Pa	16.228 kg/m2	3.345 kg

Figure 5(a) shows of value total drag in Newton unit toward rate of Froude number (Fr). From this graph total drag of three movement dive was increased at every step Froude number. The vertical and diagonal dive has similar coincide trend which sharply increased from Fr 0.3 to Fr 0.6 and then slowly growth until Fr 0.8. Contrast with horizontal dive which considered slightly increased and then steadily increase.

From the trends show the vertical dive has highest value and the horizontal dive has lowest value of total drag at the service speed or Fr 0.6. The total drag of horizontal is less than 12 N and vertical dive has almost 19 N. Both of dives motion has significant difference up to 32%. Diagonal dive has slightly lower than vertical dive. This different caused by ROV motion against fluid flow that commonly called angle of attack.

In other hand Figure 5(b) shown graph of the total pressure value in Pascal (Pa) unit toward rate of Froude number (Fr). The trends of three movement model has similar pattern. Each of motion has significant rose at each step Froude number. This graph displays diagonal dive has highest quantity and the vertical dive has lowest quantity at service speed model.

Total pressure of diagonal dive has around 15 Pa and vertical dive has about 70 Pa, which means vertical dive took only a half. In addition value of total pressure horizontal dive slightly higher than the vertical dive with approximately 95 Pa. The huge gap of diagonal and vertical dive happened caused by ROV body form travelled against fluid flow.

The detail visualization about affected of total pressure around body ROV has shown in Figure 6(a), 6(b), and 6(c). This CFD simulation captured physic phenomena around body due to fluid flow respectively. When mini ROV travelled through fluid flow, the pressure force acting on each element of body surface summed over entire body to produce total pressure. The pressure arose from viscous of fluid flow.

The figure 6(a) illustrated total pressure of body mini-ROV which simulation capture the pressure mostly affected at side of body. The figure 6(b) demonstrated total pressure of body mini-ROV when moved diagonally. It shown that diagonal dive has affected pressure on almost surface area and has biggest total pressure value among the movement. When body moved diagonally both side and bottom affected pressure that push perpendicular integrally. The last figure 6(c) described vertical dive. Same as horizontal dive, it has one side affected major pressure area, which is bottom region of mini ROV. This pressure acted normally to the body.

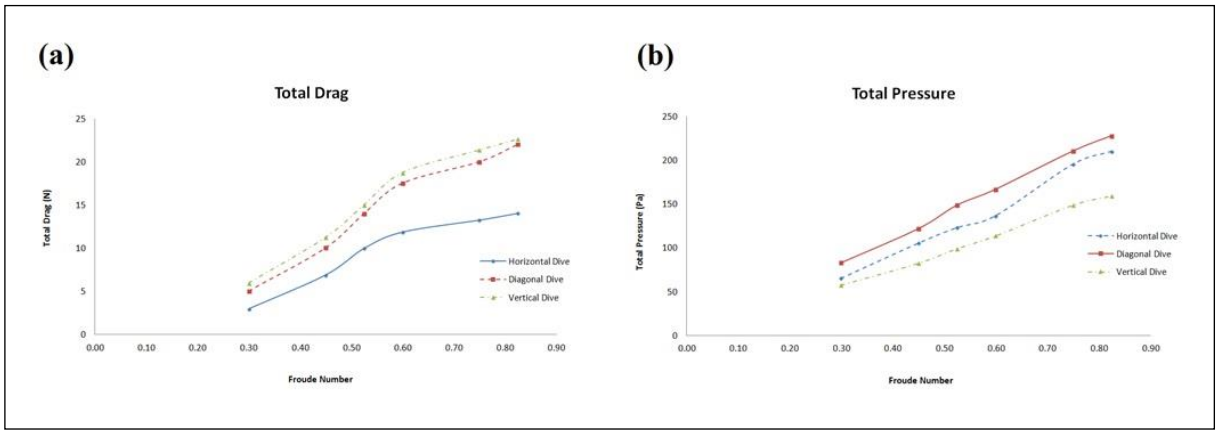

Fig. 5. Simulation Result (a) Total Drag; (b) Total Pressure l

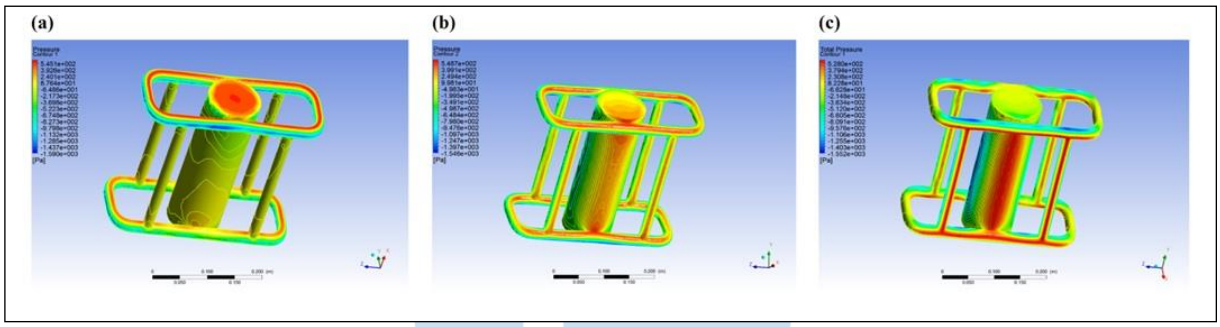

Total Pressure of ROV body form (a) Horizontal Dive; (b) Diagonal Dive; (c) Vertical Dive

IV. Material Production and Controller

A. *Material Production*

According to CFD analysis result regarding pressure value, the material of ROV main body was selected. Polyvinyl Chloride (PVC) with category rigid PVC known as Unplasticied PVC (PVC-U) was chosen to accommodate the requirement value of pressure. UPVC materials are used in the broad transportation of drinking water, water sewage and soil, underground drainage and industrial applications and eco-friendly which meant allow to disposable. UPVC has high hardness mechanical properties of tensile strength up to 51 MPa, thus body ROV allowed to free dive below the sea conducted with CFD result.

B. *Controller Hardware*

In Addition, Mini ROV was propelled by thruster with BLDC type of brushless motor fitted 4 kg of thrust power to overcome due to impact of the resistance where acted around mini ROV body up to 3.562 kg at Fr 0.6. Thus Mini ROV was allowed to travel under the sea. The velocity and axial rotation of BLDC motor controlled by 12 Volt BLDC motor driver circuit then operated by Arduino UNO R3.

V. Conclusion

ROV has major role for environmental research and surveying underwater purpose for evidence, especially the micro-ROV with light body geometry can reach through narrow and dangerous area. It provides a cost-effective alternative to fully utilize research grants and funding. The investigation of mini ROV using simulation CFD based RANSE software was successfully determined. Hydrodynamic parametric has been accomplished particularly in total force and total pressure. CFD simulation provides comprehend visualization of fluid flow around body thus performance of ROV can be examined.

When performing numerical analysis, it is important to ensure that the numerical errors are as small as possible. Except from the error associated with the fact that the solution is attained at discrete points in the domain, there are three important sources of error. First the governing equations need to be able to describe the fluid flow in a satisfactory way, this lead to the second source of error which is the algebraic equations and lastly the physical model used in the simulation (e.g. turbulence models).

The total force is used to determined amount of motor thrust with around weigh 4 kg. Then total pressure is employed the load pressure can be hold up about 8 bar when ROV operated and diving depth into underwater. The mini ROV succeed fulfill of design and performance requirement. Further research for mini ROV still developed to adjust in many research fields.

ACKNOWLEDGMENT

The authors are thankful to Vocational School Faculty, University of Diponegoro for partially funding the study.

REFERENCES

[1] A. M. Tahir and J. Iqbal, "UNDERWATER ROBOTIC VEHICLES: LATEST DEVELOPMENT TRENDS AND POTENTIAL CHALLENGES," Sci.Int.(Lahore), 2014.

[2] M. Nancekievill et al., "Detection of simulated fukushima daichii fuel debris using a remotely operated vehicle at the naraha test facility," Sensors (Switzerland), 2019.

[3] V. Raoult et al., "Remotely operated vehicles as alternatives to snorkellers for video-based marine research," J. Exp. Mar. Bio. Ecol., vol. 522, 2020.

[4] Rahimuddin, H. Hasan, H. A. Rivai, Y. Iskandar, and P. Claudio, "Design of Omni Directional Remotely Operated Vehicle (ROV)," 2018.

[5] R. Jones and J. Drabble, "U.K.'s submarine rescue efforts," Sea Technol., 1993.

[6] L. Bezanson, S. Reed, E. M. Martin, J. Vasquez, and C. Barbalata, "Coupled control of a lightweight ROV and manipulator arm for intervention tasks," 2017.

[7] A. Costanza, G. D'Anna, A. D'Alessandro, and G. Vitale, "Micro-ROV instrumental customization and canister design under pressure," 2017.

[8] J. H. Tarneckii and W. F. Patterson, "A mini ROV-based method for recovering marine instruments at depth," PLoS One, 2020.

[9] R. Capocci, G. Dooly, E. Omerdić, J. Coleman, T. Newe, and D. Toal, "Inspection-class remotely operated vehicles-a review," Journal of Marine Science and Engineering, vol. 5, no. 1. 2017.

[10] T. H. Samosir, K. W. A. Masengi, P. N. I. Kalangi, M. Iwata, and I. F. Mandagi, "Aplikasi remotely operated vehicle (ROV) dalam penelitian kelautan dan perikanan di sekitar perairan Sulawesi Utara dan Biak Papua," J. ILMU DAN Teknol. Perikan. TANGKAP, 2012.

[11] M. Chyba, T. Haberkorn, R. N. Smith, and S. K. Choi, "Autonomous Underwater Vehicles: Development and Implementation of Time and Energy Efficient Trajectories," Sh. Technol. Res., 2008.

[12] A. Amory and E. Maehle, "Modelling and CFD Simulation of a Micro Autonomous Underwater Vehicle SEMBIO," 2019.

[13] C. S. Chin, W. P. Lin, and J. Y. Lin, "Experimental validation of open-frame ROV model for virtual reality simulation and control," J. Mar. Sci. Technol., 2018.

[14] D. C. Wilcox, Turbulence modeling for CFD. 1993.

[15] J. D. Anderson and J. D. Anderson Jr, Computational Fluid Dynamics The Basics with Applications. 1995.

[16] F. D. Kurniawati and I. K. A. Pria Utama, "An Investigation into the Use of Ducktail at Transom Stern to Reduce Total Ship Resistance," IPTEK J. Proc. Ser., 2017.

ISSN 2355-3286

The Development of an IoT-based Indoor Air Monitoring System Towards Smart Energy Efficient Classroom

Moeljono Widjaja[1], Dareen Halim[2], Rahmi Andarini[3]
[1] Department of Informatics, Universitas Multimedia Nusantara, Tangerang, Indonesia
[2] Department of Computer Engineering, Universitas Multimedia Nusantara, Tangerang, Indonesia
[3] Department of Engineering Physics, Universitas Multimedia Nusantara, Tangerang, Indonesia
[1] moeljono.widjaja@umn.ac.id, [2] dareen.halim@umn.ac.id, [3] rahmi.andarini@lecturer.umn.ac.id

Accepted on 03 May 2022
Approved on 16 June 2022

***Abstract*— Indoor air quality has become a crucial issue, specifically during COVID 19 pandemic. The good indoor air quality will lead to occupants' comfort condition, thus affecting their productivity. Indoor air temperature and relative humidity are two essential components of thermal comfort. This paper presents the development of a temperature and relative humidity monitoring system for the classroom using the Internet of Things (IoT). This system consists of three main components: logger nodes, a gateway logger, and an interconnected cloud server. The logger node (ESP8266 / ESP32 microcontroller and DHT22 sensor) is a device at the edge of the IoT system and is placed at the monitoring location. The logger gateway is built on a Raspberry Pi 4, which serves as an intermediate server. It receives periodic data (temperature and humidity) from the logger nodes through the publish-subscribe MQTT protocol and sends it to the MongoDB Atlas cloud database. The logger gateway saves all received logs into the SQLite database as temporary local storage and then uploads the data to the MongoDB Atlas cloud at a predefined interval. The MongoDB data is then displayed on a monitoring dashboard using MongoDB charts. The logger node with the DHT22 sensor has been adjusted using a linear model and successfully tested to monitor indoor and outdoor air conditions with satisfactory results. The recorded data has also been successfully modeled using the Gaussian Mixture Model and a simple Fuzzy model. These models can capture the dynamic of air condition in the room and predict the state of the cooling system.**

***Index Terms*— Fuzzy Model; Gaussian Mixed Model; Internet of Things; MQTT Protocol; Sensors.**

I. INTRODUCTION

Air conditioning systems are increasingly widespread for homes, office buildings, shopping centers, factories, campuses and schools. As a result, the consumption of electrical energy for the cooling system also increases from year to year. Often the use of the cooling system is inefficient due to several factors, including an adequate monitoring system is not yet available, so efficiency actions cannot be carried out optimally [1].

Instead of energy consumption issues, thermal comfort is also a crucial factor that must be achieved for a room with an air conditioning system (conditioned room) [2]. The good indoor air quality of a room will lead to the occupants' productivity [3]. In order to achieve thermal comfort conditions, it is crucial to maintain the indoor air parameter such as temperature, relative humidity, and CO2 level of the room [4].

Currently, there are various ways to monitor the condition of the room, either manually or automatically. Air conditioning units are usually equipped with a conventional room temperature controller (thermostat), but the tools that are commonly used are usually unable to record the measured data for further analysis. In order to maintain a comfortable room temperature, the system must be able to monitor the dynamic of air condition as affected by many factors, including the weather outside (exposure to sunlight through glass windows or rain), room occupancy rate, time of day (morning, afternoon or evening) and the impact of heat generated by electronic equipment [5], [6].

An Internet of Things (IoT) is a device connected through the Internet network so that it can be monitored and controlled remotely as long as an Internet network is available. This IoT technology is relatively affordable and quite easy to implement so that its use has been included in the daily activities of various industries; its application includes and is not limited to smart city applications [7], [8], smart campuses [9]–[11], smart grid, smart home [12], security [13] and smart building management system [14], [15]. There has been no standard as a reference in the application of IoT in the field of building management, so there are still plenty of opportunities for exploration of various methods and related technologies [16]. This study aims to develop a temperature and humidity monitoring system for classrooms based on the Internet of Things which offers more comprehensive measurements and broader

coverage areas. The first stage of this research was to design the IoT-based monitoring system architecture. The development of this system was then continued by testing two IoT loggers: one to monitor indoor air conditions and the other to monitor outdoor air conditions. Prior to field testing, the two IoT loggers were adjusted so that the measurement results of the two loggers were identical when measuring the same air condition. The adjusted measurement was modelled linearly using the least-squares method. The saved data was then analysed and used to build a simple model using GaussianMixture and Fuzzy approaches to capture the dynamic of air condition as it is influenced by the outdoor weather and the air cooling system.

II. METHODOLOGY

The development of this IoT-based temperature/humidity monitoring system includes the design of the IoT system architecture, the setup of the MongoDB database in the Atlas cloud, the development of a dashboard monitoring system using MongoDB Charts, and the process of calibrating the sensors.

A. IoT Architecture System

In general, this IoT-based temperature/humidity monitoring system consists of three main components: (1) logger nodes, (2) logger gateways, and (3) cloud servers that are connected to each other as described in Figure 1.

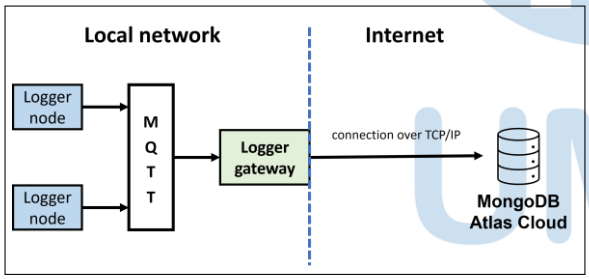

Fig. 1. IoT-based monitoring system architecture

The logger node is the far end device of the IoT system and is placed at the monitoring location. In this study, the logger device is composed of the ESP8266 / ESP32 microcontroller family is equipped with Wi-Fi connectivity and paired with a DHT-22 temperature and humidity sensor. The logger is connected via a local WLAN network (Wi-Fi technology) with the logger gateway. This local WLAN can be an ad-hoc network created by a logger gateway or a WLAN network originating from a public Wi-Fi router device.

The logger gateway is a Raspberry Pi 4, which functions as an intermediary server, which receives periodic temperature and humidity data from the logger node, and sends it to the MongoDB Atlas cloud database, which will be discussed in more detail later. Communication between the logger gateway and logger node is carried out through the publish-subscribe MQTT [17] protocol, where the logger node unit becomes the MQTT client and the logger gateway become the MQTT broker as well as the MQTT client. Communication between the logger gateway to the MongoDB Atlas is done via the MongoDB wire protocol over the TCP/IP standard socket connection. The intermediary server function in this research is designed in two versions, namely: NodeJS and Python script.

The query-driven communication flow between the logger gateway and the node can be seen in Figure 2. Two MQTT communication channels were provided, namely the 'control' channel and the 'log/data' channel. The logger gateway periodically (every 10 minutes in this study) sends a message to the 'control' channel, which will be received by all logger nodes. When receiving the control message, the logger node will respond by sending a message containing the loggerID and the current temperature/humidity to the 'log/data' channel.

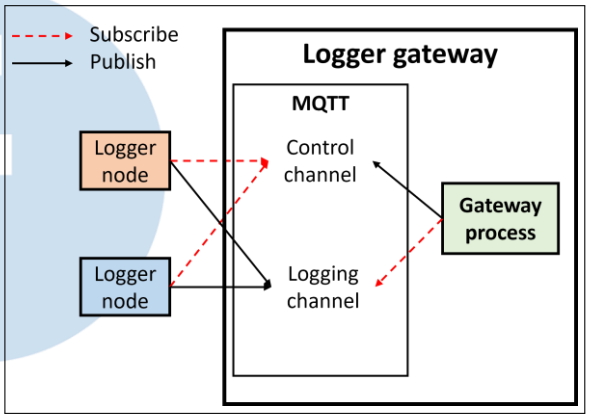

Fig. 2. The query-driven communication flow between logger gateway and node

The use of these two separate channels is carried out with the following considerations:

1) *Security*

When the system has been implemented with loggers on a large scale, the 'control' channel can be opened to the public so that all devices can join the channel to get information about when temperature and humidity logging should be carried out, or for development other more complex control schemes (including initiation when a new logger joins the network for the first time). Meanwhile, information regarding the 'log/data' channel can be provided only for 'trusted' loggers, so those other unverified devices cannot send fake logging info because they cannot access the 'log/data' channel. This scheme can be further developed so that the information dissemination process regarding the 'log/data' channel is integrated with the authentication process. For example, the logger can be registered with the system via a management dashboard. A secret 'log/data' channel and access token are provided by

the dashboard upon successful registration. The logger then can access the given MQTT channel while providing access token [18]. This schematic is described in Figure 3.

2) *Efficiency*

Similar to the first point, a system that is implemented on a large scale will result in a large number of MQTT message transactions as well. If only one channel is used both for 'control' and 'log/data', control commands from the logger gateway will be mixed with data logging messages from the logger node. As a result, it will cause unnecessary processing on the logger node side [19]. In operation, the logger node must monitor the communication channel to get commands from the logger gateway, which in this study is the command to do logging. If the command is mixed with messages containing logging data from other nodes (a large number), then each node must filter the incoming messages only to recognize control messages from the gateway logger, thus affecting performance. Processing this large amount of messages may not be a problem for devices with more resources, but it can have an impact on microcontroller devices

Event #	Logger node	Channel 'control'	Channel 'log/data'	Logger gateway
1		Content: {Auth API info, log command}	Content: {existing logger's logs}	Periodically publishing *Auth API* and *log command* to '**control**'
2	Join logger network, only knows channel '**control**'	...	...	...
3	Subscribe to '**control**', get Auth API	...	...	...
4	Hit Auth API with proper credentials	...	...	Receive API request, authentication attempt
5	OK, subscribe to '**log/data**'	...	...	Auth successful, reply with channel '**log/data**' information (*name*)
6	Log and publish to '**log/data**' upon logger gateway command on '**control**'	...	...	
		Content: {Auth API info, log command}	Content: {existing logger's logs}	

Fig. 3. Data transmission security scheme using 'control' and 'log/data' channels

The gateway logger then saves all received logs into an SQLite database as temporary local storage before being uploaded to the MongoDB Atlas cloud. In this research, we create two schemes related to local storage. We have tested both storage schemes, and both are working fine.

1) All log data received via MQTT is stored in the SQLite database first and will be uploaded to the MongoDB Atlas cloud at specified periods (if internet connection exists).

2) All log data received via MQTT will be directly uploaded to the MongoDB Atlas cloud. If during upload there is an interruption in the internet connection, the logs that failed to upload will be stored in the SQLite database first, and try to be uploaded again in the next logging period (10 minutes later) together with the new data.

B. MongoDB Atlas

The measurement data of several loggers is stored in a MongoDB database provided by MongoDB Atlas. MongoDB Atlas is a global cloud database service for modern applications [20]. Unpaid service is available with limited 512 MB storage capacity, sharing RAM, Highly available replica sets (provided three nodes), end-to-end encryption, automatic patches, and REST API.

The data stored in the MongoDB database is loggerID, timestamp (ts), temperature (temp) and relative humidity (hum) in JSON format (JavaScript Object Notation) as shown in Figure4.


```
{
  "_id": {
    "$oid": "605366675e8b6b713a449066"
  },
  "loggerID": "loggerA",
  "ts": {
    "$date": {
      "$numberLong": "1616073609494"
    }
  },
  "temp": {
    "$numberDouble": "29.4"
  },
  "hum": {
    "$numberDouble": "52.2"
  }
}
```


Fig. 4. A sample document from the MongoDB database

The MongoDB database automatically adds a unique identity _id for every record saved. Figure 5 shows an overview of the data stored in a MongoDB database. The report is based on a sample of 1000 documents. The total amount of data stored is 5925. The two loggerIDs are logger3 and logger4. The recorded air temperature was in the range of 27.7$^{\circ}C$ to 36.2$^{\circ}C$ with an average temperature of about 30$^{\circ}C$ and a skew-normal distribution with a long tail on the right side. Air humidity is in the range of 35.9%RH to 87.5%RH and it can be seen that there are two peaks of data distribution (local and global maximum) so it can be concluded that the data distribution is bi-modal. Data stored in the database were in the period from 5 to 26 November 2020.

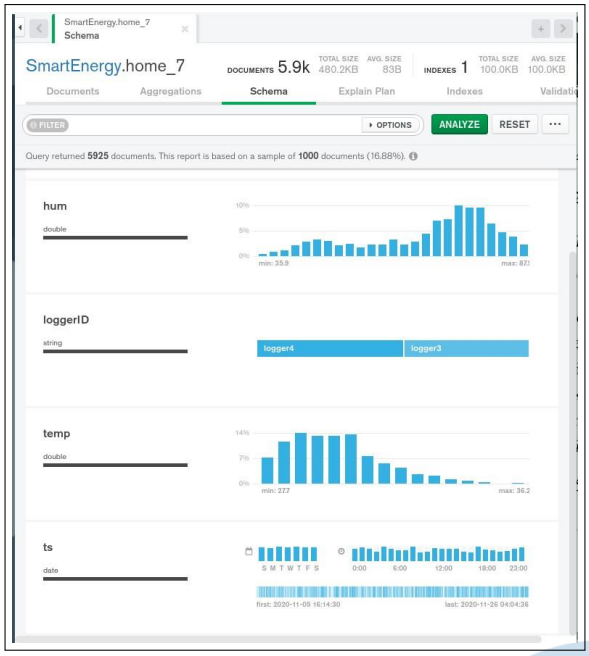

Fig. 5. Overview of data stored in the MongoDB database

C. *MongoDB Chart*

MongoDB charts are tools to visualise data in MongoDB Atlas. There are various types of charts available such as column/bar charts, line/area charts, combo charts, grid charts (heatmap and scatter), circular charts (donut and gauge), text charts (number, word cloud and top item), and geospatial charts (heatmap, scatter and chloropleth). It is easy to create a dashboard with a collection of charts using MongoDB charts. Charts update automatically as real-time data comes into the MongoDB database. The dashboard is updated in real-time and can be made interactive by enabling filters.

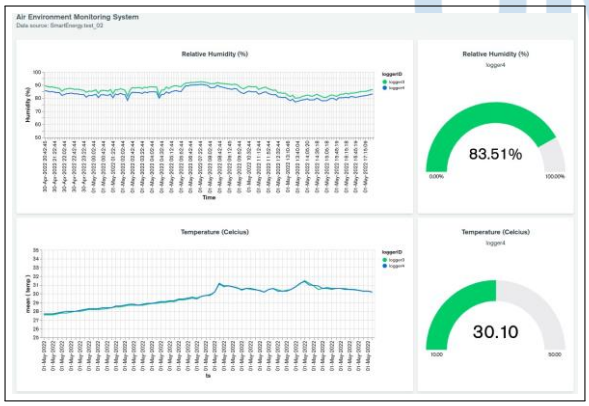

Fig. 6. Air condition monitoring dashboard

Figure 6 shows the dashboard of the air condition monitoring system. The dashboard shows the current measured humidity and temperature as gauge charts. It also shows the historical measurements of humidity and temperature as line charts.

D. *DHT22 Sensor Adjustment*

Two IoT loggers equipped with DHT22 temperature/humidity sensors generated different reading measurements when placed in the same room, so an adjustment process was required for both sensors. The process was carried out in a room equipped with air conditioning and windows so that it could condition a reasonably wide range of temperature and humidity. One of the DHT22 sensors will be used as a reference, for example, the sensor used in the loggerB. Under ideal conditions, a calibrated temperature/humidity sensor can be used as a reference.

The data from the temperature and humidity measurement during the adjustment process on two DHT22 sensors can be seen in Figure 7. The process was carried out from 8.10 pm local time on 18 March 2021 until the morning at 9.00 am on 19 March 2021.

Figure 7 shows that there is a difference between loggerA and loggerB in both temperature and humidity measurements. There is a fairly large gap (about 5%) seen in the results of air humidity measurements. The adjustment process was performed using the DHT22 sensor on the loggerB as a reference. The result of linear modelling for air temperature on loggerA is given in the following linear equation:

$$t_{adjusted} = 0.93 \times t_{measured} + 1.91 \quad (1)$$

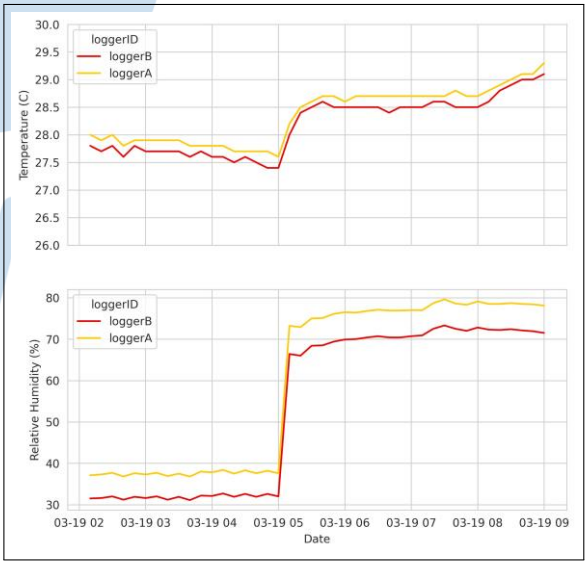

Fig. 7. Results of measurement of air temperature and humidity before the adjustment process

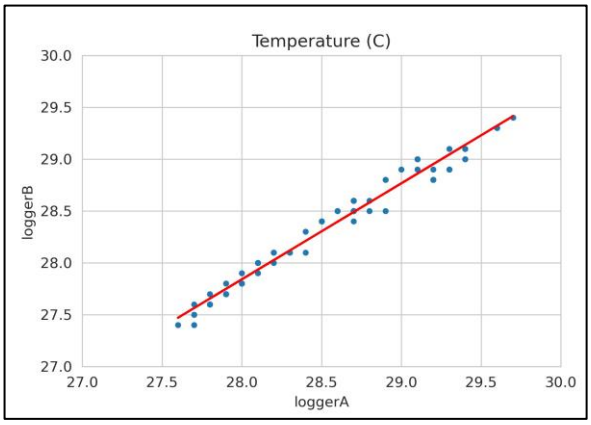

Fig. 8. The results of fitting air temperature data from loggerA and loggerB

Where $t_{adjusted}$ is the result of temperature measurement on loggerA that has been adjusted and $t_{measured}$ is the original result of temperature measurement on loggerA. This linear model is the result of fitting with the least-squares method on the measurement data, which is displayed as a scatter plot as shown in Figure 8.

Linear modelling was also carried out on the loggerA humidity measurement with the results in the form of the following linear equation:

$$h_{adjusted} = 0.98 \times h_{measured} - 5.06 \quad (2)$$

where $h_{adjusted}$ is the result of measuring humidity on an adjusted loggerA and $h_{measured}$ is the original result of measuring humidity on the loggerA. This modelling is the result of fitting with the *least-squares* method on the measurement data and displayed as a scatter plot as shown in Figure 8.

Table I shows the parameters and metrics of the regression models for temperature and relative humidity. A high correlation value (0.975656) for the temperature model indicates that the modelling results have high accuracy; in other words, the results of air temperature measurements with adjusted loggerA and loggerB are very similar. A very high correlation value (0.99985) for the relative humidity model indicates that the modelling results have very high accuracy; in other words, the results of air humidity measurements with adjusted loggerA and loggerB are almost identical.

TABLE I. THE PARAMETERS AND METRICS OF THE FITTED LINEAR MODELS (TEMPERATURE AND RELATIVE HUMIDITY)

Parameters of Regression Model	Temperature	Relative Humidity
Slope	0.92596934	0.982
Intercept	1.91308973	-5.06556
Metrics of Regression Model		
RMS error	0.006698	0.042672
R2 score	0.975656	0.99985

After adjusting the loggerA, the plot results for the same period can be seen in Figure 10. The results of temperature and humidity measurements during the adjustment process show that temperature and humidity measurements with loggerA and loggerB almost overlap in one plot. It indicates that loggerA and loggerB have been successfully ”calibrated” so that both loggers are ready to use.

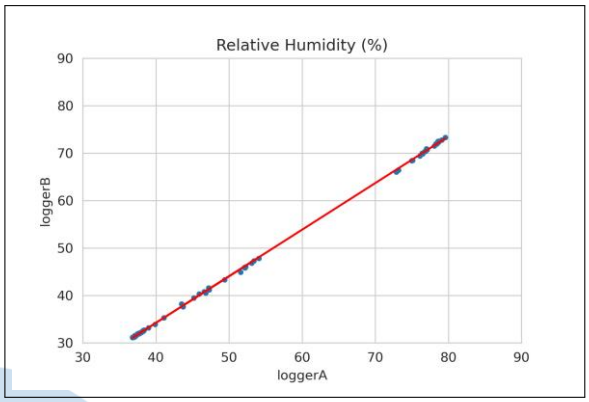

Fig. 9. The results of fitting air humidity data from loggerA and loggerB

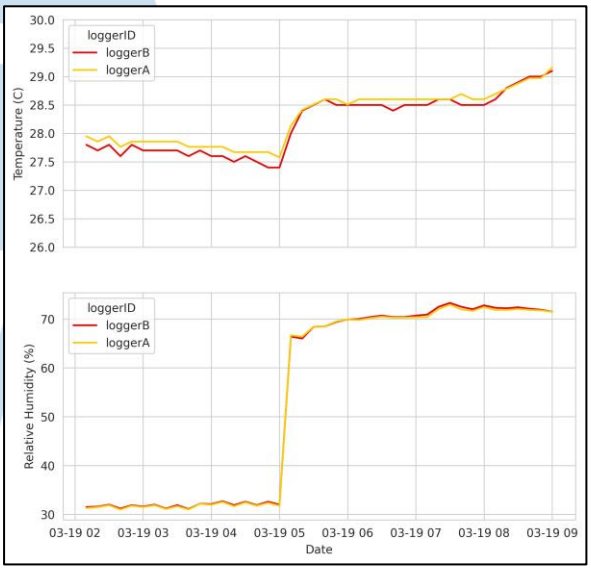

Fig. 10. The results of monitoring the temperature and humidity of the air after the adjustment process

III. Result and Discussion

The developed system has been successfully applied to monitor air conditions in the field. The system is ready to monitor the temperature/humidity of the air in an enclosed space and an open space. The data collected from the monitoring system is used to model the dynamic of air condition due to the outdoor weather condition and the effects of a cooling system.

A. Experimental Testing

Air temperature and humidity measurements were conducted at two locations: indoor and outdoor

environments. The first location was a classroom. The loggerA and a mini server (Raspberry Pi 4) were placed in this classroom. LoggerA functioned to record the indoor air temperature and humidity. The second location was a corridor with considerable access to fresh air. The loggerB was located in this corridor. LoggerB served to monitor the outdoor air condition. The measurements began at around 11 am on 19 March 2021.

Monitoring of air conditions was carried out for six days consecutively, starting from 20 March 2021 to 25 March 2021 as seen in Figure 11. The air conditioning system was only turned on (as indicated by the value of the state equal to 1) for a few hours on 24 and 25 March 2021 specifically for this monitoring purpose. The air conditioning system is usually turned on when there is a class session in progress. However, there have been no classes scheduled in the building for almost two years due to the pandemic. When the cooling system was turned off, the temperature and humidity in the classrooms were relatively stable (a temperature range of about 28°C and a humidity of about 70%RH). The outdoor air conditions are pretty extreme, namely: the air temperature range is between 24°C to 33°C, and the humidity range is between 50%RH to 100%RH.

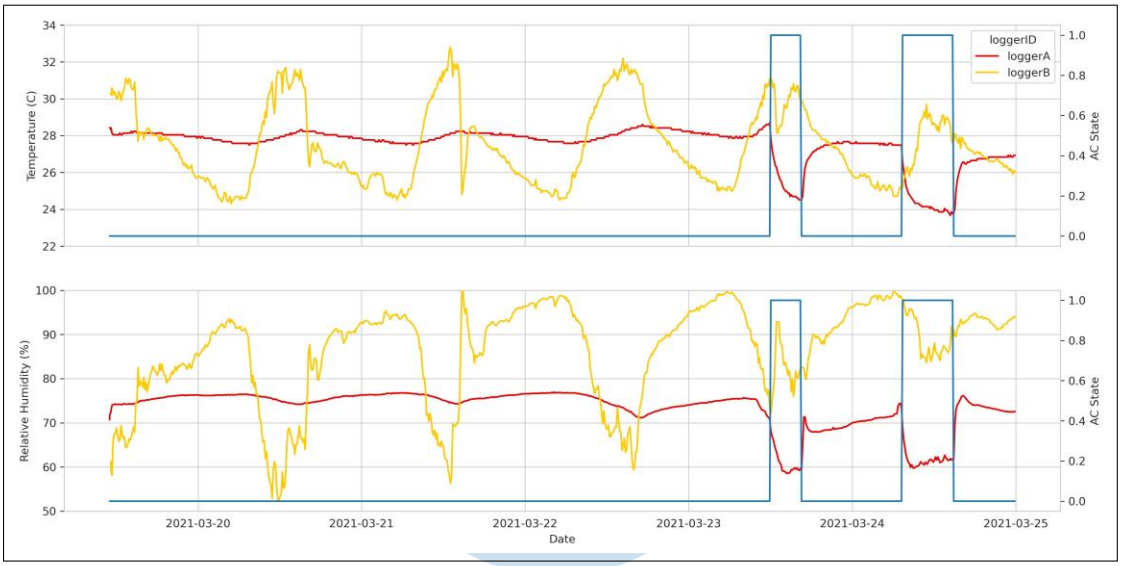

Fig. 11. The results of fitting air temperature data from loggerA and loggerB

When the air conditioning system was turned on, the air temperature quickly dropped to a range of 24°C when the outdoor temperature was in the range of 30°C. A decrease also occurred in the humidity in the classroom from the range of 75%RH to the range of 60%RH when the outdoor humidity was in the range of 90-90%RH.

The air condition in the classroom is relatively stable and isolated from the outdoor air condition because the building is equipped with a double skin facade and a heat-insulating wall that can regulate the intensity of light and reduce the heat from the sun that enters the room so that the room is bright enough and cool even when the air conditioner is turned off.

B. Modeling Results

The logged data were analyzed to understand the relationship between indoor and outdoor temperature/humidity and the effect of the cooling system on indoor air conditions. The distribution of temperature and humidity parameter values in each logger provides an overview of the distribution of each of these parameters.

Figure 12(a) shows that the distribution of data from loggerA (indoor temperature) is clustered in two centers: one is centered around 24◦C with low density, and the other is centered around 28°C with high density. The cluster with low intensity came from the measurement when the air conditioning was turned on for a short period. Meanwhile, the data from loggerB (outdoor temperature) is distributed more evenly over a more comprehensive range.

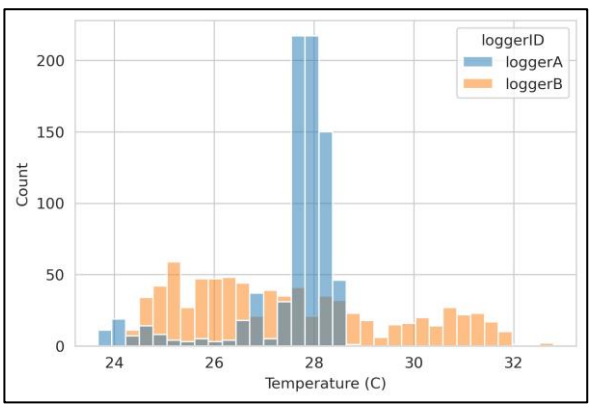

Fig. 12. Histogram of air temperature data recorded by loggerA (located indoors) and loggerB (located outdoors)

Figure 13(b) clearly shows that there are two peaks (local and global) in the humidity data from loggerA. If we fit two Gaussian distributions on the data using the *ExpectationMaximization* [21] algorithm, we will get two clusters with the following distribution:

- Gaussian distribution in low humidity cluster with μ = 68, σ =5.2, weight =0.3.
- Gaussian distribution in high humidity cluster with μ = 75, σ =1.1, weight =0.7.

The mean values of the low and high humidity clusters are 68%RH and 75%RH. The peak at the high humidity cluster is much higher than the peak at the low humidity cluster because during the monitoring process, the air conditioning system is turned on for a minimal time compared to the length of the measurement.

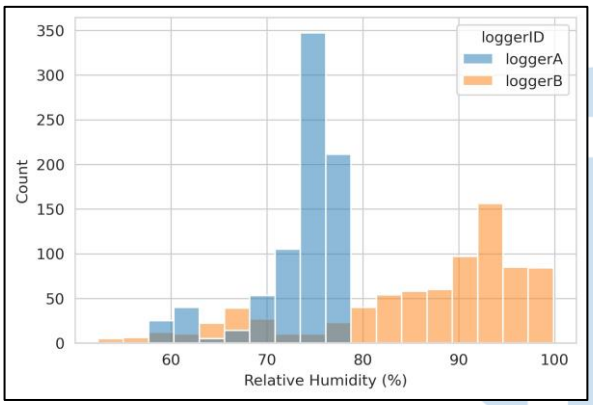

Fig. 13. Histogram of air humidity data recorded by loggerA (located indoors) and loggerB (located outdoors)

Figure 14 shows the Gaussian-Mixture model of the low and high humidity clusters. The model does not fit well to the data because Gaussian-Mixture models assume the data is distributed normally. Figure 14 clearly shows that the collected data is not normally distributed and is imbalanced between two variables. It could be due to the limited number of available data. As the number of measured data increases, the data would be expected to be normally distributed.

Alternatively, we could manually shape the fuzzy membership functions as proposed in [22] to fit the two clusters, as shown in Figure 15. It is shown that the membership functions of the low and high humidity can define the two distributions more distinctly. This fuzzy model can be used as an indicator to distinguish the state of the cooling system, either active orinactive. A simple fuzzy rule can be defined as follows: (a) if the relative humidity is low, then the cooling system is active, and (b) if the relative humidity is high, then the cooling system is inactive.

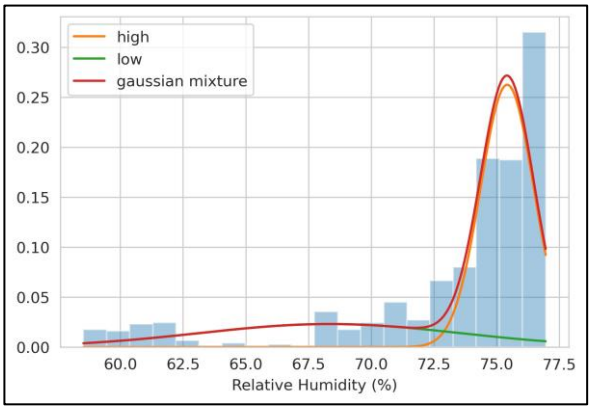

Fig. 14. Gaussian distribution modeling with two clusters (*low and high*) on humidity data from loggerA

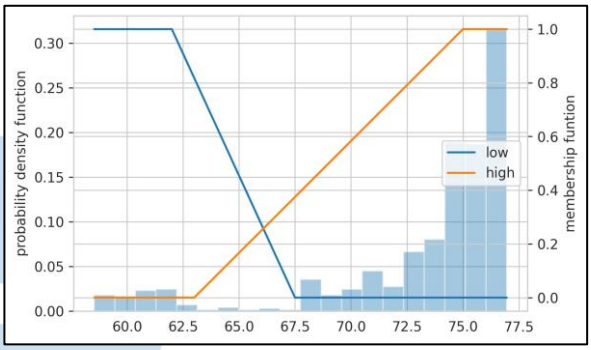

Fig. 15. Fuzzy Model with two clusters (*low and high*) on humidity data from loggerA

The data obtained can be used to predict the state of the cooling system: actively working or not. This model can be used to monitor unmeasured or hidden variables. It can be a cheaper and more effective solution than installing a current sensor in the air conditioning system.

IV. Conclusion

A temperature and relative humidity monitoring system for a conditioned classroom using the Internet of Things has been developed. The system has been successfully ”calibrated” and tested to simultaneously monitor indoor and outdoor air conditions. The monitoring results have been analyzed and used to construct a Gaussian-Mixture and a simple fuzzy model capturing the relationship between the indoor air conditions and the state of the air conditioning system. Further research can use the model as an input to a controller of the air conditioning system to achieve its optimal operation.

Acknowledgment

The authors would like to acknowledge the support given by Universitas Multimedia Nusantara for this research work.

REFERENCES

[1] R. Andarini, M. Salehuddin, and C. O. Harahap, "Pengembangan Sistem Manajemen Energi di Kampus Universitas Multimedia Nusantara," Universitas Multimedia Nusantara, Tangerang, Tech. Rep., 12 2019.

[2] M. Di Giulio, R. Grande, E. Di Campli, S. Di Bartolomeo, and L. Cellini, "Indoor air quality in university environments," Environmental monitoring and assessment, vol. 170, no. 1-4, pp. 509–517, 11 2010. [Online]. Available: https://pubmed.ncbi.nlm.nih.gov/19941062/

[3] H. B. Awbi, "Ventilation for Good Indoor Air Quality and Energy Efficiency," Energy Procedia, vol. 112, pp. 277–286, 3 2017.

[4] A. Asif, M. Zeeshan, and M. Jahanzaib, "Indoor temperature, relative humidity and CO2 levels assessment in academic buildings with different heating, ventilation and air-conditioning systems," Building and Environment, vol. 133, pp. 83–90, 4 2018.

[5] K. M. Al-Obaidi, M. Ismail, and A. M. Abdul Rahman, "A study of the impact of environmental loads that penetrate a passive skylight roofing system in Malaysian buildings," Frontiers of Architectural Research, vol. 3, no. 2, pp. 178–191, 6 2014.

[6] P. H. Shaikh, N. B. M. Nor, P. Nallagownden, I. Elamvazuthi, and T. Ibrahim, "A review on optimized control systems for building energy and comfort management of smart sustainable buildings," Renewable and Sustainable Energy Reviews, vol. 34, pp. 409–429, 6 2014.

[7] J. Shah and B. Mishra, "IoT enabled environmental monitoring system for smart cities," 2016 International Conference on Internet of Things and Applications, IOTA 2016, pp. 383–388, 2016.

[8] B. Hammi, R. Khatoun, S. Zeadally, A. Fayad, and L. Khoukhi, "IoT technologies for smart cities," IET Networks, vol. 7, no. 1, pp. 1–13, 1 2018.

[9] A. Zhamanov, Z. Sakhiyeva, R. Suliyev, and Z. Kaldykulova, "IoT smart campus review and implementation of IoT applications into education process of university," 2017 13th International Conference on Electronics, Computer and Computation, ICECCO 2017, vol. 2018Janua, pp. 1–4, 2018.

[10] K. Sharma and T. Suryakanthi, "Smart System: IoT for University," Proceedings of the 2015 International Conference on Green Computing and Internet of Things, ICGCIoT 2015, pp. 1586–1593, 1 2016.

[11] R. Andarini, M. Widjaja, and D. K. Halim, "Evaluation of Indoor Air Condition of University Building in Tropics using Building Thermal Modeling," 2021 2nd International Conference On Smart Cities, Automation & Intelligent Computing Systems (ICON-SONICS), pp. 52–57, 10 2021. [Online]. Available: https: //ieeexplore.ieee.org/document/9617192/

[12] L. Smirek, G. Zimmermann, and M. Beigl, "Just a Smart Home or Your Smart Home - A Framework for Personalized User Interfaces Based on Eclipse Smart Home and Universal Remote Console," Procedia Computer Science, vol. 58, pp. 107–116, 2016.

[13] S. S. Vedaei, A. Fotovvat, M. R. Mohebbian, G. M. Rahman, K. A. Wahid, P. Babyn, H. R. Marateb, M. Mansourian, and R. Sami, "COVIDSAFE: An IoT-based system for automated health monitoring and surveillance in post-pandemic life," IEEE Access, vol. 8, pp. 188538– 188551, 2020.

[14] D. Minoli, K. Sohraby, and B. Occhiogrosso, "IoT Considerations, Requirements, and Architectures for Smart Buildings-Energy Optimization and Next-Generation Building Management Systems," IEEE Internet of Things Journal, vol. 4, no. 1, pp. 269–283, 2017.

[15] G. Lilis, G. Conus, N. Asadi, and M. Kayal, "Towards the next generation of intelligent building: An assessment study of current automation and future IoT based systems with a proposal for transitional design," Sustainable Cities and Society, vol. 28, pp. 473–481, 1 2017.

[16] L. Atzori, A. Iera, and G. Morabito, "The Internet of Things: A survey," Computer Networks, vol. 54, no. 15, pp. 2787–2805, 10 2010.

[17] R. A Light, "Mosquitto: server and client implementation of the MQTT protocol," The Journal of Open Source Software, vol. 2, no. 13, p. 265, 5 2017.

[18] D. K. Halim and S. Hutagalung, "Towards data sharing economy on Internet of Things: a semantic for telemetry data," Journal of Big Data, vol. 9, no. 1, pp. 1–24, 12 2022.[Online]. Available: https://journalofbigdata.springeropen.com/articles/ 10.1186/s40537-021-00549-0

[19] A. van den Bossche, N. Gonzalez, T. Val, D. Brulin, F. Vella, N. Vigouroux, and E. Campo, "Specifying an MQTT Tree for a Connected Smart Home," in International Conference On Smart homes and health Telematics (ICOST 2018). Springer, Cham, 2018, pp.236–246. [Online]. Available: https://link.springer.com/chapter/10.1007/ 978-3-319-94523-1 21

[20] "Learn More About MongoDB — MongoDB." [Online]. Available: https://www.mongodb.com/discover-mongodb-atlas

[21] A. P. Dempster, N. M. Laird, and D. B. Rubin, "Maximum Likelihood from Incomplete Data via the EM Algorithm," Journal of the Royal Statistical Society. Series B (Methodological), vol. 39, no. 1, pp. 1–38, 1977.

[22] M. Widjaja, A. Darmawan, and S. Mulyono, "Fuzzy classifier of paddy growth stages based on synthetic MODIS data," in 2012 International Conference on Advanced Computer Science and Information Systems, ICACSIS 2012 - Proceedings, 2012, pp. 239–244.

ISSN 2355-3286

Sensor Design for Building Environment Monitoring System based on Blynk

Fahmy Rinanda Saputri[1], Sekar Fattima Dhaneswari[2]
[1,2] Department of Engineering Physics, Universitas Multimedia Nusantara, Tangerang, Indonesia
[1] fahmy.rinanda@umn.ac.id, [2] sekar.dhaneswari@student.umn.ac.id

Accepted on 10 June 2022
Approved on 06 July 2022

***Abstract*— A green building is a building wherein planning, construction, operation until the maintenance reduces the negative impacts, such as efficient use of energy, water, and other resources, maintaining the excellent quality of the building, and considering the quality of life of occupants. Good environmental damage in the building will affect the health, comfort and, safety of the occupants' lives. Therefore, it takes green buildings concept for buildings where people do activities in a home, an office, a school, a hospital, or a community center. To implement the green building concept, the building needs a monitoring system to monitor the quality of its environment. This research aim is to design sensor systems to monitor the building environment. The parameters monitored are temperature, humidity, illuminance, and noise intensity. The sensor system needs to the integrated with microcontroller and Blynk applications. The sensor system obtains the environment parameter. The accuracy rating for the temperature sensor is 94.41%, the humidity sensor is 93.53%, the light sensor is 91.26%, and the sound sensor is 97.13%. Blynk's warning system can make it easier for users to monitor the environment of a building.**

***Index Terms*— Blynk; green building; humidity sensor; light sensor; microcontroller; monitoring system; sensor system; sound sensor; temperature sensor.**

I. INTRODUCTION

A green building is a building wherein planning, construction, operation until the maintenance reduces the negative impacts, such as efficient use of energy, water, and other resources, maintaining the excellent quality of the building, and considering the quality of life of occupants. Good environmental damage in the building will affect the health, comfort and, safety of the occupants' lives. Currently, green building is a requirement for sustainable development. Not only applied to office buildings, but the green building also applied in campus buildings, hotels, department stores, even houses.

Green Building Council Indonesia (GBCI) has issued GREENSHIP Interior Space Version 1.0. This standard contains appropriate site development (ASD), Energy Efficiency and Conservation (EEC), Water Conservation (WAC), Material Resource and Cycle (MRC), Indoor Health and Comfort (IHC) and, Building Environment Management (BEM) criteria [1]. To meet these criteria standards, especially IHC 5, 6, and 7 and, to improve the comfort of occupants, a building environment monitoring system is needed to monitor the condition of the building and its environment.

In this paper, the sensor system able to monitor the environment parameters, such as temperature, humidity, illuminance, and noise intensity. The comfort standard for these parameters is regulated in the Standar Nasional Indonesia (SNI). Thermal comfort is regulated in SNI 03-6572-2001 [2]. The standard shows that optimal comfort in tropical areas is 22,8°C – 25.8°C. For tropical areas, relative air humidity is recommended between 40% - 50%, but for rooms where the number of people is dense such as meeting rooms, relative humidity is still allowed ranging from 55% - 60%. Based on SNI 03-6197-2000, the recommended average lighting level is set based on the room's function, for example, for kitchens in residential houses of 250 Lux, office workspaces of 350 Lux, and classrooms in educational institutions are 250 Lux [3]. In terms of noise intensity, SNI 16-7063-2004, which regulates noise control, said that the noise intensity is 88 dB(A) for the exposure time of 4 hours per day [4].

In general, buildings in Indonesia are complex buildings because there are various rooms by their functions. In this case, monitoring of environmental parameters in the building is required. In addition, it needs technology that can monitor these parameters at all times. It can solve these problems by designing a building environment monitoring system. With this system, the values of each parameter can be monitored in real-time so that occupants can know the information provided by the system. Occupants can also compare it with comfort standards according to SNI.

Vanessa Lee and Fahmy Rinanda S. researched about the design of monitoring system for laboratory. They can monitor the condition of illumination using LDR sensor and microcontroller in laboratory through the website in real-time using Blogger and an Internet of Things (IoT) platform [5]. Bimo et al. researched the design of sensor systems using Arduino Uno boards. Data acquisition testing is conducted separately for each sensor. The method compares the results of the

data taken by the sensors and their respective measuring instruments under different conditions. So it is known the measurement error [6]. Research from M. Dwisnanto Putro et al. used LDR sensors for light intensity readings in various rooms in a house. However, the results had varying degrees of accuracy ranging from 70.6% to 99.6% after comparison with a luxmeter [7]. In addition, Wanto uses AT89S52 microcontrollers from ATMEL as a data processing system. This microcontroller has 8-bit input/output terminals, 8 KB flash memory, 256 BYTES OF RAM [8] [9]. Meanwhile, Ahmed H. H. Imam uses NodeMCU as a controller where the control has been equipped esp8266 as a communication module with a WIFI internet connection. No longer needed components of communication module devices separately [10].

In this study, a microcontroller is using the WeMos D1 Mini. The sensors used are the DHT22 sensor for temperature and humidity, the BH1750 sensor for the lighting level, and the KY-038 sensor for noise intensity. These sensors will be used as a medium to monitor environmental parameters that want to know their value at all times. The sensors used will record the data obtained. It also will give notify on the device used as a monitoring tool of the parameters above. If in a condition where the data obtained by the sensor exceeds the standard set, then there will be a warning through a notification on the phone using the Blynk application. After knowing the environmental conditions in a building, it will be information for the occupants.

II. Green Building Theory

Green Building is a practice in the series of green buildings, which create structures from a building and use environmentally responsible processes and use efficient material sources throughout the building creation cycle. From placement to design, construction, operation, maintenance, renovation, and deconstruction. This practice expands and reduces design issues classic buildings in terms of economy, utility, durability, and comfort [11].

Green buildings are designed to reduce the overall impact from the environment of a building to human health and the environment in three ways, namely:

- Use electrical energy and water efficiently,
- maintain the health of building users and improve the work performance of employees,
- reduce waste disposal, pollution, and environmental degradation.

III. Tools And Materials For Research

A sensor is a tool that receives a stimulus and responds with an electrical signal. Stimulus is the quantity, properties, or conditions received and converted to electrical signals. There are two types of sensors, active sensors, and passive sensors. Active sensors require an additional source of energy to work. Passive sensors do not require additional energy sources to work and directly emit electrical signals to respond to stimuli. The input and output relationships can be represented by a mathematical equation, the transfer function. Under ideal conditions, the transfer function is stable both graphically, in value, and equations. In general, the transfer function can be written as follows [12]:

$$y = a + bx \quad (1)$$

The value a is intercepting, and b is sensor sensitivity. Not all transfer functions are linear, but they can also be polynomial, logarithmic, or exponential. Sensors have several characteristics, namely sensitivity, span, accuracy, threshold, nonlinearity, saturation, resolution, saturation, repeatability.

A. Temperature Sensor

A temperature sensor is a component that can convert the amount of heat into an electric magnitude so that it can detect the symptoms of temperature changes in a particular object. The temperature sensor measures the amount of heat/cold energy produced by an object, allowing us to know or detect the symptoms of these temperature changes in the form of analog and digital outputs. There are four types of temperature sensors: thermocouple, thermistor, Resistant Temperature Detector (RTD), and temperature sensor IC.

A DHT22 sensor is a sensor that can provide input of temperature and humidity data from a surrounding environment. The DHT22 sensor outputs a calibrated digital signal. These sensors use digital signal collection and technology to sense moisture to ensure the stability and reliability of DHT22 sensors. For its sensing element used to sense input from the outside environment connected with a single chip of an 8-bit computer [13].

B. Humidity Sensor

Humidity sensors are electronic components used to assist in the measurement of moisture contained in the air. Types of humidity sensors include a capacitive sensor, electrical conductivity sensor, thermal conductivity sensor, optical hygrometer, and oscillating hygrometer. A moisture sensor uses a capacitive sensor. In this sensor, a dielectric between capacitor plates is made of hygroscopic material that can absorb water molecules. The constant of dielectric material varies according to the amount of moist vapor absorbed. It will convert the capacitance that can be measured and converted into a relative moisture value.

C. Light Sensor

A light sensor is an electronic component that can provide changes in electrical magnitude when receiving and sensing changes in light intensity in the environment. Components include light sensors, namely LDR, photovoltaic, photoconductive, photodiode, phototransistor, and optocoupler.

The BH1750 sensor is a sensor for measuring the value of ambient light. This sensor allows detecting a wide range with high resolution (1-65535 Lux). The BH1750 sensor uses an I²C interface, has a response that approaches the human eye, can convert illumination to digital signals, and uses only a tiny amount of power [14] [15].

D. Sound Sensor

Sound sensors are electronic components that can change the size of the sound becomes the amount of electricity. The sound sensor works based on the magnitude/small force of the sound wave that hits the sensor membrane causing the sensor membrane to move up and down. Behind this membrane is a small coil that flows magnetic waves due to the movement of the sensor membrane. The speed of motion of the coil affects the strength/weakness of the electric waves it generates .

The sound that disturbs human activity is called noise. So KY-038 sensor will measure the noise in this research. The KY-038 sensor is the microphone sensor used for the Arduino. The sensor has three main components on its circuit board. The first component is a sensor located in front of the module to measure the physical state of the environment and transmit data in the form of analog signals to the second component, the amplifier. The amplifier serves to amplify the analog signal by the potentiometer that has been determined from the beginning. The third component is a comparator that turns off the LED if the signal obtained is below the specified value [16].

E. Sound Sensor

MCU (Microcontroller Unit) is an electronic component or IC (Integrated Circuit) with computer-like properties, such as centralized processing units, memory codes, memory data, and ports for input/output. Microcontrollers have a small shape and are relatively cheap so that they can be integrated into various parts. Microcontrollers are programmed through software programs that can write, read, and delete content from microcontrollers [17].

The WeMos D1 Mini is a board based on an open-source electronic microcontroller whose main component is an ESP-8266EX micro-8266EX chip. Microcontroller can be programmed using a computer. The chip has a function to embed the microcontroller program to read the input, then the input will be processed, and after processing, the input will produce output. In WeMos D1 Mini, there is already a wireless network module, so it no longer requires additional wireless network module components [18].

F. Blynk

Blynk is Internet of Things (IoT) platform that allows user to build the apps to control certain devices over the internet. It provides dashboard by which user can create graphic interface using different widgets. It also displays and stores the data from the sensor. Blynk provides libraries for hardware platforms like Arduino, ESP8266, Raspberry Pi, SparkFun, WeMos D1 Mini, etc. There are three main components in the Blynk, app, server, and libraries. The app is used to create the interface. The server is for communication between app and hardware. Then, libraries enable for hardware communications with the server using commands [19].

IV. Working Of The System

The sensor systems consist of the DHT22 sensor, BH1750 sensor, KY-038 sensor, WeMos D1 Mini, mobile phone and, Blynk. Fig. 1 is the block diagram of the building environment monitoring system.

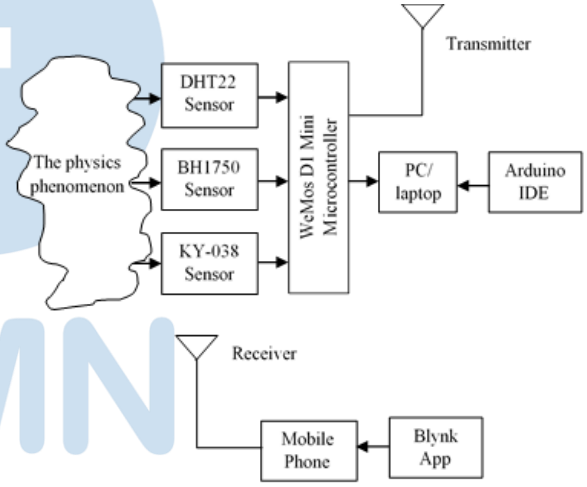

Fig. 1. Block diagram of building environment monitoring system

The sensors will sense the environment parameters. A DHT22 sensor is a sensor that can provide input of temperature and humidity data from a surrounding environment. The BH1750 sensor is a sensor for measuring the value of ambient light. Then, the KY-038 sensor is the microphone sensor used for this microcontroller. The WeMos D1 Mini is a board based on an open-source electronic microcontroller whose main component is an ESP-8266EX micro-8266EX chip. It will process the data from the sensor. The process need the program in Arduino IDE. Then, the output will be displayed on serial monitor Arduino IDE and also on mobile phone with the Blynk applications. Some notifications also can be set, so the alarm will work on if the value of parameters is trimmer and more than standards. The standards also can be set to allow the SNI.

Fig. 2 displays the system flowcharts. Start with set parameters, in this research, is temperature, humidity, illuminance, and sound intensity. This parameter would be input for the sensors. If the value match with the range of standard, this value will be displayed in Blynk applications. However, if the data do not match the standard range, Blynk will alarm and notify the user, so the user will know if the environment does not appropriate the standard.

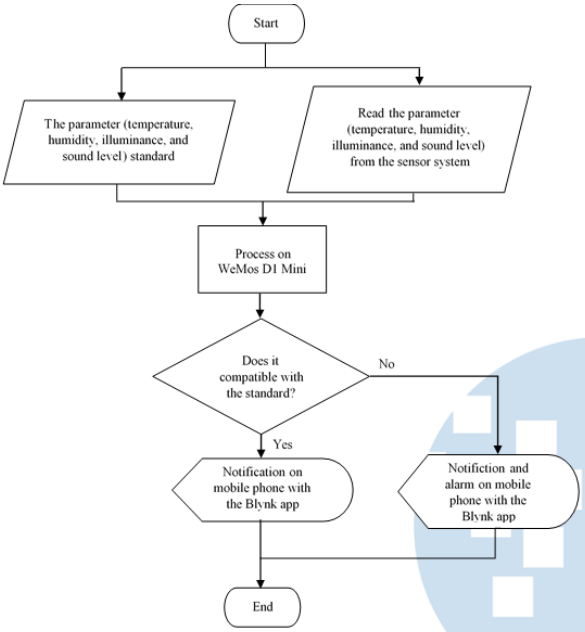

Fig. 2. Building environment monitoring system flowchart

For the entire sensor system consisting of a DHT22 sensor, the BH1750, and ky-038 sensors, will all be connected to the WeMos D1 Mini. Here is Fig. 3, which shows the complete hardware of the sensor system consisting of KY-038 sensor (number 1), DHT22 sensor (number 2), BH1750 sensor (number 3), and WeMos D1 Mini (number 4).

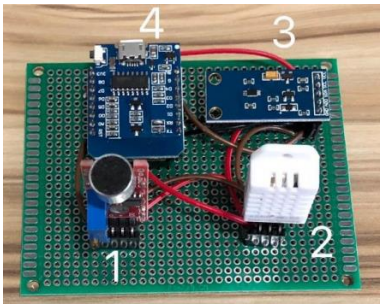

Fig. 3. System wiring

In using this sensor system, these steps must be taken:

1. Place the sensor system by working in a stable state and away from the noise.
2. Add input voltage to turn on the system.
3. The light indicator will turn on if it is connected to the voltage source.
4. Open the Blynk app on the mobile phone and make sure it has a stable internet connection.
5. Then press the start sign, and the program will run.
6. If the device is already connected via Wi-Fi, it will appear as 'Connected' on the Blynk app.
7. Data from the sensor will be displayed in this application located on the mobile phone.

Before this system is implemented in a building, it will be compared with the Environment Meter DT-8820 as a calibrator. There are thirty data of the temperature and humidity, illuminance, and sound intensity. The accuracy, precision, and error are analyzed based on the data.

Measurement system is applied in this research to obtain the accuracy, precision, and error calculation based on the temperature, humidity, illuminance and noise data measurement. There are thirty measurement data for each variable. The data is taken every two seconds real-time. Fig. 4, 5, 6, and 7 show the real-time data of temperature, humidity, illuminance, and noise level. This graph shows a comparison of data from sensor systems and Environment Meter. Based on the that data, the accuracy, precision, and error can be calculated.

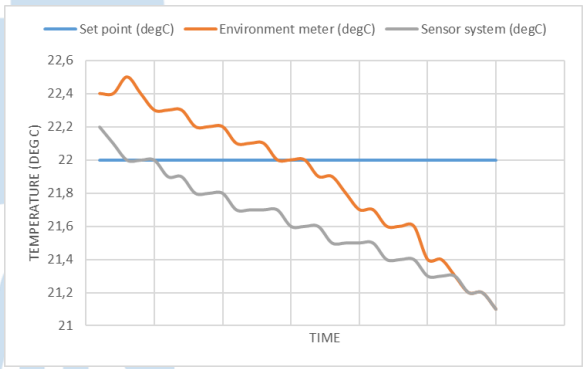

Fig. 4. Graph of temperature measurement

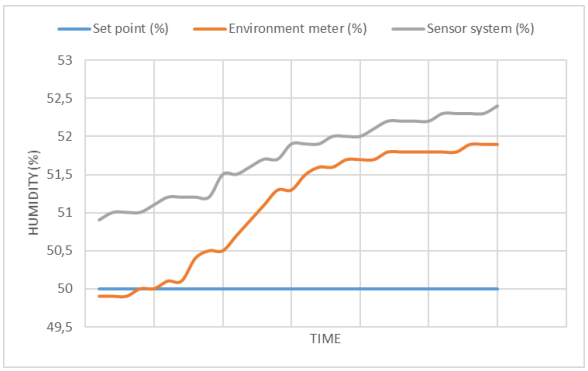

Fig. 5. Graph of humidity measurement

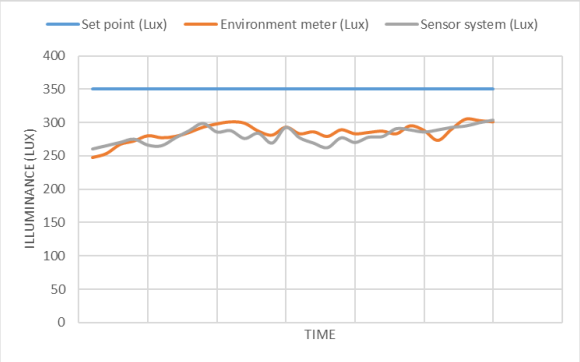

Fig. 6. Graph of illuminance measurement

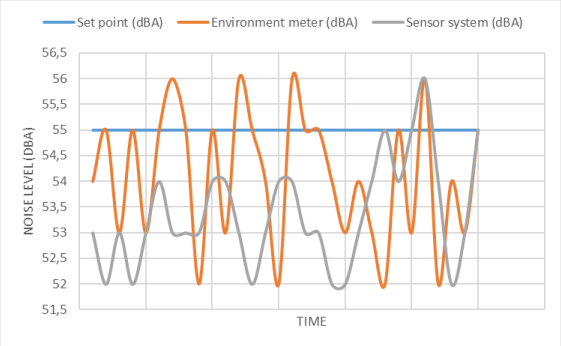

Fig. 7. Graph of the noise level measurement

Table 1. results from the accuracy, precision, and error calculation based on the temperature data measurement. When compared to the results, it is obtained that the accuracy and precision of the sensor system in measuring the temperature is higher compared to the environment meter measuring instrument. So the error is also more minor compared to the environment meter. The results are that the accuracy rating for the temperature sensor is 94.41%. The precision and error of the sensor system are 96.06% and 5.59%. It shows in the Table 1.

TABLE I. ACCURACY, PRECISION, AND ERROR CALCULATION RESULTS IN TEMPERATURE MEASUREMENT

Accuracy (%)		Precision (%)		Error (%)	
Environment M.	Sensor System	Environment M.	Sensor System	Environment M.	Sensor System
93.91	94.41	94.37	96.06	6.09	5.59

Then, the result of the calculation on humidity data measurement shows in Table 2. The sensor system has a higher accuracy and precision value but lower error when compared to the environment meter. Accuracy, precision, and error of humidity sensor is 93.53%, 97.12%, and 6.47%.

TABLE II. ACCURACY, PRECISION, AND ERROR CALCULATION RESULTS IN HUMIDITY MEASUREMENT

Accuracy (%)		Precision (%)		Error (%)	
Environment M.	Sensor System	Environment M.	Sensor System	Environment M.	Sensor System
93.21	93.53	95.51	97.12	6.79	6.47

Also in Table 3 is for the result of illuminance measurement using light sensor. Environment meters are capable of measuring illumination with higher accuracy and precision than sensor systems. The light sensor obtained 91.26% in accuracy, 84.49% in precision, and 8.74% in error.

TABLE III. ACCURACY, PRECISION, AND ERROR CALCULATION RESULTS IN ILLUMINANCE MEASUREMENT

Accuracy (%)		Precision (%)		Error (%)	
Environment M.	Sensor System	Environment M.	Sensor System	Environment M.	Sensor System
93.32	91.26	84.50	84.49	6.68	8.74

Based on Table 4, in measuring noise intensity, the sensor system has a higher precision level than the environment meter. However, the accuracy level is lower than the environment meter, so the error is higher than the environment meter. The sound sensor obtains 97.13% in accuracy, 94.08% in precision, and 2.87% in error.

TABLE IV. ACCURACY, PRECISION, AND ERROR CALCULATION RESULTS IN NOISE MEASUREMENT

Accuracy (%)		Precision (%)		Error (%)	
Environment M.	Sensor System	Environment M.	Sensor System	Environment M.	Sensor System
94.08	97.13	92.04	94.08	5.92	2.87

Many things that affect the sensor system obtain a level of accuracy, poor precision compared to the environment meter, such as systematic errors and even random errors. The error can be minimized for further research related.

After the accuracy is obtained, the data will be transmitted over WiFi (Wireless Fidelity) via the ESP8266 module on the WeMos D1 Mini port. Fig. 4 shows the interfaces of Blynk that are already connected with the system sensor and the interface of alarm and notification if the data do not compatible with the standard range that has been set.

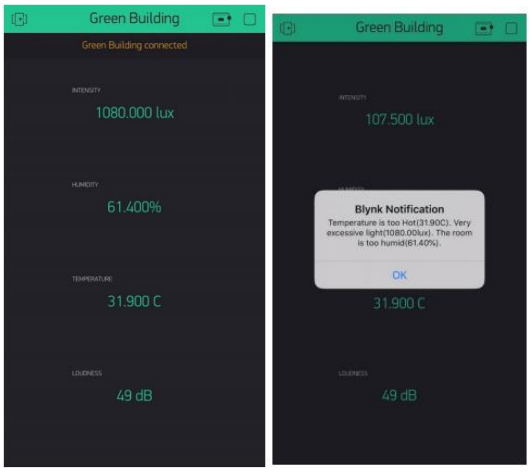

Fig. 8. Screen display of Blynk app on mobile phone and the notification

V. CONCLUSION

This research has designed the sensor system for building an environment monitoring system. The sensor system obtains the environment parameter. The accuracy rating for the temperature sensor is 94.41%, the humidity sensor is 93.53%, the light sensor is 91.26%, and the sound sensor is 97.13%. Blynk's warning system can make it easier for users to monitor the environment of a building. The parameter information which is sensed by the sensor system can be displayed on mobile phones using the Blynk application. In addition, Blynk's warning system can make it easier for users to monitor the environment of a building.

ACKNOWLEDGMENT

The authors would like to thanks Universitas Multimedia for supporting the facilities for research. So this research can complete well.

REFERENCES

[1] G. B. C. Indonesia, Greenship Interior Space Version 1.0, Jakarta: Green Building Council Indonesia, 2012.

[2] B. S. Nasional, SNI 03-6572-2001 Tata Cara Perencanaan Sistem Ventilasi dan Pengkondisian Udara pada Bangunan Gedung, Jakarta: BSN, 2001.

[3] B. S. Nasional, SNI 03-6197-2000 Konservasi Energi pada Sistem Pencahayaan, Jakarta: BSN, 2000.

[4] B. S. Nasional, SNI 16-7063-2004 Nilai Ambang Batas Iklim Kerja (Panas), Kebisingan, Getaran Lengan-Lengan dan Radiasi Sinar Ultra Ungu di Tempat Kerja, Jakarta: BSN, 2004.

[5] V. Lee and F. R. Saputri, "Website-Based Lighting Monitoring System Design in a Laboratory of Universitas Multimedia Nusantara," in 2021 2nd International Conference On Smart Cities, Automation & Intelligent Computing Systems (ICON-SONICS), Tangerang, 2021.

[6] B. A. Pamungkas, A. F. Rochim and E. D. Widianto, "Perancangan Jaringan Sensor Terdistribusi untuk Pengaturan Suhu, Kelembaban, dan Intensitas Cahaya," Jurnal Teknologi dan Sistem Komputer, vol. I, no. 2, pp. 42-48, 2013.

[7] M. D. Putro and F. D. Kambey, "Sistem Pengaturan Pencahayaan Ruangan Berbasis Android pada Rumah Pintar," Jurnal Nasional Teknik Elektro, vol. 5, no. 3, p. 297–307, 2016.

[8] Wanto and P. S. Priambodo, "Rancang Bangun Pengukur Intensitas Cahaya Tampak Berbasis Mikrokontroler," Universitas Indonesia Library, Depok, 2008.

[9] A. Corporation, 8-bit Microcontroller with 8K Bytes In-System Programmable Flash AT89S52, Atmel, 2001.

[10] A. H. H. Imam, "A Simple Smart Home Based on IoT Using NodeMCU and Blynk," UMS Library, Surakarta, 2019.

[11] U. G. B. Council, LEED Reference Guide for Green Building Design and Construction with Global ACPs, Washington DC: U.S. Green Building Council, 2009.

[12] J. Fraden, Handbook of Modern Sensors: Physics, Designs, and Applications Fourth Edition, San Diego: Springer, 2010.

[13] T. Liu, "Aosong Electronics Co.,Ltd," [Online]. Available: https://www.sparkfun.com/datasheets/Sensors/Temperature/DHT22.pdf. [Accessed 10 June 2022].

[14] M. Rawashdeh, "Instructables Circuits," [Online]. Available: https://www.instructables.com/BH1750-Digital-Light-Sensor/. [Accessed 10 June 2022].

[15] L. ROHM Co., "BH1721FVC Digital 16bit Serial Output Type Ambient Light Sensor IC," ROHM. Co.,Ltd., 2015. [Online]. Available: https://fscdn.rohm.com/en/products/databook/datasheet/ic/sensor/light/bh1721fvc_spec-e.pdf. [Accessed 10 June 2022].

[16] ElectroPeak, "How to Use KY-037 Sound Detection Sensor with Arduino," 2019. [Online]. Available: https://create.arduino.cc/projecthub/electropeak/how-to-use-ky-037-sound-detection-sensor-with-arduino-a757a7. [Accessed 10 June 2022].

[17] Yudhaniristo, "Prototipe Alat Monitoring Radioaktivitas Lingkungan, Cuaca dan Kualitas Udara Secara Online dan Periodik Berbasis Arduino (Studi Kasus: BATAN Puspitek Serpong)," Universitas Islam Negeri Syarif Hidayatullah, Jakarta, 2014.

[18] R. Thiara, "Design and Implementation of IoT based Remote Monitoring System at Electrical Engineering Laboratory in President University," President University, Cikarang, 2019.

[19] H. Durani, M. Sheth, M. Vaghasia and S. Kotech, "Smart Automated Home Application using IoT with Blynk App," in 2018 Second International Conference on Inventive Communication and Computational Technologies (ICICCT), Coimbatore, 2018.

ISSN 2355-3286

Preliminary Study on Indonesian Word Recognition for Elder Companion Robot

M.B.Nugraha[1], Dyah Ayu Anggreini Tuasikal[2], Ni Made Satvika Iswari[3]
Luthfialmas Fakhrizki Irwanto[4]
[1,2,4] Department of Electrical Engineering, Universitas Multimedia Nusantara, Tangerang, Indonesia
[3] Department of Informatics, Universitas Multimedia Nusantara, Tangerang, Indonesia
[1] mb.nugraha@umn.ac.id, [2] dyah.tuasikal@umn.ac.id, [3] satvika@umn.ac.id,
[4] lutfiaamas.fakhriski@student.umn.ac.id

Accepted on 06 July 2022
Approved on 15 July 2022

***Abstract*— Word recognition using deep learning is a simple approach to speech recognition in general. From this word-level recognition, the emotional expression recognition model. The emotion recognition model can be used to describe the important level of action on future planned hardware implementation. This research was conducted using MFCC as the feature extraction method from the audio data and using the CNN-LSTM approach for the emotional expression classifier. The model itself will be implemented into a humanoid robot to become a companion robot for the elderly. The model itself has 67% accuracy for emotion recognition and 97% accuracy for word recognition. However, the model only attained 20% accuracy in real-life testing using the humanoid robot as the model tends to overfitting as a result of the lack of data used in model training.**

***Index Terms*— CNN-LSTM; emotion recognition; MFCC.**

I. INTRODUCTION

Speech recognition recently become a popular research subject in Machine Learning and Artificial Intelligence research studies. The speech recognition studies also expand into emotion recognition derived from speech data [1]. This phenomenon occurs because emotion is one of the fundamentals of day-to-day communication between humans. Speech emotion recognition studies grow because researchers expect machines could learn how to distinguish an emotion by audio and visual data [2], [3]. As the machine's capability to recognize emotion in audio or visual data could augment user experience in several areas, especially in services such as automatic call centers, virtual reality games, etc. [4]

Previous studies in speech emotion recognition have already tried different approaches to building a learning network for emotional recognition. Wan [5] uses DTW in emotion recognition. But recently, deep neural networks using CNN and LSTM or RNN are gaining popularity for recognizing human emotion [6][7][8] and compared with established methods like SVM, LSTM and CNN have greater accuracy results [9]. And recently, the researcher also tried to recognize speech and emotion from their respective natural language, as shown in the study of Wan [5], Guiming [10], and Wang [1]. Specific language emotion recognition, in this case, Indonesian also studied by Lasiman [9]. Wunarso et al. [11] even tried to build another dataset for the Indonesian language in their study. As stated by Park et al. [12], deep neural network output really depends on how feature selection is done, and also how pooling and padding are important in improving speech recognition. They also stated that stacking many convolutional layers as they used in their work to create very deep neural networks does not have a great impact on recognition.

Word and emotion recognition technology can be used to build a companion robot for elders. Although in Indonesia the prevalence of loneliness in the elderly is not too high due to the strong eastern culture, symptoms of seniors who come from the middle to upper economy are already living alone without the company of their families. One of the solutions that can be given to this problem is to use a companion robot which is already widely used in Japan and the US. Robot companion is used by seniors who are in the middle to upper economic level and do have the appropriate understanding of technology. The companion robot function emphasizes the response that can be given by the robot based on voice input, so word recognition and speech recognition are important. And an additional feature that is also important is the robot's ability to detect danger or emergencies based on variations in intonation which will be the emotion recognition feature of this robot.

The purpose of this research is to do a preliminary study on emotion recognition in segmented words. Emotion classes were chosen based on a plan of implementation on the robotic system. In previous work, some authors of this paper successfully experimented with the word recognition system using MFCC for feature extraction and implementing the model on CNN. Hence, this work will discuss on speaker-independent word-emotion recognition system, focusing on emotional classification regardless

of the speaker. This paper only discussed the method chosen for conducting training and validation of deep learning using CNN and LSTM.

II. Data Collection

In their study, Wunarso et al. [11] try to build an Indonesian speech-emotion database called I-SpeED and use SVM as the classifier method. While Lasiman [9] studied emotion recognition using a feed-forward neural network and LSTM for the Indonesian language.

In this research, the data was collected and built by using multiple audio files with .wav format. Audio files were recorded in Bahasa Indonesia, and based on three emotional expressions, "happy," "sad," and "angry." Speakers were asked to read ten words with their respective expressions. The words are chosen from the robot implementation scenario in future works. All used words are described in Table 1.

TABLE I. Word Used

Words				
Maju (*forward*)	Mundur (*backward*)	Kanan (*right*)	Kiri (*left*)	Tegak (*stand*)
Duduk (*sit*)	Tidur (*sleep*)	Joget (*dance*)	Cari (*find*)	Angkat (*lift*)

The word-emotion database recorded from 100 different speakers consists of 9000 audio files. Each speaker must speak each word 3 times for each emotional expression. Speakers consist of 50 males and 50 females. This approach is necessary because, in the previous study, the training and testing result is biased by serious overfitting caused by a lack of diversity in the database [13]. Also, the general expression of "sad" and "angry" between males and females has different energy and frequency.

Participants were first asked to fill out a simple questionnaire regarding their mood at the time. If the participant is in a very sad or angry condition, the recording will not include the "happy" state and will be rescheduled for another day. To induce the "happy", "sad" and "angry" emotional state, participants were asked to view a video for each emotional state. The videos are purely chosen by the data sample collector and to minimize bias before recording, participants were also asked once again about their emotional state after watching the video.

TABLE II. Voice Samples Gender Distribution

Words	Male	Female
Maju (*forward*)	450	450
Mundur (*backward*)	450	450
Kanan (*right*)	450	450
Kiri (*left*)	450	450
Tegak (*stand*)	450	450
Duduk (*sit*)	450	450
Tidur (*sleep*)	450	450
Joget (*dance*)	450	450
Cari (*find*)	450	450
Angkat (*lift*)	450	450
	4500	4500

III. Methodology

The features from audio data were extracted using the MFCC method before being fed into CNN-LSTM networks to classify audio file samples into three emotion classes. Each audio is preprocessed to have the same ±1000ms length with .wav file format. Shorter data will be added with zeroes, and longer data will be cut to fit in a 1000ms timeframe.

This work will use MFCC for the feature extraction method, as shown by several studies that MFCC has greater output accuracy compared with other methods like DTW, hence MFCC become one of the main methods to process audio samples to be used in deep learning [7][14]. CNN-LSTM is chosen to provide deep learning methods for emotion recognition. A detailed explanation of the processes in this work is given below.

A. MFCC

Preprocessed data will be further processed into MFCC to get the 2D representation of the spectrogram from audio data. This is necessary because the convolutional process in CNN requires all data represented in the image, in this case, a 2D spectrogram image. Using constant value padding, all output vectors from MFCC were fixed in size. Audio files used in the MFCC process have a 16kHz framerate and mono encoding. Output from MFCC extractions are 20x11 vector matrix.

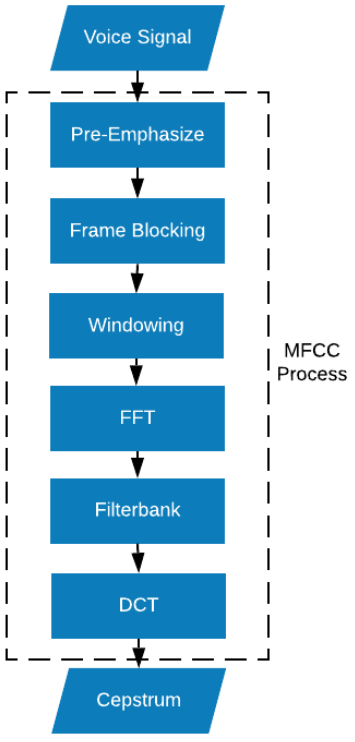

Fig. 1. Typical MFCC Process

B. CNN-LSTM

In this study, CNN-LSTM is used as a means of training, validating, and testing the learning and recognition model built in the research, by using the Keras library in Python. MFCC feature output from the process will be fed into the CNN network. The convolutional method in CNN will extract samples from dataset features provided in MFCC by convoluting the sample to extract diminishing features from the dataset. After the convolutional and pooling process, the fully-connected layer of CNN will be connected to the LSTM layers. The step-by-step of this process will be further explained below.

Convolution - we used 64 convolutional layers, with three by three kernels, to extract data from the sample with ReLU activation.

MaxPooling - to decrease the samples, we used two-by-two pool sizes with the "same" padding.

Dropout - The dropout method used for regularisation means to reduce the overfitting probability. 0.25 probability used in the Dropout layer

Convolution - 128 convolutional layers, with two by two kernels to further extract diminishing features from convoluted layers.

MaxPooling - another two-by-two pool size is used.

Dropout - same 0.25 probability used in this layer.

Flatten - flatten the output to become a fully connected layer, to make the sure output of CNN will be connected with the LSTM layer.

LSTM - we used two layers of LSTM to acquire information from the output of CNN with "ReLU" activation.

Dense - model will be condensed into 3 classes, with "Softmax" activation.

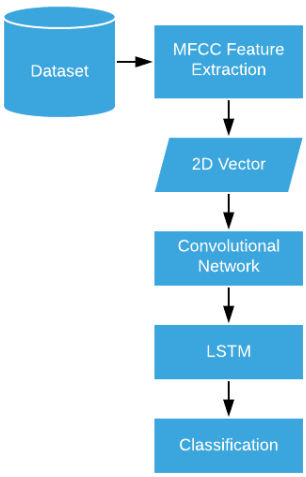

Fig. 2. Feature Extraction and Classification Process

C. CNN-LSTM

The hardware robot used in this research is a humanoid robot from UBTech. This robot will be dismantled and the main CPU in the system will be replaced with a Raspberry Pi board. The Raspberry Pi will be used as a place for running the machine learning model, and where a webcam is connected to the system. The microphone from the webcam will be used to record voice commands, which are then processed with MFCC and classified by CNN-LSTM layers. The result of the classification is a command for the robot, which will then be used as input for the Arduino Uno. This is because the robot's motor itself is driven using Arduino. The illustration of the robot will be shown in Figure 3. The wiring diagram of the robot will be shown in Figure 5.

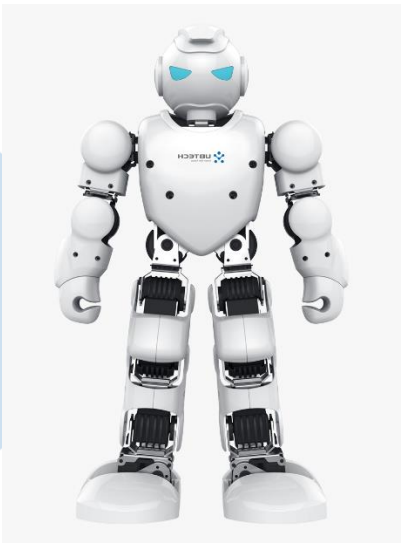

Fig. 3. Humanoid Robot used in Experiment

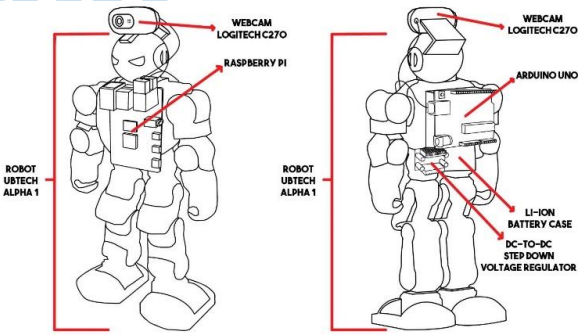

Fig. 4. Robot Design

The servo used in this robot is operated by sending a byte array to the servo. The servo itself is daisy-chained for each limb, so the Tx pin for moving the robot is split into 4 channels. The bytes array itself is consist of 10 bytes which is shown in Table III below.

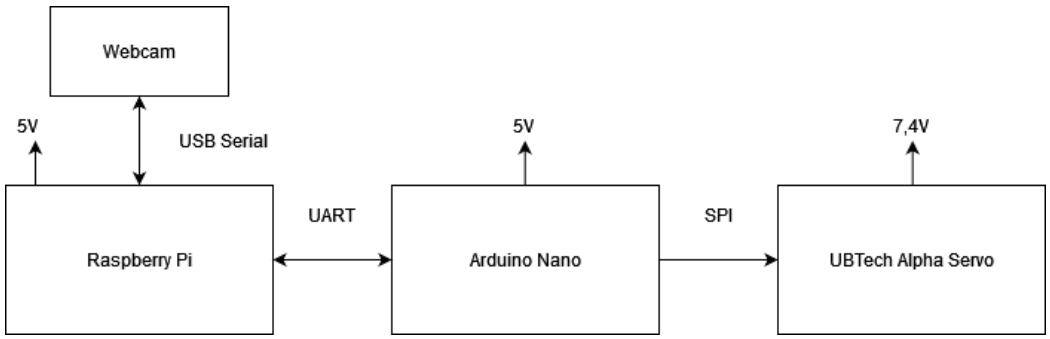

Fig. 5. System Block Diagram

The servo ID is already predetermined by the manufacturer. Op Mode is like the "servo.attach" command when using the Arduino Servo library, so the servo will be initialized and energized when "attached" and de-energized when "detached". Mode 1 is for the "attach" function and Mode 2 is for the "detach" function. The degree is the value of desired servo degree, ranging from 0 to 180. Duration is for determining how fast the servo must attain the desired degree.

TABLE III. ROBOT MOVEMENT COMMAND

Byte 1	Header
Byte 2	Header
Byte 3	Servo ID
Byte 4	Op Mode
Byte 5	Degree
Byte 6	Duration
Byte 7	N/A
Byte 8	N/A
Byte 9	Checksum
Byte 10	End of array

IV. EXPERIMENT AND RESULTS

A. *Word Recognition*

For word recognition and classification, the CNN-LSTM network is used as a means for training and testing the machine learning model. This classification is done by using the Keras library in Python. On the CNN side, 128 convolution layers were used, with a kernel size of 2x2 matrix and ReLU activation. And then, the kernel will be pooled using the 2D MaxPooling technique with a 2x2 matrix size.

As this work uses limited data on non-linear hidden layers of the deep neural network, the tendency for overfitting to occur is high [15]. So Dropout method is used to prevent overfitting to occur. The Dropout coefficient used is 0.25.

The LSTM layers in the model are engaged by defining CNN layers within the "TimeDistributed" function from Keras. After building the layer, the model will be completed by using the "Dense" function to build a Fully Connected Layer (FC Layer). The final result will be compiled using the Adadelta optimizer. After compilation, the model will be tested for 150 epochs using 80% audio samples from the data set for training and 20% for testing.

TABLE IV. TRAINING AND TESTING RESULT

Epoch	Training Accuracy	Test Accuracy
10	47,21%	38,06%
25	62,19%	41,12%
50	68,86%	44,19%
75	73,57%	45,91%
100	85,67%	57,56%
125	90,36%	61,33%
150	89,19%	66,94%

For the accuracy of training and testing from all emotion datasets, depicted in Fig. 3. The training process from 80% of data, peaked at 90,36%. And the testing process used 20% of the data and peaked at 67%.

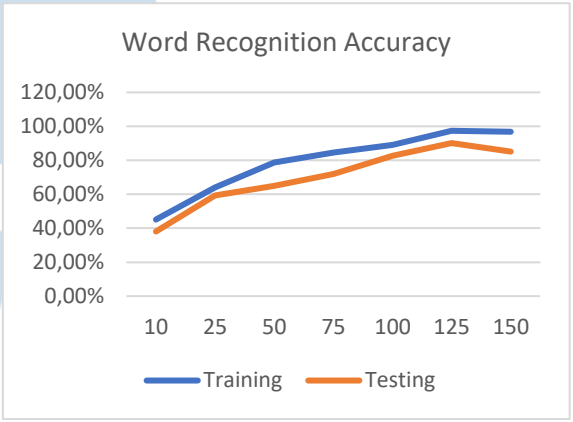

Fig. 6. Accuracy of Training and Testing

B. *Emotion Recognition*

Experiments in this research were conducted in 3 scenarios to fully validate the classification accuracy. All scenarios were conducted with 80:20 split data ratios. The parameter in CNN-LSTM networks used in the scenarios is ReLU activation CNN networks. For LSTM, the Softmax activation method is used for the final output. 150 epoch set for all scenarios with final compilation using the "Adadelta" optimizer.

1. *Scenario 1* - test the accuracy of the "happy" expression on the model.
2. *Scenario 2* - test the accuracy of the "sad" expression on the model.

3. *Scenario 3* - test the accuracy of the "angry" expression on the model.

Scenarios 1 to 3 will try to recognize which audio sample is classified as an emotional expression and to check the accuracy compared to the null model or undefined expression. The averaged result of "happy," "sad," and "angry" is shown in Table V. For the accuracy of training and testing from all emotion datasets, depicted in Fig. 7. The training process from 80% of data, peaked at 90,36%. And the testing process used 20% of the data and peaked at 67%

TABLE V. RESULT OF "HAPPY", "SAD", "ANGRY"

Emotion	Precision	Recall	f-1 Score
Happy	0,78	0,52	0,65
Sad	0,61	0,57	0,66
Angry	0,69	0,46	0,67

For the final testing scenario, all emotional expressions are processed together within the CNN-LSTM network. From this process, the output of this process can be depicted in a random confusion table, shown in Table VI.

TABLE VI. RANDOM SAMPLE CONFUSION RESULT

	Prediction			
Actual	Happy	Sad	Angry	Undefined
Happy	73	5	7	15
Sad	3	65	18	14
Angry	9	11	67	13

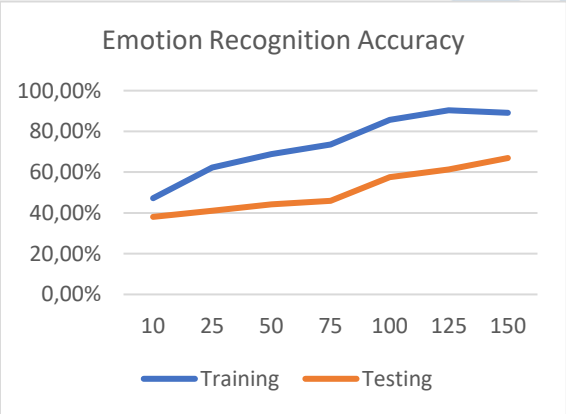

Fig. 7. Accuracy of Training and Testing

C. Robot Movement

The movement of the robot will depend on the classification results that have been obtained. The classification results that have been successfully obtained from the Raspberry Pi will be sent to the microcontroller. The robot will be driven by using serial communication between the microcontroller and the robot's servo motor. The movement of the robot being tested is for 4 types of movement, namely "Tegak", "Duduk", "Kanan", and "Kiri". This type of movement was chosen because this type of movement allows it to be carried out without analyzing the balance of the robot's movement. The first test is carried out using the data used in the machine learning model as input. The first experiment result is shown in Table VII.

TABLE VII. PRE-RECORDED INPUT TEST RESULT

No	Pre-Recorded Input	Classification Result	Robot Movement
1	Duduk	Duduk	Duduk
2	Tegak	Tegak	Tegak
3	Duduk	Duduk	Duduk
4	Tegak	Tegak	Tegak
5	Kanan	Kanan	Kanan
6	Kanan	Kanan	Kanan
7	Kiri	Kiri	Kiri
8	Duduk	Duduk	Duduk
9	Tegak	Tegak	Tegak
10	Kanan	Kanan	Kanan

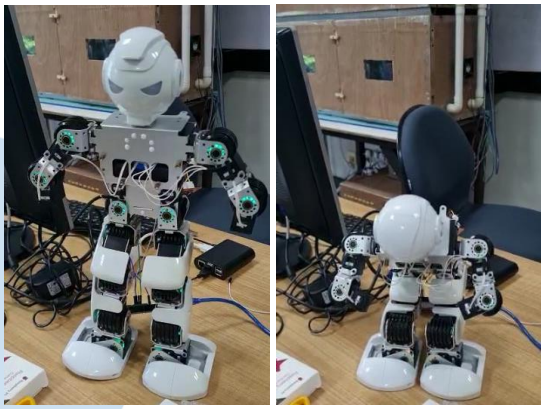

(a) (b)

Fig. 8. Robot Movement for (a) Tegak, (b) Duduk

And then for the final testing scenario, the input data for the robot uses a new voice input recorded using a webcam microphone. The user must speak within 10-20 cm of the webcam. This is because the webcam microphone was not good enough to capture the user's voice. The result of the final experiment is shown in Table VIII below.

TABLE VIII. REAL-TIME INPUT TEST RESULT

No	Pre-Recorded Input	Classification Result	Robot Movement
1	Duduk	Duduk	Duduk
2	Tegak	Tegak	Tegak
3	Duduk	Duduk	Duduk
4	Tegak	Tegak	Tegak
5	Kanan	Kanan	Kanan
6	Kanan	Kanan	Kanan
7	Kiri	Kiri	Kiri
8	Duduk	Duduk	Duduk
9	Tegak	Tegak	Tegak
10	Kanan	Kanan	Kanan

From Table VIII above, mostly the results of the model classification resulted in the word "Duduk". This causes the robot to do more "Duduk" movements even though the user gives the "Right" and "Left" commands to the robot. This could be caused by the model experiencing overfitting because the results of the input

using pre-recorded data indicate the model can work well according to the input given.

V. CONCLUSION

Our preliminary study on word-level emotion recognition results shows that this model has an acceptable performance. And from the confusion matrix result shows that the model accuracy is around 65%. These results should be improved in future works by adding more data and also using and comparing different layers of CNN and LSTM to determine how deep the network should be used for emotion recognition based on a self-built database like this. For robot implementation, the pre-recorded scenario shows the model can satisfy the movement classification with 100% classification, but when the model is introduced with new input data, it fails miserably as most input is classified as "Duduk" with accuracy only 20% from 10 data. This result is strong evidence for showing this model has an overfitting tendency. This is the main issue that must be solved in future works.

ACKNOWLEDGMENT

This study is supported by Universitas Multimedia Nusantara under an internal research grant.

REFERENCES

[1] J. Wang and Z. Han, "Research on Speech Emotion Recognition Technology based on Deep and Shallow Neural Network," *2019 Chinese Control Conf.*, pp. 3555–3558, 2019.

[2] P. Tzirakis, J. Zhang, and W. Schuller, "End-to-End Speech Emotion Recognition Using Deep Neural Networks," *IEEE Int. Conf. Acoust. Speech, Signal Process. 2018*, pp. 5089–5093, 2018.

[3] K. Tarunika, R. B. Pradeeba, and P. Aruna, "Applying Machine Learning Techniques for Speech Emotion Recognition," *2018 9th Int. Conf. Comput. Commun. Netw. Technol. ICCCNT 2018*, pp. 1–5, 2018, doi: 10.1109/ICCCNT.2018.8494104.

[4] B. T. Atmaja and M. Akagi, "Speech Emotion Recognition Based on Speech Segment Using LSTM with Attention Model," *2019 IEEE Int. Conf. Signals Syst.*, pp. 40–44, 2019, doi: 10.1109/icsigsys.2019.8811080.

[5] C. Wan and L. Liu, "Research of speech emotion recognition based on embedded system," *ICCSE 2010 - 5th Int. Conf. Comput. Sci. Educ. Final Progr. B. Abstr.*, pp. 1129–1133, 2010, doi: 10.1109/ICCSE.2010.5593692.

[6] Y. J. Lee, C. Y. Park, and H. J. Choi, "Word-Level Emotion Embedding Based on Semi-Supervised Learning for Emotional Classification in Dialogue," *2019 IEEE Int. Conf. Big Data Smart Comput. BigComp 2019 - Proc.*, pp. 1–4, 2019, doi: 10.1109/BIGCOMP.2019.8679196.

[7] S. Basu, J. Chakraborty, and M. Aftabuddin, "Emotion Recognition From Speech Using Convolutional Neural Network With Recurrent Neural Network Architecture," *ICCES 2017 - 2nd Int. Conf. Commun. Electron. Syst.*, pp. 333–336, 2017.

[8] D. Palaz, M. Magimai-Doss, and R. Collobert, "Convolutional Neural Networks-Based Continuous Speech Recognition Using Raw Speech Signal," *ICASSP, IEEE Int. Conf. Acoust. Speech Signal Process. - Proc.*, pp. 4295–4299, 2015, doi: 10.1109/ICASSP.2015.7178781.

[9] J. J. Lasiman and D. P. Lestari, "Speech Emotion Recognition for Indonesian Language Using Long Short-Term Memory," *2018 Int. Conf. Comput. Control. Informatics its Appl. Recent Challenges Mach. Learn. Comput. Appl. IC3INA 2018 - Proceeding*, pp. 40–43, 2019, doi: 10.1109/IC3INA.2018.8629525.

[10] D. Guiming, W. Xia, W. Guangyan, Z. Yan, and L. Dan, "Speech recognition based on convolutional neural networks," pp. 708–711, 2017, doi: 10.1109/siprocess.2016.7888355.

[11] N. B. Wunarso and Y. E. Soelistio, "Towards Indonesian speech-emotion automatic recognition (I-SpEAR)," *Proc. 2017 4th Int. Conf. New Media Stud. CONMEDIA 2017*, vol. 2018-Janua, pp. 98–101, 2018, doi: 10.1109/CONMEDIA.2017.8266038.

[12] S. Park, Y. Jeong, M. S. Kim, and H. S. Kim, "Linear prediction-based dereverberation with very deep convolutional neural networks for reverberant speech recognition," *Int. Conf. Electron. Inf. Commun. ICEIC 2018*, vol. 2018-Janua, no. 1, pp. 1–2, 2018, doi: 10.23919/ELINFOCOM.2018.8330593.

[13] D. A. A. Tuasikal, M. B. Nugraha, E. Yudhatama, A. S. A. S. Muharom, and M. Pura, "Word Recognition For Color Classification Using Convolutional Neural Network," in *Proceedings of 2019 5th International Conference on New Media Studies, CONMEDIA 2019*, Oct. 2019, pp. 228–231, doi: 10.1109/CONMEDIA46929.2019.8981852.

[14] A. I. S. M. Ayu and K. K. Karyono, "Audio detection (Audition): Android based sound detection application for hearing-impaired using AdaBoostM1 classifier with REPTree weaklearner," in *2014 Asia-Pacific Conference on Computer Aided System Engineering (APCASE)*, Feb. 2014, pp. 136–140, doi: 10.1109/APCASE.2014.6924487.

[15] A. Singh, K. K. Srivastava, and H. Murugan, "Speech emotion recognition using convolutional neural network (CNN)," *Int. J. Psychosoc. Rehabil.*, vol. 24, no. 8, pp. 2408–2416, 2020, doi: 10.37200/IJPR/V24I8/PR280260.

AUTHOR GUIDELINES

1. Manuscript criteria

- The article has never been published or in the submission process on other publications.
- Submitted articles could be original research articles or technical notes.
- The similarity score from plagiarism checker software such as Turnitin is 20% maximum.
- For December 2021 publication onwards, Ultima Computing : Jurnal Sistem Komputer will be receiving and publishing manuscripts written in English only.

2. Manuscript format

- Article been type in Microsoft Word version 2007 or later.
- Article been typed with 1 line spacing on an A4 paper size (21 cm x 29,7 cm), top-left margin are 3 cm and bottom-right margin are 2 cm, and Times New Roman's font type.
- Article should be prepared according to the following author guidelines in this template. Article contain of minimum 3500 words.
- References contain of minimum 15 references (primary references) from reputable journals/conferences

3. Organization of submitted article

The organization of the submitted article consists of Title, Abstract, Index Terms, Introduction, Method, Result and Discussion, Conclusion, Appendix (if any), Acknowledgment (if any), and References.

- Title
  The maximum words count on the title is 12 words (including the subtitle if available)
- Abstract
  Abstract consists of 150-250 words. The abstract should contain logical argumentation of the research taken, problem-solving methodology, research results, and a brief conclusion.
- Index terms
  A list in alphabetical order in between 4 to 6 words or short phrases separated by a semicolon (;), excluding words used in the title and chosen carefully to reflect the precise content of the paper.
- Introduction
  Introduction commonly contains the background, purpose of the research, problem identification, research methodology, and state of the art conducted by the authors which describe implicitly.
- Method
  Include sufficient details for the work to be repeated. Where specific equipment and materials are named, the manufacturer's details (name, city and country) should be given so that readers can trace specifications by contacting the manufacturer. Where commercially available software has been used, details of the supplier should be given in brackets or the reference given in full in the reference list.
- Results and Discussion
  State the results of experimental or modeling work, drawing attention to important details in tables and figures, and discuss them intensively by comparing and/or citing other references.
- Conclusion
  Explicitly describes the research's results been taken. Future works or suggestion could be explained after it
- Appendix and acknowledgment, if available, could be placed after Conclusion.
- All citations in the article should be written on References consecutively based on its' appearance order in the article using Mendeley (recommendation). The typing format will be in the same format as the IEEE journals and transaction format.

4. Reviewing of Manuscripts

Every submitted paper is independently and blindly reviewed by at least two peer-reviewers. The decision for publication, amendment, or rejection is based upon their reports/recommendations. If two or more reviewers consider a manuscript unsuitable for publication in this journal, a statement explaining the basis for the decision will be sent to the authors within six months of the submission date.

5. Revision of Manuscripts

Manuscripts sent back to the authors for revision should be returned to the editor without delay (maximum of two weeks). Revised manuscripts can be sent to the editorial office through the same online system. Revised manuscripts returned later than one month will be considered as new submissions.

6. Editing References

- **Periodicals**
  J.K. Author, “Name of paper,” Abbrev. Title of Periodical, vol. x, no. x, pp. xxx-xxx, Sept. 2013.

- **Book**
  J.K. Author, “Title of chapter in the book,” in Title of His Published Book, xth ed. City of Publisher, Country or Nation: Abbrev. Of Publisher, year, ch. x, sec. x, pp xxx-xxx.

- **Report**
  J.K. Author, “Title of report,” Abbrev. Name of Co., City of Co., Abbrev. State, Rep. xxx, year.

- **Handbook**
  Name of Manual/ Handbook, x ed., Abbrev. Name of Co., City of Co., Abbrev. State, year, pp. xxx-xxx.

- **Published Conference Proceedings**
  J.K. Author, “Title of paper,” in Unabbreviated Name of Conf., City of Conf., Abbrev. State (if given), year, pp. xxx-xxx.

- **Papers Presented at Conferences**
  J.K. Author, “Title of paper,” presented at the Unabbrev. Name of Conf., City of Conf., Abbrev. State, year.

- **Patents**
  J.K. Author, “Title of patent,” US. Patent xxxxxxx, Abbrev. 01 January 2014.

- **Theses and Dissertations**
  J.K. Author, “Title of thesis,” M.Sc. thesis, Abbrev. Dept., Abbrev. Univ., City of Univ., Abbrev. State, year. J.K. Author, “Title of dissertation,” Ph.D. dissertation, Abbrev. Dept., Abbrev. Univ., City of Univ., Abbrev. State, year.

- **Unpublished**
  J.K. Author, “Title of paper,” unpublished. J.K. Author, “Title of paper,” Abbrev. Title of Journal, in press.

- **On-line Sources**
  J.K. Author. (year, month day). Title (edition) [Type of medium]. Available: http:// www.(URL) J.K. Author. (year, month). Title. Journal [Type of medium]. volume(issue), pp. if given. Available: http://www.(URL) Note: type of medium could be online media, CD-ROM, USB, etc.

7. Editorial Adress

Jl. Scientia Boulevard, Gading Serpong
Tangerang, Banten, 15811
Email: **ultimacomputing@umn.ac.id**

Paper Title

Subtitle (if needed)

Author 1 Name[1], Author 2 Name[2], Author 3 Name[2]
[1] Line 1 (of affiliation): dept. name of organization, organization name, City, Country
Line 2: e-mail address if desired
[2] Line 1 (of affiliation): dept. name of organization, organization name, City, Country
Line 2: e-mail address if desired

Accepted on mmmmm dd, yyyy
Approved on mmmmm dd, yyyy

***Abstract*—This electronic document is a "live" template which you can use on preparing your Ultima Computing paper. Use this document as a template if you are using Microsoft Word 2007 or later. Otherwise, use this document as an instruction set. Do not use symbol, special characters, or Math in Paper Title and Abstract. Do not cite references in the abstract.**

***Index Terms*—enter key words or phrases in alphabetical order, separated by semicolon (;)**

I. INTRODUCTION

This template, modified in MS Word 2007 and saved as a Word 97-2003 document, provides authors with most of the formatting specifications needed for preparing electronic versions of their papers. Margins, column widths, line spacing, and type styles are built-in here. The authors must make sure that their paper has fulfilled all the formatting stated here.

Introduction commonly contains the background, purpose of the research, problem identification, and research methodology conducted by the authors which been describe implicitly. Except for Introduction and Conclusion, other chapter's title must be explicitly represent the content of the chapter.

II. EASE OF USE

A. Selecting a Template

First, confirm that you have the correct template for your paper size. This template is for Ultima Computing. It has been tailored for output on the A4 paper size.

B. Maintaining the Integrity of the Specifications

The template is used to format your paper and style the text. All margins, column widths, line spaces, and text fonts are prescribed; please do not alter them.

III. PREPARE YOUR PAPER BEFORE STYLING

Before you begin to format your paper, first write and save the content as a separate text file. Keep your text and graphic files separate until after the text has been formatted and styled. Do not add any kind of pagination anywhere in the paper. Please take note of the following items when proofreading spelling and grammar.

A. Abbreviations and Acronyms

Define abbreviations and acronyms the first time they are used in the text, even after they have been defined in the abstract. Abbreviations such as IEEE, SI, MKS, CGS, sc, dc, and rms do not have to be defined. Abbreviations that incorporate periods should not have spaces: write "C.N.R.S.," not "C. N. R. S." Do not use abbreviations in the title or heads unless they are unavoidable.

B. Units

- Use either SI (MKS) or CGS as primary units (SI units are encouraged).
- Do not mix complete spellings and abbreviations of units: "Wb/m2" or "webers per square meter," not "webers/m2." Spell units when they appear in text: "...a few henries," not "...a few H."
- Use a zero before decimal points: "0.25," not ".25."

C. Equations

The equations are an exception to the prescribed specifications of this template. You will need to determine whether or not your equation should be typed using either the Times New Roman or the Symbol font (please no other font). To create multileveled equations, it may be necessary to treat the equation as a graphic and insert it into the text after your paper is styled.

Number the equations consecutively. Equation numbers, within parentheses, are to position flush right, as in (1), using a right tab stop.

$$\int_0^{r_2} F(r,\phi)\, dr\, d\phi = [\sigma r_2 / (2\mu_0)] \qquad (1)$$

Note that the equation is centered using a center tab stop. Be sure that the symbols in your equation have been defined before or immediately following the

equation. Use "(1)," not "Eq. (1)" or "equation (1)," except at the beginning of a sentence: "Equation (1) is ..."

D. Some Common Mistakes

- The word "data" is plural, not singular.
- The subscript for the permeability of vacuum μ_0, and other common scientific constants, is zero with subscript formatting, not a lowercase letter "o."
- In American English, commas, semi-/colons, periods, question and exclamation marks are located within quotation marks only when a complete thought or name is cited, such as a title or full quotation. When quotation marks are used, instead of a bold or italic typeface, to highlight a word or phrase, punctuation should appear outside of the quotation marks. A parenthetical phrase or statement at the end of a sentence is punctuated outside of the closing parenthesis (like this). (A parenthetical sentence is punctuated within the parentheses.)
- A graph within a graph is an "inset," not an "insert." The word alternatively is preferred to the word "alternately" (unless you really mean something that alternates).
- Do not use the word "essentially" to mean "approximately" or "effectively."
- In your paper title, if the words "that uses" can accurately replace the word using, capitalize the "u"; if not, keep using lower-cased.
- Be aware of the different meanings of the homophones "affect" and "effect," "complement" and "compliment," "discreet" and "discrete," "principal" and "principle."
- Do not confuse "imply" and "infer."
- The prefix "non" is not a word; it should be joined to the word it modifies, usually without a hyphen.
- There is no period after the "et" in the Latin abbreviation "et al."
- The abbreviation "i.e." means "that is," and the abbreviation "e.g." means "for example."

IV. Using the Template

After the text edit has been completed, the paper is ready for the template. Duplicate the template file by using the Save As command, and use the naming convention as below

ULTIMATICS_firstAuthorName_paperTitle.

In this newly created file, highlight all of the contents and import your prepared text file. You are now ready to style your paper. Please take note on the following items.

A. Authors and Affiliations

The template is designed so that author affiliations are not repeated each time for multiple authors of the same affiliation. Please keep your affiliations as succinct as possible (for example, do not differentiate among departments of the same organization).

B. Identify the Headings

Headings, or heads, are organizational devices that guide the reader through your paper. There are two types: component heads and text heads.

Component heads identify the different components of your paper and are not topically subordinate to each other. Examples include ACKNOWLEDGMENTS and REFERENCES, and for these, the correct style to use is "Heading 5."

Text heads organize the topics on a relational, hierarchical basis. For example, the paper title is the primary text head because all subsequent material relates and elaborates on this one topic. If there are two or more sub-topics, the next level head (uppercase Roman numerals) should be used and, conversely, if there are not at least two sub-topics, then no subheads should be introduced. Styles, named "Heading 1," "Heading 2," "Heading 3," and "Heading 4", are prescribed.

C. Figures and Tables

Place figures and tables at the top and bottom of columns. Avoid placing them in the middle of columns. Large figures and tables may span across both columns. Figure captions should be below the figures; table heads should appear above the tables. Insert figures and tables after they are cited in the text. Use the abbreviation "Fig. 1," even at the beginning of a sentence.

TABLE I. TABLE STYLES

Table Head	**Table Column Head**		
	Table column subhead	***Subhead***	***Subhead***
copy	More table copy		

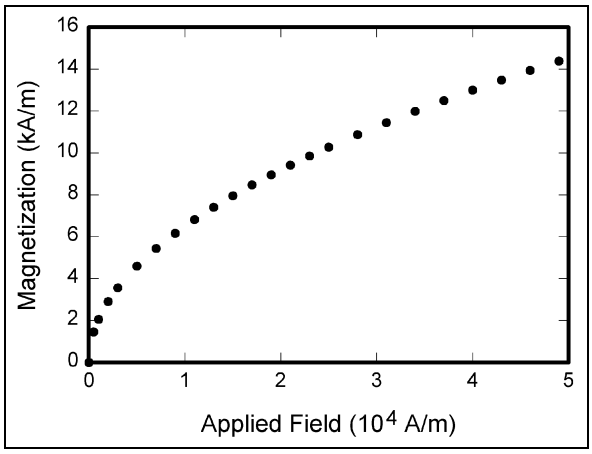

Fig. 1. Example of a figure caption

V. Conclusion

A conclusion section is not required. Although a conclusion may review the main points of the paper, do not replicate the abstract as the conclusion. A conclusion might elaborate on the importance of the work or suggest applications and extensions.

Appendix

Appendixes, if needed, appear before the acknowledgment.

ACKNOWLEDGMENT

The preferred spelling of the word "acknowledgment" in American English is without an "e" after the "g." Use the singular heading even if you have many acknowledgments. Avoid expressions such as "One of us (S.B.A.) would like to thank ... ." Instead, write "F. A. Author thanks ... ." You could also state the sponsor and financial support acknowledgments here.

References

The template will number citations consecutively within brackets [1]. The sentence punctuation follows the bracket [2]. Refer simply to the reference number, as in [3]—do not use "Ref. [3]" or "reference [3]" except at the beginning of a sentence: "Reference [3] was the first ..."

Number footnotes separately in superscripts. Place the actual footnote at the bottom of the column in which it was cited. Do not put footnotes in the reference list. Use letters for table footnotes.

Unless there are six authors or more give all authors' names; do not use "et al.". Papers that have not been published, even if they have been submitted for publication, should be cited as "unpublished" [4]. Papers that have been accepted for publication should be cited as "in press" [5]. Capitalize only the first word in a paper title, except for proper nouns and element symbols.

For papers published in translation journals, please give the English citation first, followed by the original foreign-language citation [6].

[1] G. Eason, B. Noble, and I.N. Sneddon, "On certain integrals of Lipschitz-Hankel type involving products of Bessel functions," Phil. Trans. Roy. Soc. London, vol. A247, pp. 529-551, April 1955. (*references*)

[2] J. Clerk Maxwell, A Treatise on Electricity and Magnetism, 3rd ed., vol. 2. Oxford: Clarendon, 1892, pp.68-73.

[3] I.S. Jacobs and C.P. Bean, "Fine particles, thin films and exchange anisotropy," in Magnetism, vol. III, G.T. Rado and H. Suhl, Eds. New York: Academic, 1963, pp. 271-350.

[4] K. Elissa, "Title of paper if known," unpublished.

[5] R. Nicole, "Title of paper with only first word capitalized," J. Name Stand. Abbrev., in press.

[6] Y. Yorozu, M. Hirano, K. Oka, and Y. Tagawa, "Electron spectroscopy studies on magneto-optical media and plastic substrate interface," IEEE Transl. J. Magn. Japan, vol. 2, pp. 740-741, August 1987 [Digests 9th Annual Conf. Magnetics Japan, p. 301, 1982].

[7] M. Young, The Technical Writer's Handbook. Mill Valley, CA: University Science, 1989.

UMN

UNIVERSITAS
MULTIMEDIA
NUSANTARA

ISSN 2355-3286

UMN
UNIVERSITAS
MULTIMEDIA
NUSANTARA

PRESS

Universitas Multimedia Nusantara
Scientia Garden Jl. Boulevard Gading Serpong, Tangerang
Telp. (021) 5422 0808 | Fax. (021) 5422 0800